

**Development of new manufacturing process of carbon
short fiber and carbon nano fiber reinforced aluminum
matrix composites and characterizations**

カーボン短繊維とカーボンナノファイバー強化アルミニウム基複合材料の新しい製造プロセスの開発と特性評価

March 2020

MENG XUAN

Development of new manufacturing process of carbon
short fiber and carbon nano fiber reinforced aluminum
matrix composites and characterizations

カーボン短繊維とカーボンナノファイバー強化
アルミニウム基複合材料の新しい製造プロセス
の開発と特性評価

Dissertation for the Degree of
Doctor of Philosophy

Department of Mechanical System Engineering
Graduate School of Engineering
Hiroshima University, Japan

Asst. Prof. Choi Yong Bum, Advisor

MENG XUAN

March 2020

CONTENTS

Chapter 1 Background and objectives

<i>1.1 Introduction</i>	2
<i>1.2 Development of aluminum alloys</i>	4
<i>1.2.1 Wrought aluminum alloys</i>	4
<i>1.2.2 Cast aluminum alloys</i>	7
<i>1.3 Development of aluminum matrix composites</i>	8
<i>1.3.1 Manufacturing processes of aluminum matrix composites</i>	9
<i>1.3.2 Thermal and mechanical properties of aluminum matrix composites</i>	13
<i>1.3.3 Reinforcement</i>	16
<i>1.3.3.1 PAN and pitch based carbon fibers</i>	16
<i>1.3.3.2 Vapor grown carbon fibers</i>	19
<i>1.3.3.3 Coating of carbon fibers</i>	21
<i>1.4 Theoretical models for predicting properties of CF/Al matrix composites</i>	25
<i>1.4.1 Models for predicting strength of composites</i>	25
<i>1.4.2 Models for predicting thermal conductivity of composites</i>	27
<i>1.5 Objective and outline of this thesis</i>	32
<i>References</i>	35

Chapter 2 Fabrication process and microstructure of carbon short fiber and hybrid carbon short fiber-carbon nanofiber reinforced aluminum matrix composites with SiO₂ binder by low pressure infiltration process

<i>2.1 Introduction</i>	42
<i>2.2 Experimental procedure</i>	44
<i>2.2.1 Raw materials</i>	44
<i>2.2.2 Preparation of CSF preform and hybrid CSF-CNF preform</i>	46
<i>2.2.3 Fabrication of CSF/Al and hybrid CSF-CNF/Al composites</i>	48
<i>2.2.4 Evaluation methods and equipment</i>	50
<i>2.2.4.1 Observation of microstructure</i>	50

2.2.4.2 X-ray diffraction characterization.....	50
2.3 Results and discussion.....	51
2.3.1 Microstructures	51
2.3.1.1 Microstructures of CSF preform and hybrid CSF-CNF preform.....	51
2.3.1.2 Microstructures of CSF/Al and hybrid CSF-CNF/Al composites	54
2.3.2 Interface structure between CSF and aluminum matrix.....	61
2.4 Summary.....	65
References.....	66

Chapter 3 Fabrication process and microstructure of nickel plated carbon short fiber reinforced aluminum matrix composites by low pressure infiltration process

3.1 Introduction.....	70
3.2 Experimental procedure.....	72
3.2.1 Raw materials and electroless Ni plating process	72
3.2.2 Electroless Ni plating of CSFs	73
3.2.3 Fabrication of Ni plated CSF reinforced aluminum matrix composites without preform manufacturing.....	76
3.2.4 Evaluation methods and equipment.....	78
3.2.4.1 Observation of microstructure.....	78
3.2.4.2 Measurement of thickness of Ni layer	78
3.2.4.3 X-ray diffraction characterization.....	78
3.3 Results and discussion.....	79
3.3.1 Microstructures	79
3.3.1.1 Microstructures of Ni plated CSFs.....	79
3.3.1.2 Microstructures of Ni plated CSF/Al matrix composites.....	84
3.3.2 Dispersion behavior of Ni plated CSF inside matrix	93
3.4 Summary.....	96
References.....	97

Chapter 4 Mechanical and thermal properties of CSF/Al matrix composites

4.1 Introduction.....	100
4.2 Evaluation methods and equipment.....	102
4.2.1 Hardness test	102

4.2.2	<i>Relative density</i>	102
4.2.3	<i>Tensile test</i>	102
4.2.4	<i>Thermal conductivity</i>	103
4.2.5	<i>Observation of fracture surface</i>	103
4.3	<i>Results and discussion</i>	104
4.3.1	<i>Mechanical properties of CSF/Al matrix composites</i>	104
4.3.1.1	<i>Vickers hardness and relative density of CSF/Al matrix composites</i>	104
4.3.1.2	<i>Tensile properties and fracture surface of CSF/Al matrix composites</i> ..	108
4.3.2	<i>Thermal conductivity of CSF/Al matrix composites</i>	121
4.4	<i>Summary</i>	129
	<i>References</i>	130
Chapter 5	Conclusions	133

List of Figures

- Fig. 1-1 Classification of wrought aluminum alloys and cast aluminum alloys:
(a) wrought aluminum alloys. (b) cast aluminum alloys.
- Fig. 1-2 Schematic illustration of the powder metallurgy process (PM process).
- Fig. 1-3 Schematic illustration of (a) Stir casting process and (b) Squeeze casting process.
- Fig. 1-4 The textures of mesophase pitch-based CFs.
- Fig. 1-5 Illustration of differences between (a) graphitizable CF and (b) non-graphitizable CF structures.
- Fig. 1-6 SEM and TEM images of pitch CFs heat treated at (a) 1200 °C, (b) 1500 °C, (c) 2100 °C, and (d) 2600°C.
- Fig. 1-7 SEM images of CNFs: (a) low, (b) high in magnification.
- Fig. 2-1 Schematic diagram of CSF preform and hybrid CSF-CNF preform fabricating process.
- Fig. 2-2 Schematic illustration of low-pressure infiltration equipment.
- Fig. 2-3 SEM images of (a) as-received CSF, (b) as-received CNF and (c) CNF after acid treatment.
- Fig. 2-4 SEM images of hybrid preforms, different ratio of CSF: CNF (a) 5:5, (b) 7:3, (c) 9:1 and (d) 9.5:0.5.
- Fig. 2-5 SEM images of preforms: (a), (b) CSF inside preform, (c) CSF-CNF hybrid preform (9.5:0.5) and (d) partial enlargement of (c).
- Fig. 2-6 OM and SEM images of the composites: (a) CSF/A1070 composite (OM), (b) CSF/A356 alloy composite (OM), (c) CSF/A336 alloy composite (OM), (d) CSF-CNF/A336 alloy composite (OM) and (e) enlargement of CNF cluster (SEM).
- Fig. 2-7 SEM images of composites: (a), (a'), (a'') CSF/A1070 composite, (b), (b'), (b'') CSF/A356 alloy composite, (c), (c'), (c'') CSF/A336 alloy composite and (d), (d'), (d'') CSF-CNF/A336 alloy composite.
- Fig. 2-8 Results of area elemental mapping and point analysis of CSF/A336 alloy composite.
- Fig. 2-9 Defects and area elemental mapping of CSF/Al matrix composites:
(a) CSF/A1070 composite, (b) CSF/A356 alloy composite, (c) CSF/A336 alloy composite and (d) CSF-CNF/A336 alloy composite.
- Fig. 2-10 Results of X-ray diffraction spectra of CSF/A336 alloy composite.

- Fig. 2-11 Typical transverse microstructure of pitch based and K13D2U pitch CSF used in this study. (a), (b) SEM images of CF, (c), (d) TEM images of CF.
- Fig. 2-12 TEM image and area elemental mapping of CSF/A336 alloy composite.
- Fig. 2-13 TEM images of interface and interfacial reactions between CF and Al of CSF/A336 alloy composite: (b) interface and (c), (d), (e) interfacial reactions.
- Fig. 2-14 Schematic diagram of interface formation with different structure of CF.
- Fig. 3-1 Variation of hardness of Ni-B films after heat treatment at various temperatures.
- Fig. 3-2 Schematic illustration of the new fabrication process without preform manufacturing by low-pressure infiltration method.
- Fig. 3-3 SEM images of (a) as-received CSF, (b) Ni plated CSF (60s), (c) Ni plated CSF (90s), (d) Ni plated CSF (120s), (e) Ni plated CSF (180s) and (f) EDS data of Ni plated CSF (120s).
- Fig. 3-4 SEM images of (a-e) surface view of the Ni plated CSFs, (a'-e') cross section view of the Ni plated CSFs.
- Fig. 3-5 Effect of plating time on volume fraction of Ni/CSF.
- Fig. 3-6 Effect of plating time on the density of CSF.
- Fig. 3-7 Microstructures of composites (0.4 MPa and 0.8 MPa): (a), (d) Ni plated CSF/A1070 composite, (b), (e) Ni plated CSF/A356 alloy composite, and (c), (f) Ni plated CSF/A336 alloy composite.
- Fig. 3-8 Image analysis of composites (0.4 MPa and 0.8 MPa): (a), (d) Ni plated CSF/A1070 composite, (b), (e) Ni plated CSF/A356 alloy composite, and (c), (f) Ni plated CSF/A336 alloy composite.
- Fig. 3-9 SEM images of defects of composites (0.4 MPa and 0.8 MPa): (a), (d) Ni plated CSF/A1070 composite, (b), (e) Ni plated CSF/A356 alloy composite, and (c), (f) Ni plated CSF/A336 alloy composite.
- Fig. 3-10 Element mapping analysis of Ni plated CSF/A1070 composite.
- Fig. 3-11 Results of X-ray diffraction spectra of composites: (a) Ni plated CSF/A1070 composite, (b) Ni plated CSF/A356 alloy composite, and (c) Ni plated CSF/A336 alloy composite.
- Fig. 3-12 Dispersion of CSFs inside the matrix: Ni plated CSF/A1070 composite (0.8 MPa) (a), (b) microstructure of composite, (c) enlargement of microstructure. Ni plated CSF/A336 alloy composite (0.8 MPa) (d), (e) microstructure of composite, (f) enlargement of microstructure.
- Fig. 3-13 Pattern diagram of dispersion behavior of Ni plated CSF inside matrix.
- Fig. 4-1 Shape and dimension of tensile specimens (Unit: mm).
- Fig. 4-2 Schematic diagram of laser flash method.

- Fig. 4-3 Vickers hardness and relative density of CSF/Al matrix composites fabricated with SiO₂ binder preform (0.4MPa): (a) CSF/A1070 composite, (b) CSF/A356 alloy composite, (c) CSF/A336 alloy composite and (d) CSF-CNF/A336 alloy composite.
- Fig. 4-4 Vickers hardness and relative density of Ni plated CSF/Al matrix composites fabricated without preform manufacturing (0.4MPa): (a) Ni plated CSF/A1070 composite, (b) Ni plated CSF/A356 alloy composite and (c) Ni plated CSF/A336 alloy composite.
- Fig. 4-5 Tensile stress–strain curves of Ni plated CSF/Al matrix composites fabricated without preform manufacturing (0.4 MPa): (a) Ni plated CSF/A1070 composite, (b) Ni plated CSF/A356 alloy composite and (c) Ni plated CSF/A336 alloy composite.
- Fig. 4-6 Tensile fracture surfaces and image analysis of Al matrix: (a), (b) A1070, (c), (d) A356 alloy and (e), (f) A336 alloy.
- Fig. 4-7 Tensile fracture surfaces of Ni plated CSF/Al matrix composites fabricated without preform manufacturing (0.4 MPa): (a)-(c) Ni plated CSF/A1070 composite, (d)-(f) Ni plated CSF/A356 alloy composite and (h)-(j) Ni plated CSF/A336 alloy composite.
- Fig. 4-8 Tensile stress–strain curves of CSF/Al matrix composites fabricated without preform manufacturing (0.4 and 0.8 MPa): (a), (b) Ni plated CSF/A1070 composites, (c), (d) Ni plated CSF/A356 alloy composites and (e), (f) Ni plated CSF/A336 alloy composites.
- Fig. 4-9 Tensile fracture surfaces of Ni plated CSF/Al matrix composites (0.4 MPa and 0.8 MPa): (a), (c), (e) 0.4 MPa, and (c), (d), (f) 0.8 MPa.
- Fig. 4-10 Tensile stress–strain curves of CSF/Al matrix composites fabricated under 0.8 MPa without preform manufacturing and with SiO₂ binder: (a), (c) and (e) Ni plated CSF/Al matrix composites fabricated without preform manufacturing and (b), (d) and (f) CSF/Al matrix composites fabricated with SiO₂ binder preform.
- Fig. 4-11 Tensile fracture surfaces of Ni plated CSF/Al matrix composites fabricated without preform manufacturing (0.8 MPa): (a)-(c) Ni plated CSF/A1070 composite, (d)-(f) Ni plated CSF/A356 alloy composite and (h)-(j) Ni plated CSF/A336 alloy composite.
- Fig. 4-12 Tensile fracture surfaces of CSF/Al matrix composites fabricated with SiO₂ binder preform (0.8 MPa): (a)-(c) CSF/A1070 composite, (d)-(f) CSF/A356 alloy composite and (h)-(j) CSF/A336 alloy composite.

Fig. 4-13 Comparison of microstructures and fracture surfaces of CSF/A336 alloy composites: (a) Ni plated CSF/A336 alloy composites without preform manufacturing (0.4 MPa), (b) Ni plated CSF/A336 alloy composites without preform manufacturing (0.8 MPa) and (c) CSF/A336 alloy composites with SiO₂ binder (0.8 MPa).

Fig. 4-14 TC of CSF/Al matrix composites fabricated with SiO₂ binder preform (0.4MPa): (a) CSF/A1070 composite, (b) CSF/A356 alloy composite, (c) CSF/A336 alloy composite and (d) CSF-CNF/A336 alloy composite.

Fig. 4-15 TC of Ni plated CSF/Al matrix composites fabricated without preform manufacturing (0.4MPa and 0.8 MPa): (a) Ni plated CSF/A1070 composite, (b) Ni plated CSF/A356 alloy composite and (c) Ni plated CSF/A336 alloy composite.

List of Tables

- Table 1-1 Series and properties of Wrought Aluminum.
- Table 1-2 Series of Cast Aluminum.
- Table 1-3 Comparison of powder metallurgy, stir casting and squeeze casting.
- Table 1-4 Thermal properties of various materials for the application of composite materials in electronic packaging materials.
- Table 1-5 Thermal properties of different C-based composites.
- Table 1-6 Comparison of polyacrylonitrile (PAN) and pitch-based carbon fibers.
- Table 1-7 Metallic coatings on CFs and their effects.
- Table 1-8 Effects of metallic coatings and coating methods on the strength of CF.
- Table 1-9 Ceramic coatings on carbon fiber and their effects on interfaces in aluminum matrix composites.
- Table 2-1 Chemical composition of A1070 aluminum, A336 alloy and A356 alloy (mass%).
- Table 2-2 Properties of CSF and CNF.
- Table 2-3 Conditions of low-pressure infiltration.
- Table 2-4 EDS point analysis result of IMC of CSF/A336 alloy composite in Fig. 2-7 (b'), white phase.
- Table 3-1 Chemical composition of A1070, A336 alloy and A356 alloy (mass%).
- Table 3-2 Properties of CSF and Al matrix for CF/Al matrix composites.
- Table 3-3 Solutions used for the different stages in the Electroless Ni plating process.
- Table 3-4 Results of Electroless Ni plated CFs with different plating time.
- Table 3-5 Volume fraction of CSFs, Al-Ni compounds and Si phases in Ni plated CSF/Al matrix composites fabricated under 0.4 MPa and 0.8 MPa.
- Table 3-6 EDX analysis of the Al-Ni compound.
- Table 4-1 Comparison of Vickers hardness and relative density of CSF/Al matrix composites fabricated with SiO₂ binder and Electroless Ni plating (0.4MPa).
- Table 4-2 Tensile properties of Al matrix and Ni plated CSF/Al matrix composites fabricated without preform manufacturing (0.4MPa).
- Table 4-3 Tensile properties of CSF/Al matrix composites fabricated without preform manufacturing (0.4 MPa and 0.8 MPa) and with SiO₂ binder preform (0.8MPa).
- Table 4-4 Comparison of TC of CSF/Al matrix composites fabricated with SiO₂ binder (0.4 MPa) and without preform manufacturing (0.4 and 0.8 MPa).

Chapter 1

Background and objectives

1.1	Introduction.....	2
1.2	Development of aluminum and aluminum alloys.....	4
1.2.1	Wrought aluminum alloys	4
1.2.2	Cast aluminum alloys.....	7
1.3	Development of aluminum matrix composites	8
1.3.1	Manufacturing processes of aluminum matrix composites.....	9
1.3.2	Thermal and mechanical properties of aluminum matrix composites	13
1.3.3	Reinforcement	16
1.3.3.1	PAN and Pitch based carbon fibers	16
1.3.3.2	Vapor grown carbon fibers	19
1.3.3.3	Coating of carbon fibers	21
1.4	Theoretical models for predicting properties of CF/Al matrix composites.....	25
1.4.1	Models for predicting strength of composites	25
1.4.2	Models for predicting thermal conductivity of composites	27
1.5	Objective and outline of this thesis	32
	References	35

1.1 Introduction

In recent years, global warming caused by the increase in carbon dioxide emissions has become a serious problem. On the other hand, the improvement of automobile fuel consumption is needed from the viewpoint of resource exhaustion. Therefore, materials with lightweight and excellent properties in the internal combustion engine are urgently needed to reduce carbon dioxide emission and to improve fuel efficiency in automobiles. The single set of material (metal or alloy) has been difficult to fulfill modern industrial requirements, lightweight metal composite materials can combine the advantage of physical and chemical properties of different components that are gaining a lot of attention.

Metal matrix composites (MMCs) consist of a metal or alloy as the matrix and reinforcement which could be a particle, short fiber or continuous fiber. In lightweight MMCs, important metal matrices contain aluminum alloys, magnesium alloys, titanium alloys, copper alloys etc. Aluminum and aluminum alloys are one of the most promising lightweight metals that offer low density, high thermal conductivity (TC), high specific strength and stiffness, excellent machinability and superior cast ability. Therefore, aluminum and its alloys are the most major matrix material for manufacturing composites. However, compared to other functional and structural metals, aluminum and its alloys have a relatively not so high strength and TC which limited their applications.

Concerning weight reduction of moving parts of the internal combustion engine, aluminum with low density is a good alternative material. However, the internal combustion engine related parts, such as pistons and cylinder block required to meet the high strength and TC, low coefficient of thermal expansion (CTE) and well wear resistance, etc. Heat sink applies for the high heat generation components, required high TC, low CTE, and a certain strength. The single aluminum metal cannot satisfy the requirements. Aluminum matrix composites (AMCs) have attracted the interests of researchers and design experts due to their promising superior properties which could further improve the properties and extend application areas of aluminum and aluminum alloys. AMCs refer to a kind of material containing aluminum matrix and reinforcement,

which combine the physical characteristics of aluminum (high specific strength, high TC, and ductility) and reinforcement (high strength, high modulus, and high TC), leading to greater strength and TC capabilities. Carbon materials such as carbon fiber (CF) in chopped and vapor grown carbon fiber (VGCF, CNF) have been considered as effective reinforcements for AMCs due to their high specific strength and specific modulus, lightweight, low CTE as well as high thermal and electrical conductivities which have attracted attentions and widely used in electrical and engineering applications. Therefore, CF reinforced aluminum and aluminum alloys composites with high thermal conductive and strength have the most potential to be utilized as functional and structural materials in the future.

1.2 Development of aluminum and aluminum alloys

Aluminum and aluminum alloys are the most extensively used materials as functional and structural materials, which have the potential for application in power electronics, aviation, aerospace, automobile, naval and weapons fields due to the low density, excellent thermal and electric conductivity, high specific strength, superior machinability, and good corrosion resistance [1, 2].

The typical alloying elements are silicon (Si), copper (Cu), magnesium (Mg), manganese (Mn), and zinc (Zn). In view of the composition and process characteristics, aluminum alloys can be divided into wrought aluminum alloys and cast aluminum alloys. Both of which are further divided into heat-treatable and non-heat-treatable categories. About 85% of aluminum products are made from wrought aluminum alloys. Cast aluminum alloys are used to fabricate cost-effective products due to the low melting point.

1.2.1 Wrought aluminum alloys

Wrought aluminum is obtained after the metal is subject to a mechanical working process containing extrusion, rolling and forging. Wrought aluminum can be identified with a four-digit number, where the first digit is the indicator of alloying elements, second is a dash, and then a letter for identifying the type of heat treatment and the number 1 to 4 represents the specific temperature. The letters which identifying the kinds of heat treatment contain T, H and O. T meaning a heat-treatable alloy, H meaning a non-heat-treatable alloy with the final properties acquired by mechanical working processes, and O meaning not heat treated or annealed metal. In general, the alloying elements of wrought aluminum alloys is 1%- 2% (in some case it can be as high as 6%-8%). Figure. 1-1 (a) shows the classification of wrought aluminum alloys, which can be divided into heat treatable and non-heat treatable aluminum alloys in accordance with whether the alloy can be a response to precipitation hardening. Table 1-1 shows the series and properties of wrought aluminum alloys. Wrought aluminum alloys contain elements such as Cu-Mg (2xxx series), Mg-Si (6xxx series) and Zn-Mg (7xxx series) belong to heat treatable alloys, the elements can go into solution to an

appreciable degree and provide the opportunity for appreciable precipitation hardening by various heat treatment processes^[3, 4], as a result, that the strength can be enhanced, therefore, the 2xxx, 6xxx and 7xxx series are the higher-strength wrought aluminum alloys.

Pure aluminum (1xxx series) and alloys contain principally elements such as Mn (3xxx series), Si (4xxx series) and Mg (5xxx series) belong to non-heat treatable alloys which must be strengthened primarily by strain hardening. Because the pure aluminum has no appreciable amounts of other elements that can provide solution strengthening or precipitation hardening. And elements such as Mg, Si and Mn provide a good response to precipitation hardening. Thus, for pure aluminum and the 3xxx, 4xxx and 5xxx alloys, rolling, drawing and stretching are the main means of strengthening methods. Especially, 1070 pure aluminum has relatively low strength, even when strain hardened, however, it has extremely high ductility and formability and so may be readily worked or formed. The 1070 aluminum also has exceptionally high thermal and electrical conductivity, and resistance to all types of corrosive environments and may be readily joined by a number of commercial processes.

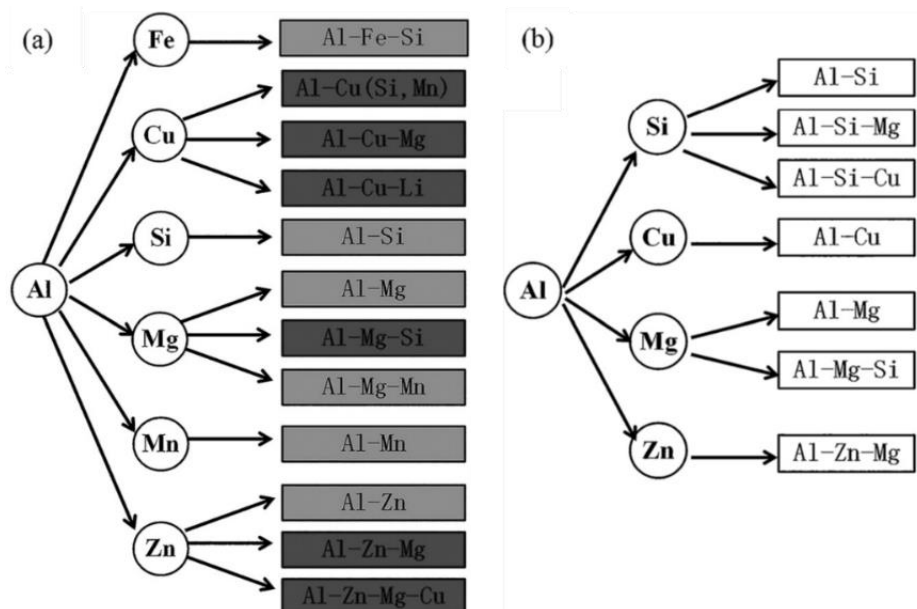


Fig. 1-1 Classification of wrought aluminum alloys and cast aluminum alloys ^[5]:

(a) wrought aluminum alloys. (b) cast aluminum alloys. Heat treatable aluminum alloys are in black and non-heat treatable aluminum alloys are in gray.

Table 1-1 Series and properties of Wrought Aluminum [5].

Series	Types	Elements	Performance
1xxx	non-heat treatable	Pure Al ($\geq 99.00\%$)	Low strength, good corrosion resistance and conductivity, easy processing
2xxx	heat treatable	Al-Cu/Al-Cu-Mg	Hard-aluminum alloy. High strength, good heat resistance, poor corrosion resistance
3xxx	non-heat treatable	Al-Mn	Antirust aluminum alloy. Low strength, cold-working-hardening, good plasticity
4xxx	non-heat treatable	Al-Si	High silicon, low melting point, good weldability, good heat and wear resistance
5xxx	non-heat treatable	Al-Mg	High magnesium, good corrosion resistance and weldability
6xxx	heat treatable	Al-Mg-Si	Medium strength, good formability, weldability and machinability
7xxx	heat treatable	Al-Zn-Mg	Very high strength, cannot be welded, poor corrosion resistance

1.2.2 Cast aluminum alloys

Cast aluminum alloys are the most attractive of all common alloys and have the highest cast ability. Cast aluminum alloys depend on the same alloy systems with wrought aluminum alloys, are also classified into non-heat-treatable and heat-treatable types. Cast aluminum alloys can be identified with a four-digit number, where the first digit indicates the alloy group according to the major alloying element. Figure. 1-1 (b) shows the classification of cast aluminum alloys, cast alloys can be mainly divided into the Al-Si system, Al-Cu system, Al-Mg system and Al-Zn system. The most widely used cast aluminum alloys system is the Al-Si system, the sufficient amounts of eutectic forming elements (usually Si) fulfill adequate fluidity to feed the shrinkage during casting. The second and third two digits indicate the purity of alloys or identify alloys. In designations of 1xx.x series, the second and third two digits indicate minimum aluminum content (99.0% or greater). In designations of 2xx.x to 8xx.x series, the second and third two digits have no numerical significance but only identify the various alloys in the group. The last digit indicates the product form: casting (designated by “0”) or ingot (“1” denotes standard ingot or “2” denotes the ingot limited to those cases where a narrower composition range of one or more of the elements). Table 1-2 shows the series, types and elements of cast aluminum alloys. It is noted that the 1xx.x and 5xx.x series belong to non-heat treatable alloys, the others belong to heat treatable alloys exception for 6xx.x and 9xx.x series. Despite 3xx.x and 4xx.x series are identified as heat treatable alloys, the separate solution heat treatment is seldom conducted on these alloys in the die-casting industry. Al-Si-Cu/Mg cast alloys (3xx.x series) are the most attractive cast alloys with the advantages of high strength, low ductility, good wear resistance, good fluidity and excellent machinability can be applied in the application of automotive used to fabricate car wheels, internal combustion engine related parts such as pistons, cylinder blocks and head, and so on.

Table 1-2 Series of Cast Aluminum [6].

Series	Types	Elements
1xx.x	non-heat treatable	Unalloyed compositions
2xx.x	heat treatable	Cu (4% - 5%)
3xx.x	heat treatable	Si (5% - 17%) plus Cu and/or Mg
4xx.x	heat treatable	Si (5% - 12%)
5xx.x	non-heat treatable	Mg (4% - 10%)
6xx.x	-	Currently unused
7xx.x	heat treatable	Zn (6.2% - 7.5%)
8xx.x	heat treatable	Tin
9xx.x	-	Currently unused

1.3 Development of aluminum matrix composites

AMCs material systems offer superior properties combination of aluminum matrix and reinforcements, in such a manner that today no existing monolithic material can competitive. AMCs are intended to substitute the existing monolithic materials including aluminum alloys, magnesium alloys, and polymer-based composites in several applications. Rapid growth and development of AMCs are concerned in recent years that AMCs are expected as the material of choice in a broad range of functional and structural applications. Various properties can be tailored to composites by varying the types of constituents and their volume fraction. For high temperature applications, the incorporation of high thermal property reinforcements into aluminum composite can fulfill high heat transfer requirements. The formation of a composite is an effective means of strengthening aluminum alloys for high performance materials. Defined by the type and shape of reinforcements, AMCs can be generally divided into several classes: particle-reinforced AMCs, continuous fiber-reinforced AMCs, whisker-or short fiber-reinforced AMCs, and hybrid AMCs. AMCs utilization provides significant benefits including performance benefits, economic benefits, and environmental benefits.

AMCs can be tailored to be light-weight and with various properties that offer more possibilities in applications of the automotive industry including piston (ring groove and crown), cylinder (block and liner), connecting rod, push rod, drive shaft, and retainer rings of high-speed motors.

1.3.1 Manufacturing processes of aluminum matrix composites

The main challenge of processing of composites is to achieve a good combination of reinforcement and matrix (a homogeneously and defect-free microstructure). A variety of manufacturing processes for AMCs had been developed to obtain high performance composites. The main fabrication processes at the industrial scale can be classified into two groups: the solid-state process and liquid-state process.

Main solid-state processes contain powder metallurgy (PM), diffusion bonding, hot extrusion and rolling as well as physical vapor deposition. PM is the most representative process of the solid-state processes. The PM process is usually introduced to blending the aluminum powder with particles, short fiber/ whisker and flakes, and then the mixture is sintered at a certain temperature under a certain pressure in vacuum or the other atmosphere. Fig. 1-2 shows the schematic illustration of the powder metallurgy process. The PM process is suitable for a high melting point alloys matrix which is difficult to use for the liquid-state process [7]. The AMCs fabricated by the PM process can be achieved high density due to high pressurization, and the reinforcements can be uniformly dispersed in the matrix by the blending process before sintering. Therefore, PM is a versatile technique to produce AMCs. A variety of aluminum matrix composites have been fabricated through powder metallurgy such as SiC/Cu–Al [8], CF/Al [9], VGCF/Al [10], Hybrid VGCF-CNT/Al [11], However, the raw materials of PM process cost higher than bulk material, the size of product that can be manufactured is generally limited and is not practicable for complex shape fabrication [12].

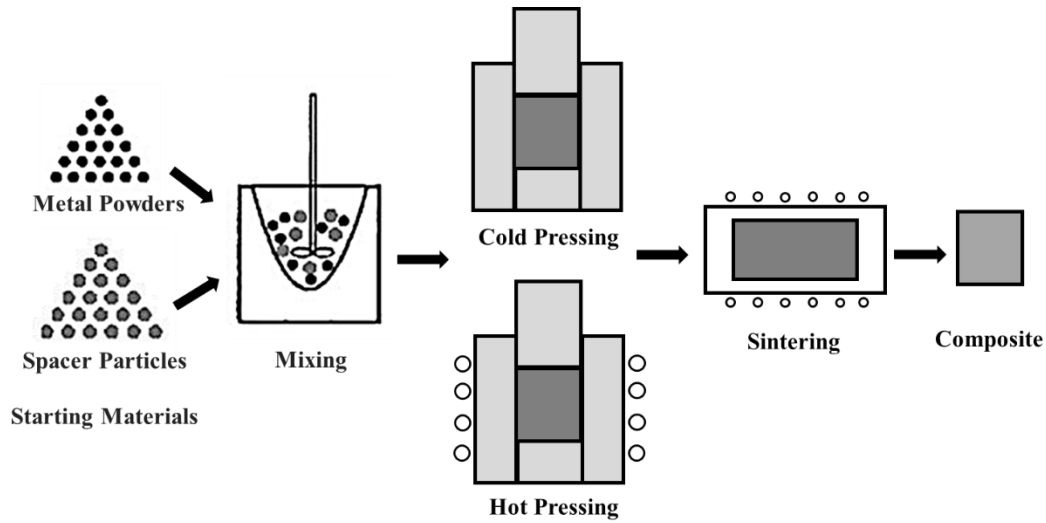


Fig. 1-2 Schematic illustration of the powder metallurgy process (PM process) [13].

The liquid-state processes are further classified into liquid-metal-mixing processes and liquid-metal-infiltration processes. As a representative of the liquid-metal-mixing process, stir casting is an economical process for the fabrication of aluminum matrix composites. The stir casting process involves the incorporation of reinforcements such as particles or short fibers into the liquid aluminum matrix through a stirring process and allowing the mixture to solidify. Stir casting process has been extensively used to incorporate ceramic, metal oxide particles, graphene, and carbon fibers to aluminum matrices, such as SiC/Al [14, 15], nano-Al₂O₃ particles/Al 6061 [16], Graphene/Al 7050 [17], and CF/Al-3Mg alloy [18]. Stir casting technique also has been adopted for wide applications such as automotive and other industrial fields due to the advantages of simplicity, flexibility, and applicability to large amounts of production. However, the disadvantages of stir casting such as high casting equipment cost, the agglomerated reinforcement in the matrix caused low ductility of product limits its widespread commercial use.

Liquid-metal-infiltration contains a pressure-assisted infiltration process and a pressureless infiltration process. Squeeze casting is recognized as a typical high pressure-assisted casting method through injecting or infiltrating liquid molten aluminum as the matrix into the interstices of the porous preforms of continuous fiber/short fiber or whisker or particle as reinforcements to produce AMCs [19, 20]. AMCs

with reinforcement volume fraction ranging from 10 to 70% can be produced using a squeeze casting technique. In the squeeze casting process, the concept was to take advantage of the excellent properties of reinforcements in a product that was essentially formed to net shape by the casting process.

In order to retain the integrity and shape of the preform, it is often necessary to use silica or alumina based mixtures as binder. The bad wettability between the matrices and reinforcements made it hard to fabricate composites without pressure. The squeeze casting enables liquid aluminum to overcome the strong flow resistance and pressure drop during casting to achieve fast fabrication and high density of AMCs by using high pressures. However, the excessively high pressure at the liquid inlet side can cause local preform compaction and damage which would reduce the mechanical properties of composites [21]. The cost of squeeze casting is very high due to the requirements for high capacity equipment and tools. Consequently, it is hard to fabricate complex shapes and large size products by high pressure infiltration process. The schematic illustration of the stir casting process and squeeze casting process is shown in Fig. 1-3.

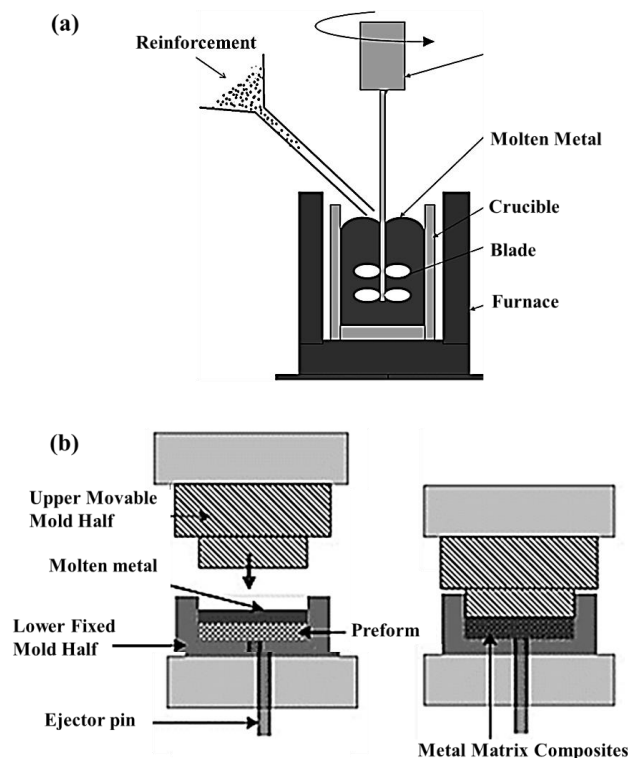


Fig. 1-3 Schematic illustration of (a) Stir casting process [22] and (b) Squeeze casting process [23].

The pressureless infiltration process is a spontaneous infiltration process that can be achieved to fabricate the AMCs with high volume fractions of reinforcement. This process involved that an Al or Al alloy ingot is placed on the preform (such as continuous fiber/short fiber or whisker preform) in a graphite mold, the entirety is heated in a furnace with nitrogen atmosphere until the Al melts and finally molten Al is infiltrated into preform under less than 1MPa infiltration pressure. Meanwhile, a good wettability between molten Al and the reinforcement is essential to LPI process. When it comes to the fabrication of CF/Al composites, metallic or ceramic coating should be conducted to CF for improving the wettability between molten Al and CF in order to obtain a compact composite structure. Plenty of AMCs were fabricated by LPI process such as Al₂O₃-SiC/Al [24], SiC/A356 alloy [25], Hybrid CF-Al₂O₃ fibers/Al [26], CF/Al [27]. The advantages of low-pressure infiltration process (LPI process) involve simple equipment which decreases the cost of fabrication, flexible reinforcement content for specific applications and can be able to fabricate net-shape composites.

The main fabrication methods of AMCs composites described above are well established and a comparative evaluation of these traditional processes techniques is summarized in Table 1-3 [28].

Table 1-3 Comparison of powder metallurgy, stir casting and squeeze casting [28].

Method	Working range	Metal yield	Volume fraction	Damage to reinforcement	Fabrication cost
Powder metallurgy	Wide range, restricted size	High	-	Fracture	Expensive
Stir casting	Wide range of shape, larger size (up to 500 kg)	Very high, >90%	~30 vol%	No damage	Least expensive
Squeeze casting (LPI process)	Limited by preform shape (up to 20 cm height)	Low	~45 vol%	Moderately damage	Moderately expensive

1.3.2 Thermal and mechanical properties of aluminum matrix composites

Many efforts have been made to overcome the challenge of thermal management in high heat generation components such as semiconductors and the challenge of high mechanical performance requirements such as internal combustion engine related parts (piston or cylinder). In order to maintain the temperature ranges of semiconductors or other heat generation parts, the heat sink materials attaching directly to them are required light weight as well as high TC. MMCs are considered as the promising heat sink materials due to their high TC and good cost performance. Table 1-4 shows the properties of the candidate materials for the fabrication of MMCs. Carbon based materials such as diamond, CF, CNT and VGCF show excellent TCs with extremely low CTEs and densities than other reinforcements. Al shows the relatively low density, high TC and cost are considered as a candidate matrix for fabrication composites. Table 1-5 presents the results of TC and CTE for the different carbon-based composites. Based on the thermal properties presented in Table 1-5, hybrid graphite flakes/CF or hybrid graphite flakes/SiC reinforced Al-Si matrix composites show a remarkably high TC than the other composites, but the 88% reinforcement causes a problem of machining and lower mechanical property. In the case of the diamond-based composite, it shows a high value of TC ($350 \text{ W} \cdot \text{m}^{-1} \cdot \text{K}^{-1}$) and reasonably low CTE ($11 \times 10^{-6} \text{ K}^{-1}$) which seems to be the suitable choice as heatsink material. However, the “high cost of diamond” as raw material and “impossibility of machining” for post-processing makes this composite unsuitable for mass commercialization. The thermal properties of composites based on carbon fibers (55%) show respectable values of TC and the lowest CTE which could well match the requirement of heatsink material. The continuous fibers reinforced Al composites show a highly isotropic of TC which demands a high-volume fraction of reinforcement lead to a high cost of raw materials. In contrast, the tailorable thermal or physical property could be obtained for discontinuously fibers reinforced Al composites, the adequate composition ratio between the reinforcement and matrix is required to accomplish the high TC, CTE matching and light weight.

Table 1-4 Thermal properties of various materials for the application of composite materials in electronic packaging materials.

Material	Density (M·gm ⁻³)	CTE (×10 ⁻⁶ K ⁻¹)	TC (W·m ⁻¹ ·K ⁻¹)	Reference
<i>Reinforcement</i>				
Diamond	3.5	2.3	1300-1800	[29]
Silicon carbide (SiC)	3.1-3.21	2.8-5.0	80-490	[29, 30]
Aluminum oxide (Al ₂ O ₃)	3.9	6.7	20	[30, 31]
Aluminum nitride (AlN)	3.26-3.3	3.3-4.5	125-250	[29, 23]
Carbon fiber (CF)	2.21	-1.2	800	Mitsubishi
Carbon nano tube (CNT)	2	-1	6600	[29]
Vapor grown CF (VGCF)	1.8-2	-1	1950	[29]
<i>Matrix</i>				
Aluminum	2.7	22.3-23	230-237	[30, 31]
Copper	8.9	16.5-17	398-400	[29, 30]
Gold	19.3	14	316	[32]
Silver	10.5	19	431	[32]

Table 1-5 Thermal properties of different C-based composites [33].

Reinforcement	Volume Fraction (vol.%)	Matrix	Infiltration pressure (MPa)	TC (W·m ⁻¹ ·K ⁻¹)	CTE (10 ⁻⁶ K ⁻¹)
90% Graphite flakes + 10% CF	88	Al-12Si	1.5	367	24
60% Graphite flakes + 40% SiC	88	Al-12Si	1.5	368	11
Diamond	61	Al-12Si	4	350	11
Graphite particles	67	Al-12Si	4	118	11
CF	55	Al-12Si	4	131	2.8
Graphite foam	60	Al-12Si	4	330	10

As a lightest metal structural material, AMCs exhibit many advantages over monolithic Al or Al alloys, such as high specific strength, superior creep and wear resistances. The desired mechanical properties can be achieved by a judicious selection of the type and size of the reinforcement. Discontinuous reinforcements such as particles, short fibers, or whiskers, have been used to produce AMCs aiming to improve mechanical properties for wide applications. Li et al. [34] researched the mechanical behavior of n-TiB₂ particles reinforced Al 5083 composites which were fabricated via cryomilling and spark plasma sintering (SPS) and concluded that the compressive strength of the composite is 20% higher than Al 5083 matrix. Zhang et al. [35] fabricated Al-based hybrid composites reinforced with SiC whiskers and SiC nanoparticles by squeeze casting and revealed that the addition of SiC whiskers and SiC nanoparticles into 2024 Al alloy increases its elastic modulus and strength.

Among the various reinforcements, fibers are the important class which effects on the directional strength and stability of the composites. Fibers can transfer the strength to the matrix constituent influencing and enhancing properties of composites as desired. Carbon short fibers possess high strength and elastic modulus which could offer more options for high strength materials applications. Naji et al. [36] investigated the role of aspect ratio of carbon fiber on fracture toughness of aluminum matrix composite and concluded that the fracture toughness of composites depends on both fiber volume fraction and aspect ratio, fracture toughness increases with increasing carbon fiber volume fraction and its aspect ratio. Han et al. [37] analyzed the wear properties of the CNF/A7xxx composites fabricated by the liquid process. They revealed that the wear loss of the composites showed a steadily decreasing trend with a weight fraction of CNF in the composites. Concluded that the composite exhibits significant increases in modulus and ultimate tensile strength, but the elongation to failure of the composite is considerably reduced.

Therefore, anisotropic carbonaceous material especially CF reinforced Al matrix composites combine the properties of CF and Al which could achieve lightweight, high TC and mechanical performance that provided credible pathways to improved affordability and processability and represented an area of opportunity for commercial applications.

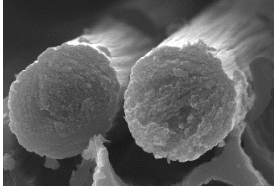
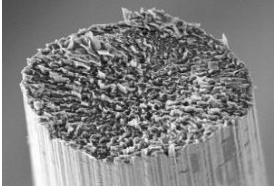
1.3.3 Reinforcement

Today, lightweight, high strength and elastic modulus, high electrical and thermal conductivities CFs are used mainly as a base material for advanced composites. Therefore, CF reinforced Al matrix composites have become a dominant material in the aerospace, automotive and sporting goods industries adopted in the field of material design more frequently. Usually, CFs are divided into organic substance based CFs and vapor grown carbon fibers (VGCFs/CNFs).

1.3.3.1 PAN and Pitch based carbon fibers

Carbon fibers are produced through the conversion of several fiber precursors such as polyacrylonitrile (PAN) fibers, pitch-based CFs made from coal tar and petroleum products (isotropic and mesophase types). PAN-based CFs are considered as the preferred raw material for obtaining CF, as it allows a better homogeneity of its final properties. Pitch-based CFs are needed to be processed through complicated processing. Table 1-6 shows the comparison of PAN and pitch-based CFs. PAN-based CFs have a very small crystal size, having flexibility, high tensile strength and good electrical conductivity [38]. Pitch-based CFs possess a large crystal size, having higher modulus/stiffness than PAN-based CFs and excellent thermal and electrical conductivities. In recent years, carbon fiber has developed rapidly with the advancement of the preparation method. High performance CFs with an elastic modulus of 200 GPa and strength of 2 to 6 GPa are obtained from PAN and mesophase pitch precursors. More notable is that high TC and elastic modulus mesophase pitch-based CFs are attracting public attention as reinforcement of composites for high temperature services such as in space and aircraft applications.

Table 1-6 Comparison of polyacrylonitrile (PAN) and pitch-based carbon fibers [38].

Property	PAN-based fiber	Pitch-based fiber
Morphology		
Density(g/cm ³)	1.73-1.93	2.10-2.20
Axial Thermal conductivity (W·m ⁻¹ K ⁻¹)	14-100	320-800
Radial Thermal conductivity (W·m ⁻¹ K ⁻¹)	0.5-10	0.5-10

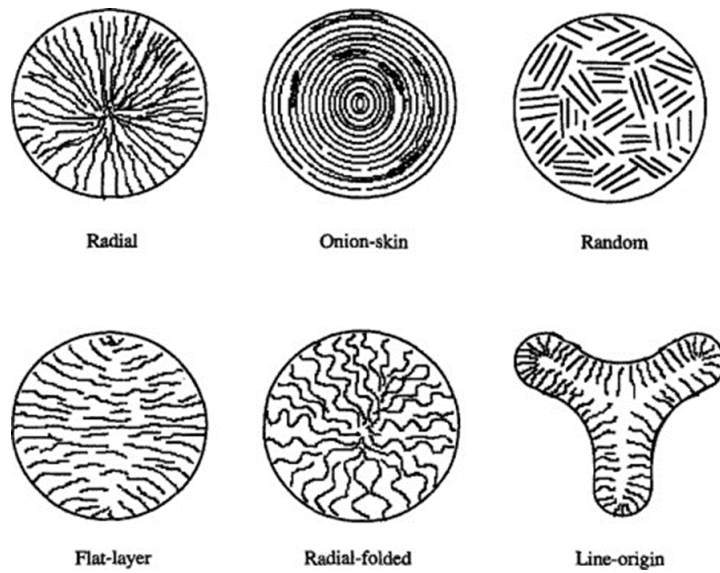


Fig. 1-4 The textures of mesophase pitch-based CFs [39].

The structure of a CF is similar to that of graphite, consisting of carbon atom layers (graphene sheets) arranged in a regular hexagonal pattern. Fig. 1-4 shows the textures of mesophase pitch-based CFs. The transverse texture of most commercial pitch CFs is either random, onion skin, flat layer, radial, or radial folded. Different textures can be obtained either by disrupting the flow during extrusion, varying extruder geometry, or through variation of temperature and flow during spinning.

As shown in Fig. 1-5, there is a distinction between graphitizable and non-graphitizable carbons. Graphitizable carbons show good planar alignment and stacking of graphene layers, on the other hand, non-graphitizable carbons do not have long-range parallel order of graphene layers. Fig. 1-6 shows the SEM and TEM images of pitch CFs heat treated at different temperatures. It can be found that the structure of CF changes from disordered (1200°C) to planar alignment (2600°C) which proves that the CF transforms from non-graphitizable to graphitizable. CF with different structure embodies different properties such as graphitic structure give pitch-based CFs higher elastic modulus and higher thermal and electrical conductivity along the fiber direction, and non-graphitic structure gives pitch-based CFs higher tensile strength. Nowadays, CFs as reinforcements of metal or polymer matrix composites have been attracted extensive research and the CFs reinforced composites have played an important role in a variety of applications.

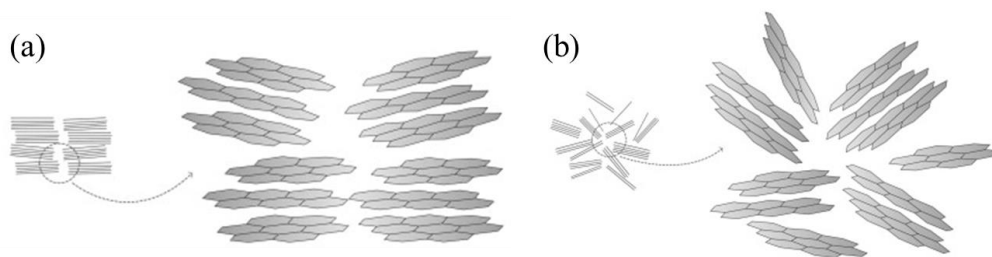


Fig. 1-5 Illustration of differences between (a) graphitizable CF and (b) non-graphitizable CF structures ^[40].

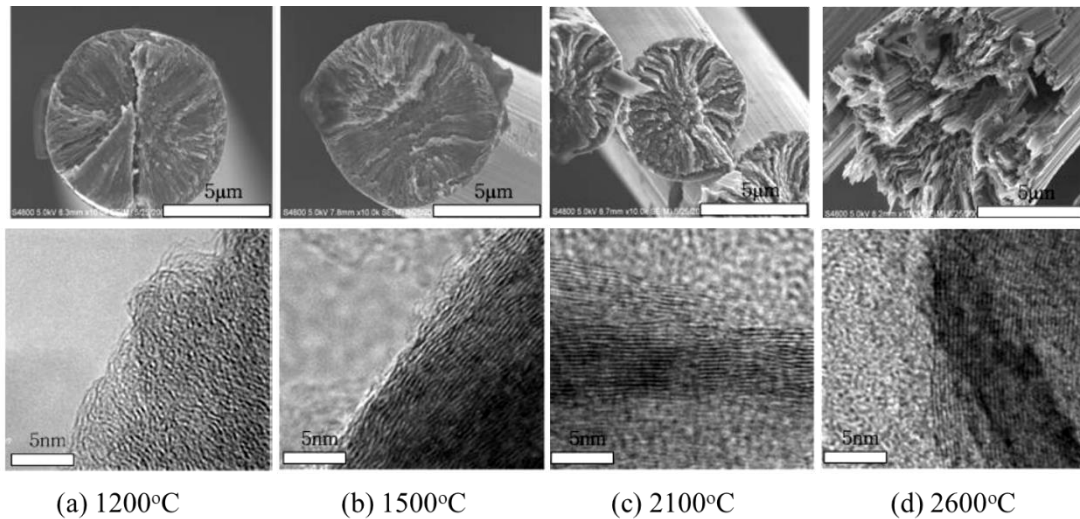


Fig. 1-6 SEM and TEM images of pitch CFs heat treated at (a) 1200 °C, (b) 1500 °C, (c) 2100 °C, and (d) 2600°C [41].

1.3.3.2 Vapor grown carbon fibers

Vapor grown carbon fibers (VGCFs or CNFs) are a new class of CF that have a highly preferred orientation parallel to the fiber axis and an annular ring texture in the cross section. The structure gives rise to the outstanding properties such as high mechanical strength of 3.5 GPa, the high elastic modulus of 760 GPa and high electrical conductivity of $1200 \text{ W} \cdot \text{m}^{-1} \text{K}^{-1}$. SEM images of as received CNF are shown in Fig. 1-7 [42]. It is seen that the CNFs have random orientations and some CNFs are aggregated together in Fig. 1-7 (a). CFibers have a morphology of semispherical tip and uniformly diameter (Fig. 1-7 b), this structure is favorable for improving electrical and thermal conductivities of composites when CNFs are applied as filler.

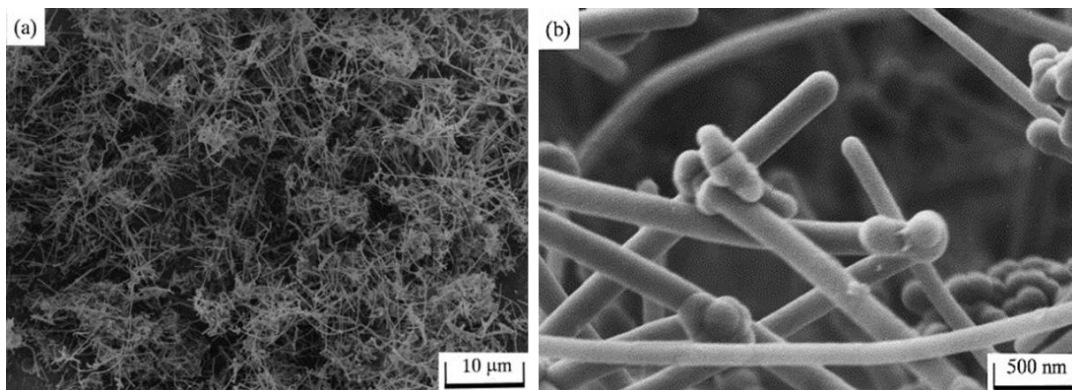


Fig. 1-7 SEM images of CNFs: (a) low, (b) high in magnification [42].

In the early 1970s, it was proved that the relatively expensive conventional PAN and pitch CFs could be incorporated in composites to yield excellent properties. After that, efforts were underway in many countries to efficiently produce “vapor-grown” carbon fibers from hydrocarbons with an equivalent performance at a more affordable price [43-46]. In the 1970s and 1980s, M. Endo, et al. had made great efforts to analyze the vapor grown methods of CNFs and make a helpful review on CNFs which greatly promoted the development of CNFs [47-51].

CNFs have been grown by the decomposition of hydrocarbons, for example, methane and benzene, with a catalyst (transition metal particles) at the temperature of 1273 K to 1573 K. The main commercial process for the fabrication of CNFs is chemical vapor deposition (CVD) process which divided into two categories: 1) bath process and 2) floating-catalyst process. Tibbetts [52] concluded a bath process by using stainless steel tubes for growing the fibers. He also investigated a bath process contained two disjoint steps for fibers lengthening and thickening in ceramic tubes at 1273 K, the catalyst was a fine iron particle, the atmosphere was methane in the concentration of 15 vol.% [53].

Koyama and Endo had patented the floating-catalyst process in 1982 by utilizing organometallic compounds dissolved in hydrocarbon gas at the temperature of 1373 K to form ultrafine metal particles as a catalyst. In the furnace, the fibers growth initiated on the surface of the catalyst particles and grew up until the catalyst deactivation caused by the impurities of the system [54].

The start of nanotechnology is thought to have begun with the discovery of single-walled carbon nanotube (SWCNT) and multi-walled carbon nanotube (MWCNT) by S. Iijima at 1991 [55]. SWNTs are formed of a single rolled up hexagonal graphene plane, their tightly bonded structure is thought to be advantageous for many mechanical and electrical applications. However, these SWNTs have been available only in gram quantities, and their high cost and poor availability have hampered efforts to exploit the anticipated composite properties. MWCNTs consist of multiple nanotubes nested within one another. The diameter of both the internal nanotube and the external nanotube change from 2nm to over 50nm for the innermost tube to the outer wall. MWCNTs exhibit outstanding thermal, electrical, and mechanical properties. However,

a large number of walls may lead to a higher possibility of defects which results in reduced performances. Although the CNTs possess excellent mechanical and electrical-thermal properties, they have still not been largely used in commercial applications because of the high preparation cost and difficulty of dispersion.

CNFs have a small diameter and existing at the nanometer scale of 100~150 nm which are considered as nanosize materials belonging in the same nanosize family of materials as CNT's. In addition, compare to CNT, CNFs have larger diameters of 100 to 150nm than MWCNTs and can thus be relatively easily dispersed in aluminum matrices. CNFs also have a lower preparation cost. In recent years, numbers of CNFs reinforced epoxy, polymer or metal matrix composites have been widely developed which possess notable mechanical and electrical properties. Consequently, CNFs are considered as promising reinforcement to provide solutions to many vexing problems in composite applications.

1.3.3.3 Coating of carbon fibers

Carbon is one of the most important reinforcements used in the fabrication of Al matrix composites. The carbon reinforced Al composites find extensive applications in the aerospace, automobile, and electrical application. Carbon short fibers (CSFs) with length less than 3 mm offered the composite a better isotropic property since they were able to keep uniform distribution in all directions ^[56]. However, associating with the processing of CFs reinforced Al matrix composites, the CFs have a large contact angle (140°) with the liquid Al at lower processing temperature (950 to 1050 K) which exhibits a non-wettable system. And chemical reactions between carbon and Al matrix at high temperatures always obstruct the improvement of mechanical and thermal properties of composites ^[57-60]. Carbon becomes wetted with Al at 1273 K, but the Al₄C₃ are prone to generate at the surface with increasing processing temperature which, in turn, reduces the strength of composites. In addition to optimizing the manufacture process aforementioned, coating the carbon materials is the more effective way to solve these problems.

The widely used coating materials contain metallic coating and ceramic coating. The

main metallic coatings of fibers are copper (Cu) and nickel (Ni). Other seldom used metallic coatings include titanium (Ti) and silver (Ag) and so on. The kinds of coating metal also play a crucial role in the properties of composites. Table 1-7 summarizes the metallic coatings on CFs and their effects on composites [61-65]. The surface of the fiber is Ni and Cu coated to reduce the contact angle between CFs and liquid Al. The Al matrix is in direct contact with the coating layer rather than CFs, as a consequence, the application of Ni and Cu coatings can promote the wettability with the Al matrix effectively and improve the interface bonding between CFs and matrix. Meanwhile, the existence of Ni and Cu coated layers could change the matrix composition by dissolving into the Al matrix to form a solid solution such as Al_3Ni and Al_2Cu which increases the strength of composites. The deposition of metals on CFs is usually conducted by cementation, electrolytic and electroless processes. Table 1-8 introduces the effects of Ni and Cu coatings and coating methods on the strength of CFs [66]. It can be concluded that the CFs coated by electroless process presented the best ultimate tensile properties to that of uncoated fibers, however, the coated CFs by electrolytic and cementation processes exhibit lower ultimate tensile properties compared to uncoated fibers. Meanwhile, the electroless process is much simpler to operate because it does not require electricity and the deposition layer on the surface of fibers is more uniformly than other processes. Consequently, the electroless process is considered as a good choice for fibers coating.

The main ceramic coatings utilized in the fibers include SiC, Al_2O_3 and SiO_2 , etc. Ceramic coatings on carbon fiber and their effects on interfaces in Al matrix composites are given in Table 1-9 [67-70]. SiC coating has been concerned as a useful coating process for preventing carbons react with oxygen and has been proved its effectiveness in oxidation protection of carbon materials [71]. Wang et al. [72] had analyzed the effects of coating on interface bonding of CF reinforced Al-10Si alloy composites by coating SiC on CFs. It has been observed that the wettability of CFs with molten Al and oxidation resistance of CFs can be both improved significantly by the SiC coating, the interfacial reaction was prevented by the SiC coating which increased the strength of the composite.

Al_2O_3 and SiO_2 coating are also used for fibers coating. It is demonstrated that the

Al₂O₃ and SiO₂ coating are both effective diffusion barriers in the protection of fibers and the SiO₂ coating shows a decrease in contact angle from 165° to 50° at temperatures of 973 K [69]. However, the Al₂O₃ coating showing an unsatisfactory enhancement to wettability. In summary, both carbide coatings and oxide coatings can act as diffusional barriers to reduce interfacial reactions. Oxide coatings are more stable and easily synthesized compared to carbon coatings. The application of coatings to the CF during fabrication of Al matrix composites is an important step, which has promising effects on the interfacial, mechanical, electrical and thermal properties of the composites.

Table 1-7 Metallic coatings on CFs and their effects [61-65].

Coating material	Coating method	Matrix	Fabrication technique	Effect
Copper [61]	Electroless	Al	Liquid metal infiltration	1. Improved wetting 2. Uniform distribution of fibers 3. Al ₂ Cu formation
Nickel [62]	Electroless	Al	Centrifugal pressure infiltration	1. Improved the throwing power of precipitant into the multifilament 2. Al ₃ Ni formation
Nickel [63]	Electroless	Al	Stir casting	1. Good wetting 2. Al ₃ Ni around fibers
Titanium [64]	CVD	Al	Liquid metal infiltration	1. Difficult to coat due to the reaction 2. Rutile and anatase are formed
Silver [65]	Electroless	Al-6063	Liquid metal infiltration	1. Promoted wetting 2. The interfacial reaction between Al and CF

Table 1-8 Effects of metallic coatings and coating methods on the strength of CF [66].

Coating material	Coating method	UTS (GPa)	Elongation (%)
Unplated		2.6-3.2	-
	Cementation	1.5-1.81	0.8
Ni	Electroless	2.4-2.81	1.23
	Electrolytic	1.5-2.25	1.35
Cu	Cementation	1.32-2.53	1.1
	Electroless	1.79-3.66	1.8

Table 1-9 Ceramic coatings on carbon fiber and their effects on interfaces in aluminum matrix composites

Coating material	Coating method	Matrix	Fabrication technique	Effect
SiC [67]	CVD	Al	Squeeze casting	1. Effective protection of fibers during processing 2. Improved mechanical properties
Al ₂ O ₃ [68]	Ion-plating	Al	-	1. Good reaction barrier 2. Poor wettability
SiO ₂ [69]	Dry mixing	Al	Gravity infiltration	1. Improve wettability by the reaction of Al and SiO ₂ 2. Higher modulus of elasticity
TiO ₂ [70]	Solgel	Al	Liquid infiltration	1. No reaction at TiO ₂ /C interface 2. Improved wetting with the formation of (Al, Ti)O ₂ mixed oxide

1.4 Theoretical models for predicting properties of CF/Al matrix composites

Discontinuous CF reinforced Al composite forms an important category of materials used in electronic devices and engineering applications. The discontinuous CFs grant the composites anisotropy properties and the performance of the composite is controlled by factors like the aspect ratio of CF, the orientation of CFs and fiber-matrix adhesion. It is important to provide reliable data for comparison with the experimental data in developing short-fiber composites. Many researchers have studied a variety of methods to predict the thermal and mechanical properties of fibers reinforced metal matrix composites which provide support for better study of factors affecting performance.

1.4.1 Models for predicting strength of composites

For MMCs, the matrix is usually metal alloy-based material and there are also an increasing number of available reinforcements, composite can be fabricated by choosing different combinations of matrix alloy and reinforcements. Regarding the prediction of properties of MMCs from the properties of the individual components, numerous models have been formulated for predicting the mechanical properties of short-fiber composites.

1) Rule-Of-Mixtures (ROM) Model ^[73]

The usual simplest theoretical UTS model concerned with the evaluation of mechanical behavior of the fiber reinforced composite is the ROM, assumes that the components are non-interacting during straining and fibers are perfectly aligned and spaced, the matrix is void free, both matrix and fibers are linearly elastic, and bonding between matrix and fibers is perfect. The strength of a unidirectional composite, σ_c can be obtained according to the ROM from the equation:

$$\sigma_c = \eta \sigma_f V_f + \sigma_m V_m \quad (1.4.1)$$

where σ and V are the respectively the strength and volume fraction of the component, the subscripts c, f and m refer to the composite, fiber and matrix. η is the fibers orientation coefficient, η is 1 where the fibers are parallel to the axial stress, 1/2 for the occasion of two-dimensional random distribution, 3/8 for the occasion of three-

dimensional random distribution [74]. However, the ROM cannot calculate the theoretical value with high precision.

2) Shear-lag Model [75]

The above-mentioned ROM is an often-used model for predicting continuous fiber reinforced composites, while, it is a rough prediction for short fiber reinforced composites. Nardone and Prewo [75] had proposed a shear-lag theory model to describe the strength prediction of the composites. They assumed that the redistribution of matrix stress to the reinforcement is caused by the interfacial shear load transfer, which is considered as the main contributing factor resulting in the significant increase of yield strength. The theoretical yield stresses of the composite (shear-lag model) is expressed as:

$$\sigma_{yc}/\sigma_{ym} = 0.5V_f(2 + 1/d) + (1 - V_f) \quad (1.4.2)$$

where σ_{yc} and σ_{ym} are the respectively the yield stresses of the composite and the matrix. This theory model is based on interfacial shear stress which focuses on tensile stress transmitted from matrix to fiber by force.

3) Hirsch Model [76]

Hirsch has proposed a prediction model which is a combination of parallel and series models. The equation for calculation of tensile strength is as follow:

$$\sigma_c = x (\sigma_f V_f + \sigma_m V_m) + (1-x) (\sigma_m \sigma_f) / (\sigma_m V_f + \sigma_f V_m) \quad (1.4.3)$$

where σ and V are the respectively the strength and volume fraction of the component, the subscripts c, f and m refer to the composite, fiber and matrix. X is a parameter of the equation which is 0.4 for longitudinally oriented composites and 0.1 for the randomly oriented composites. In the case of short-fiber composites, the stress transfer depends mainly on fiber orientation, stress concentration at the fiber ends and the critical fiber length, etc. For this equation, it can be found that the x parameter determines the stress transfer between fiber and matrix and acts a role in describing the real behavior of short-fiber composites.

1.4.2 Models for predicting thermal conductivity of composites

CF reinforced Al matrix composites have been used extensively in electronic devices. Short fibers composites are also highly demanded as a material for electronic devices where short fibers are distributed in a completely random manner. The TC of short fibers composites affects by the fiber type, fiber orientation and volume fraction. Furthermore, it is known that the interfacial thermal contact resistance between different constituent phases in a composite can arise from the combination of a poor mechanical or chemical adherence at the interface and a thermal expansion mismatch. Therefore, the analysis of the thermophysical behavior of short fibers composites becomes important and it is essential to comprehend the effects of each component and to diminish the negative influencing factors. There are numerous analytical models have been proposed to predict the TC of a short fiber composite which was focused on either aligned short fiber composite or completely random short fiber composite. The analytical models provide theoretical support and make it possible to design high TC composites using for electronic devices

1) Maxwell and Maxwell-Eucken Models ^[77, 78]

Maxwell was the first to provide analytical expressions for effective TC of the heterogenic medium. Maxwell's model ^[77] was used for composites with continuous and uniformly distribution particle reinforcements. Maxwell's model is described as follow:

$$\lambda_c = \lambda_m \frac{2 + \frac{\lambda_d}{\lambda_m} - 2V_m \left(1 - \frac{\lambda_d}{\lambda_m}\right)}{2 + \frac{\lambda_d}{\lambda_m} + V_m \left(1 - \frac{\lambda_d}{\lambda_m}\right)} \quad (1.4.4)$$

where λ and V are the respectively the TC and volume fraction of the component, the subscripts c, d and m refer to the composite, dispersed phase and matrix. The Maxwell's formula was found to be valid only in the case of low volume fraction (under about 25%).

Maxwell-Eucken model has been used to represent the TC of composites by considering the inclusion of reinforcements isolated and dispersed in a continuously

homogeneous matrix. It assumes a distribution of small spheres within a continuous matrix with the spheres being far away enough so that the local temperature distributions do not interfere with each sphere [78].

$$\lambda_c = \lambda_m \left[\frac{\lambda_f + 2\lambda_m - 2V_f(\lambda_m - \lambda_f)}{\lambda_f + 2\lambda_m + V_f(\lambda_f - \lambda_m)} \right] \quad (1.4.5)$$

where λ and V are the respectively the TC and volume fraction of the component, the subscripts c, f and m refer to the composite, reinforcement and matrix. The Maxwell-Eucken model was fit to the reinforcement at low volume fraction (15% or less).

2) Landauer Model [79]

Landauer had proposed a model fitting for the binary alloy system which considered the contact resistance between reinforcements and the second phase. The model is also suitable for high volume fractional second phase, the equation is as followed:

$$\lambda_c = \frac{1}{4} \left[\lambda_f(3V_f - 1) + \lambda_m(3V_m - 1) + \sqrt{[\lambda_f(3V_f - 1) + \lambda_m(3V_m - 1)]^2 + 8\lambda_f\lambda_m} \right] \quad (1.4.6)$$

The model assumed that the reinforcements were spherical and uniformly dispersed in the matrix. When $V_f < 0.15\%$, the result is the same as the Maxwell equation. When $V_f > 0.15\%$, the TC of composites is greatly affected by the contact resistance of reinforcements. However, the calculation of TC requires the consideration of the interfacial thermal resistance between the fiber and matrix, and the porosity also affect the TC due to the interfacial thermal resistance with air is almost 0. Therefore, it is difficult to accurately estimate the TC of composites by using Landauer's model.

3) Hatta-Taya Model [80]

A prediction theory model of composites with three-dimensional randomly oriented cylindrical fibers in a matrix was proposed by Hatta-Taya. Unlike other models, Hatta-Taya found that the present model can account for the interaction among various fiber orientations which were not considered in the before models. However, the Hatta-Taya model didn't take the interfacial thermal resistance into consideration, it lacks the ability to predict the accurate TC of composites.

4) Hasselman-Johnson Model [81]

It is known that the interfacial thermal contact resistance between different

component phases in a composite can arise from the combination of a poor adherence at the interface and a thermal expansion mismatch which is now known as the Kapitza resistance. A number of analyses [82-84] have shown that the interfacial thermal resistance has a dramatical effect on the effective TC of composites.

Hasselman and Johnson extended the classical work of Maxwell and derived an effective medium approximation for calculating the Kapitza resistance by including the interface effect and particle size. They emphasized that the TC of composites depends on not only the reinforcement volume fraction but also the particle size as well. Hasselman and Johnson derived expressions for a continuous matrix phase with dispersions with spherical (1.4.7) and cylindrical (1.4.8).

$$K_{eff} = K_m \frac{2 \left(\frac{K_f}{K_m} - \frac{K_f}{ah_c} - 1 \right) V_f + \frac{K_f}{K_m} + \frac{2K_f}{ah_c} + 2}{\left(1 - \frac{K_f}{K_m} + \frac{K_f}{ah_c} \right) V_f + \frac{K_f}{K_m} + \frac{2K_f}{ah_c} + 2} \quad (1.4.7)$$

$$K_{eff} = K_m \frac{\left(\frac{K_f}{K_m} - \frac{K_f}{ah_c} - 1 \right) V_f + \left(1 + \frac{K_f}{K_m} + \frac{K_f}{ah_c} \right)}{\left(1 - \frac{K_f}{K_m} + \frac{K_f}{ah_c} \right) V_f + \left(1 - \frac{K_f}{K_m} + \frac{K_f}{ah_c} \right)} \quad (1.4.8)$$

where K and V are the respectively the TC and volume fraction of the component, the subscripts eff, c, f and m refer to the effective, composite, reinforcement and matrix, respectively, h_c is the interfacial thermal conductance, and a is the radius of dispersion. The novelty in the Hasselman-Johnson model is the dependence of the effective TC on the particle radius a, and the boundary conductivity h_c [W/(m²·K)] which is the reciprocal of interfacial thermal resistance. But the limitation is that the model is only for cylinders perpendicular to the heat flow, which cannot be used for wide calculation.

5) Ce-Wen Nan Model [85, 86]

Nan had obtained the expression of the effective TC of composites with cylindrical dispersed dispersions in a three-dimensionally randomly oriented occasion which had been used for prediction of TC of CFs composites. Nan assumed that the fiber/matrix interface is effective for the transport of energy across it and the matrix phase as the homogeneous reference medium. The model takes into account the anisotropy in TC of

a CF, the aspect ratio and volume fraction of the fibers, as well as the interfacial thermal resistance at the fiber/matrix interface. The effective TC calculate equations and explanations are as follow:

$$K_{eff} = K_m \frac{3 + 2f[\beta_x(1-L_x) + \beta_z(1-L_z)]}{3 - f(2\beta_x L_x + \beta_z L_z)} \quad (1.4.9)$$

where f is volume fraction of the CF, K_m is the TC of the matrix. β_x , β_y and β_z are expressed in eqs. (1.4.10) and (1.4.11)

$$\beta_x = \beta_y = \frac{K_x^c - K_m}{K_m + L_x(K_x^c - K_m)} \quad (1.4.10)$$

$$\beta_z = \frac{K_z^c - K_m}{K_m + L_z(K_z^c - K_m)} \quad (1.4.11)$$

where K_x^c and K_y^c are K_z^c the thermal conductivities of the CF in x, y and z directions with the consideration of the interfacial thermal resistance between matrix and CF. L_x and L_z are well-known geometrical factors dependent on the CF aspect ratio p , aspect ratio p is expressed as l/d , l and d are the diameter and length of the CF, respectively. For $p > 1$ fibers, L_x and L_z are are given by eqs. (1.4.12) and (1.4.13)

$$L_x = \frac{p^2}{2(p^2 - 1)} - \frac{p}{2(p^2 - 1)^{\frac{3}{2}}} \cosh^{-1} p \quad (1.4.12)$$

$$L_z = 1 - 2L_x \quad (1.4.13)$$

K_x^c and K_y^c are K_z^c are calculated by the following eqs. (1.4.14) and (1.4.15).

$$K_x^c = K_y^c = \frac{K_d^c}{1 + \frac{2a_k K_d^c}{dK_m}} \quad (1.4.14)$$

$$K_z^c = \frac{K_l^c}{1 + \frac{2a_k K_l^c}{lK_m}} \quad (1.4.15)$$

where K_d^c and K_l^c represent thermal conductivities of the CF in transverse and longitudinal directions, and their values used in the present study are $10 \text{ W} \cdot \text{m}^{-1} \cdot \text{K}^{-1}$ and $800 \text{ W} \cdot \text{m}^{-1} \cdot \text{K}^{-1}$, respectively. α_K is called Kapitza radius and expressed in (1.4.16).

$$a_k = R_{Bd} K_m \quad (1.4.16)$$

where R_{Bd} is a coefficient of the interfacial thermal resistance, which controls the characteristics of interfacial heat transfer. Here $8.3 \times 10^{-8} \text{ W}^{-1} \cdot \text{m}^2 \cdot \text{K}$ was used for the coefficient [85].

The above summarized several composite TC conventional prediction models. It is important to use reasonable conventional models to predict TC of fiber reinforced composites. Noted that the models with consideration of interfacial thermal resistance provide a more accurate prediction for TC of composites.

1.5 Objective and outline of this thesis

With the rapid development of the electronic and automobile industries and the increasing attention to environmental issues, the demanding for lightweight, high thermal and mechanical properties materials is urgently needed. CF reinforced Al matrix composites could combine the excellent thermal and mechanical characteristics of CF and Al matrix which are expected to be applied in the automobile industry. The previous studies [87, 88] are much focusing on the effects of volume fraction of CF on properties, it is found that the fibers tend to aggregate and hard to disperse uniformly when the volume fraction of fibers beyond 10%, and also the defects such as pores tend to form as V_f increase. As for V_f of CF is 10%, the relative density of the composite is 96.3%, the reinforcing effect is notable simultaneously, therefore, the volume fraction of CSFs in this study was fixed to 10 vol.%. There are a few types of research have been carried on the effects of type of matrix alloys. It has a significant impact on the thermal and mechanical properties by the type of matrix. As A1070 aluminum contains no alloying elements, A356 alloy and A336 alloy contain different alloying elements content, the selection of three types of Al matrix is to analyze the effects of alloying elements on microstructure, thermal and mechanical properties of CF reinforced composites. Meanwhile, A1070 aluminum possesses high TC but low mechanical property, A356 and A336 aluminum alloys possess high tensile strength a but not ideal TC. The CSF reinforced three types of Al matrix composites are expected to improve the thermal and mechanical performances of the matrix, and to extend the range of applications of three types of Al matrix. The CSF reinforced A1070 composite is aimed to be used as functional materials (such as heat sink) in the automobile industry, and the CSF reinforced A356 alloy and A336 alloy composites are aimed to be used as structural materials (such as piston and cylinder) in the automobile industry.

Most of CSFs reinforced composites' properties are controlled by interfacial adhesion between CSFs and matrix. However, the poor wetting characteristics and chemical reaction between CSFs and molten Al are the main obstacles that limit the properties' improvement of CSF reinforced composites [89]. For solving the problems, surface coating of CSF is the most effective way to improve the wettability and to

prevent the formation of interfacial reactions. SiO_2 [90] and Ni [91] have been proved to be effective coating materials as they increase the wettability between CSFs and molten Al.

The typical manufacturing process such as PM and squeeze casting had some disadvantages by using high pressure. The high pressure limited the degree of freedom on the shape of the MMCs and raised the fabrication cost. The LPI fabrication process is similar to the squeeze casting method however it applies extremely low pressure. It was reported that the low pressure casting is also able to fabricate MMCs with complex and large shape [92, 93]. The LPI apparatus is simple and easy to operate which also reduces the fabrication cost. Therefore, the CF/Al matrix composites with high thermal and mechanical properties, in conjunction with the LPI process can be competitive for the other MMCs of the applications in the automobile industry. The traditional manufacturing of short fiber reinforced composites by liquid processes require preform manufacturing using inorganic binders (such as SiO_2 binder). However, conventional preform manufacturing techniques using inorganic binders are nontrivial procedures requiring high-energy inputs and preparation time for the binder sintering process. Therefore, a novel alternative fabrication process with cost effective and high production efficiency is urgent needed for developing carbon short fiber (CSF) reinforced Al matrix composite.

In this study, for developing the CSF reinforced Al matrix composites, the CSF reinforced A1070, A356 alloy and A336 alloy composites were fabricated with SiO_2 binder preform and the new process without preform manufacturing, respectively, by LPI process. The volume fraction of CSF was fixed to 10 Vol.%. Effects of the kind of matrix with different alloying elements, fabrication pressure as well as SiO_2 and Ni coating materials on microstructure, thermal and mechanical properties of composites were investigated and characterized.

Chapter 1 reviews the scientific background, the manufacturing processes and the development status of AMCs. Moreover, from the problems of the previous studies of AMCs, the direction of newly developing AMCs, CSF reinforced Al matrix composite is proposed. Various predictive models for the mechanical and thermal properties of the composite are enumerated. It points out the objective and illustrates the overall content

of the thesis.

Chapter 2 introduces the fabrication of only CSF and hybrid CSF-CNF reinforced Al matrix composites by LPI process with SiO₂ binder. Prior to fabricating the composites, the fabrication process of the porous CSF preform and hybrid CSF-CNF preform is discussed, the most suitable condition of hybrid CSF-CNF is analyzed. The microstructure of preforms and composites, as well as the interface structure between CSF and matrix are investigated.

In Chapter 3, the Ni plated CSF reinforced Al matrix composites were fabricated by the new process without preform manufacturing under different pressure. Before manufacturing the composites, the most appropriate electroless Ni plating condition is discussed. The effects of the Ni plated layer of CSF and the applied pressure on microstructures of composites are investigated.

In Chapter 4, the characterization of TC and mechanical properties on the CSF reinforced Al matrix composites fabricated with SiO₂ binder and without preform manufacturing is investigated. The influences of microstructure and alloying elements on the thermal and mechanical properties of composites are studied.

The results from the above-mentioned investigation are summarized in Chapter 5.

References

- [1] W. F. Xu, Y. X. Luo, W. Zhang and M. W. Fu: *J. Mater. Sci. Technol.* **34** (2018) 173–184.
- [2] J. C. Williams and E. A. S. Jr: *Acta. Mater.*, **51** (2003) 5775–5799.
- [3] E.A.S. Jr and J.T. Staley: *Prog. Aerospace. Sci.* **32** (1996) 131–172.
- [4] S. Fu, Y. Zhang, H. Liu, D. Yi, B. Wang, Y. Jiang, Z. Chen and N. Qi: *J. Mater. Sci. Technol.* **34** (2018) 335–343.
- [5] J. L. Zhang, B. Song, Q. S. Wei, D. Bourell and Y. S. Shi: *J. Mater. Sci. Technol.* **35** (2019) 270-284.
- [6] J. Gilbert Kaufman: *Introduction to Aluminum Alloys and Tempers*, (2000), p33.
- [7] S. Mallik, N. Ekere, C. Best, R. Bhatti: *App. Therm. Eng.* **31** (2011) 355-362.
- [8] H. L. Wang, R. Zhang, X. Hu, C. A. Wang and Y. Huang: *Journal of Materials Processing Technology*, **197** (2008) 43-48.
- [9] M.H. Lee, Y. B. Choi, K. Sugio, K. Matsugi and G. Sasaki: *Science and Engineering of Composite Materials*, **18** (2009) 167-171.
- [10] Z. F. Xu, Y. B. Choi, K. Matsugi, D.C. Li and G. Sasaki: *Mater. Trans.* **50** (2009) 2160-2164.
- [11] K. Fukuchi, K. Sasaki, K. Katagiri, T. Imanishi and A. Kakitsuji: *Procedia Engineering*, **10** (2011) 912–917.
- [12] S. Mallik, N. Ekere, C. Best, R. Bhatti: *App. Therm. Eng.* **31** (2011) 355-362.
- [13] R. K. Everett and R. J. Arsenault: *Metal Matrix Composites: Processing and Interface*, (1991) p. 43-102.
- [14] S. Soltani, R. A. Khosroshahi, R. T. Mousavian, Z. Y. Jiang, A. F. Boostani and D. Brabazon: *Rare Metals*, **36** (2017) 581-590.
- [15] A. D. Hamedan and M. Shahmiri: *Mater. Sci. Eng A*, **556** (2012) 921–926.
- [16] H. R. Ezatpour, S. A. Sajjadi, M. H. Sabzevar and Y. Huang: *Materials Design*, **55** (2014) 921-928.
- [17] S. Venkatesan and M. A. Xavier: *Journal of Chemical and Pharmaceutical Sciences*, **10** (2017) 55-59.

- [18] T. Miranda, L. Bolzoni, N. Barekar, Y. Huang, J. Shin, S. H. Ko and B. J. McKay: *Materials Design*, **156** (2018) 329-339.
- [19] S. Ravi Kumar, M. K. Panigrahi, S. K. Thakur, K. U. Kainer, M. Chakraborty, B. K. Dhindaw: *Mater. Sci. Eng. A*, **415** (2006) 207-212.
- [20] B. Moser, A. Rossoll, L. Weber, O. Beffort and A. Mortensen: *Composites A*, **32** (2001) 1067-1075.
- [21] K. S. Sohn, K. Euh, S. Lee, and I. Park: *Metall. Mater. Trans. A*, **29** (1998) 2543-2554.
- [22] E. A.M. Shalaby and A. Y. Churyumov: *J. Alloy. Comp.* **727** (2017) 540-548.
- [23] L. Natrayan and M. Senthil Kumar: *Advanced Manufacturing and Materials Science*, (2018) p. 75-83.
- [24] A. Demir and N. Altinkok: *Compos. Sci.* **64** (2004) 2067-2074.
- [25] J. J. Wu, C. G. Li, D. B. Wang and M. C. Gui: *Compos. Sci.* **63** (2003) 569-574.
- [26] Y. B. Choi, Y. Kataoka, Z. F. Xu, K. Matsugi and G. Sasaki: *Mater. Trans.* **58** (2017) 1097-1099.
- [27] M. H. Lee, Y. B. Choi, K. Sugio, K. Matsugi and G. Sasaki: *Compos. Sci.* **97** (2014) 1-5.
- [28] H. Z. Ye, and X.Y. Liu: *J. Mater. Sci.* **39** (2004) 6153-6171.
- [29] J. Barcena, J. Maudes, M. Vellvehi, X. Jorda, I. Obieta, C. Guraya, L. Bilbao, C. Jimenez, C. Merveille, J. Coletto: *Acta. Astron.* **62** (2008) 422-430.
- [30] S. Jin: *JOM*, **50** (1998) 46.
- [31] C. Zweben: *JOM*, **50** (1998) 47-51.
- [32] H. S. Chris, J.C. Withers, C. Pan, D. Wallace, R.O. Loutfy: *Surf. Coat. Tech.* **76** (1995) 681-686.
- [33] R. Prieto, J.M. Molina, J. Narciso and E. Louis: *Scr. Mater.* **59** (2008) 11-14.
- [34] M. J. Li, K. K. Ma, L. Jiang, H. Yang, E. J. Lavernia, L. M. Zhang and, J. M. Schoenung: *Mater. Sci. Eng. A*, **656** (2016) 241–248.
- [35] X. N. Zhang, L. Geng and G.S. Wang: *Journal of Materials Processing Technology*, **176** (2006) 146–151.
- [36] H. Naji, S. M. Zebarjad and S. A. Sajjadi: *Mater. Sci. Eng. A*, **486** (2008) 413–420.

- [37] J. H. Han, Y. B. Lee, J. Y. Lim, K. K. Jee and J. Yoon: ECCM15-15th European Conference on Composite Materials, Venice, Italy, (2012)
- [38] K. Naito, J. M Yang, Y. Xu, Y. Kagawa: *Carbon*, **48** (2010) 1849–1857.
- [39] D. D. Edie: *Carbon*, **36** (1998) 345-362.
- [40] A. Parry and A. Windle: *J. Mater. Sci.* **47** (2012) 4236-4250.
- [41] Y. B. Yao, J. M. Chen, L. Liu. Y. M. Dong and A. H. Liu: *J. Mater. Sci.* **49** (2014) 191-198.
- [42] M. Endo , Y.A. Kim, T. Hayashi, K. Nishimura, T. Matusita, K. Miyashita and M.S. Dresselhaus: *Carbon*, **39** (2001) 1287–1297.
- [43] T. Koyama and M. Endo: *O Buturi*, **42** (1973) 690–696.
- [44] A. S. Fialkov, N. M. Sidorov, B. N. Smirnov and B. I. Dyuzhikov. *Doklady Akademii Nauk SSSR*, **211** (1973) 158–160.
- [45] G. G. Tibbetts: *J Crystal Growth*, **73** (1986) 431–438.
- [46] F. Benissad, P. Gadalle, M. Coulon and L. Bonnetain: *Carbon*, **26** (1988) 425–432.
- [47] T. Koyama and M. Endo: *Jpn J Appl Phys*, **3** (1974) 1175–1176.
- [48] T. Koyama and M. Endo: *Jpn J Appl Phys*, **13** (1974) 1933–1939.
- [49] A. Oberlin and M. Endo: *J Cryst Growth*, **32** (1976) 335-349.
- [50] Endo M: *Chemtech*, **18** (1988) 568–576.
- [51] J. S. Speck and M. Endo: *J Cryst Growth*, **94** (1989) 834-848.
- [52] G. G. Tibbetts: *Appl. Phys. Lett.* **42** (1983) 666-668.
- [53] G. G. Tibbetts: *J. Crys. Growth.* **73** (1985) 431-438.
- [54] T. Koyama and M. Endo: *Japanese Patent*, **58** (1982) p. 966
- [55] S, Iijima: *Nature*, **354** (1991) 56–58.
- [56] J. Y. Lim, S. I. Oh, Y. C. Kim, K. K. Lee, Y. M. Sung and J. H. Han: *Mater. Sci. Eng. A*, **556** (2012) 337-342.
- [57] T. Etter, P. Schulz, M. Weber, J. Metz, M. Wimmmler, J. F. Loffler, P. J. Uggowitzzer, *Mater. Sci. Eng. A*, **448** (2007) 1-6.
- [58] M. Lancin, C. Marhic, *J. Euro. Ceramic Society*, **20** (2000) 1493-1503.
- [59] H. Yang, M. Gu, W. Jiang, G. Zhang, *J. Mater. Sci.* **31** (1996) 1903-1907.
- [60] S. R. Bakshi, A. K. Keshri, V. Singh, S. Seal, A. Agarwal, *J. Alloys Compd.*

- 481** (2009) 207-213.
- [61] S. I. Oh, J. Y. Lim, Y. C. Kim, J. Yoon, G. H. Kim, J. Lee, Y. M. Sung and J. H. Han: *J. Alloys Compd.* **542** (2012) 111-117.
- [62] T. Suzuki, H. Umehara, R. Hoyashi and S. Watanabe: *J. Mater. Res.* **8** (1993) 2492-2498.
- [63] N. Kumar, H. C. Chittappa and S. E. Vannan: *Materials Today, Proceedings*, **5** (2018) 11336–11345 .
- [64] K. T. Kashyap, K. Govindarajulu, M. C. Mittal and P. V. Sharma: *J. Mater. Sci. Lett.* **14** (1995) 1691-1693.
- [65] S. G. Warriar, C. A. Blue and R. Y. Rin, *J. Mater. Sci.* **28** (1993) 760-768.
- [66] S. Abraham, B. C. Pai , K. G. Satyanarayana and V. K. Vaidyan, *Journal of Minerals and Materials Characterization and Engineering*, **25** (1990) 2839-2845.
- [67] Y. Q. Wang, B. L. Zhou and L. J. Zhou: *Compos Part A: Applied Science and Manufacturing*, **27** (1996) 1139-1145.
- [68] A. Kithakara, S. Akiyama and H. Veno: *J. Jpn. Inst*, **40** (1990) 305-311.
- [69] P. G. Karandiker and T. W. Chou: *Proceedings of the Conference on Fundamental Relationships between Microstructures and Mechanical Properties of MMCs*, (1990) 59.
- [70] J. P. Clement, H. J. Rack, K. T. Wu and H. G. Spencer: *Mater. Manuf. Process*, **5** (1990) 17.
- [71] J.R. Srife and J.E. Sheehan: *Ceram. Soc. Bull*, **67** (1988) 369-374.
- [72] Y.Q. Wang and B. L. Zhou, L. J. Zhou: *Compos Part A: Applied Science and Manufacturing*, **27** (1996) 1139-1145.
- [73] M. Abdel Ghafaar, A. A. Mazen and N. A. El Mahallawy: *J. Eng. Sci.* **34** (2006) 227-236.
- [74] Y. C. Park, G. C. Lee, T. Mihara and K. Date: *J. Japan Inst. Metals.* **57** (1993) 301-306.
- [75] V. C. Nardone and K. M. Prewo: *Scripta Metallurgica*, **20** (1986) 43-48.
- [76] T. J. Hirisch: *J. Am. Con. Inst.* **59** (1962) 427-452.
- [77] J. C. Maxwell: Pergamon, Oxford, vol. 1. 3rd ed. 1904.
- [78] A. Eucken: *Forschung Gabiete Ingenieur*, **11** (1940). 6–20

- [79] R. Landauer: *J. Appl. Phys.* **23** (1952) 779-784.
- [80] H. Hatta and M. Taya: *J. Appl. Phys.* **59** (1986) 1851.
- [81] D. P. H. Hasselman and L. F. Johnson: *J. Compos. Mater.* **21** (1987) 508–515.
- [82] H. Bhatt, K. Y. Donaldson, D. P. H. Hasselman, and R. T. Bhatt: *J. Am. Ceram. Soc.* **73** (1990) 312 -316.
- [83] D. M. Liu and W. H. Tuan: *Acta Metall. Mater.* **44** (1996) 813-818.
- [84] D. P. H. Hasselman, K. Y. Donaldson, and A. L. Geiger: *J. Am. Ceram. Soc.* **75** (1992) 3137-3140.
- [85] C.W. Nan, Z. Shi and Y. Lin: *Chem. Phys. Lett.* **375** (2003) 666–669.
- [86] C.W. Nan, G. Liu, Y. H. Lin and M. Li: *Appl. Phys. Lett.* **85** (2004) 3549-3551.
- [87] H. Najji, S.M. Zebarjad and S.A. Sajjadi: *Mater. Sci. Eng. A*, **486** (2008) 413–420.
- [88] M. Deshpande, R. Gondil, R. Waikar, S. V. S. N. Murty and T. S. Mahata: *Materials Today: Proceedings*, **5** (2018) 7115–7122.
- [89] S. H. Li and C. G. Chao: *Metall. Mater. Trans. A*, **35** (2004) 2153–2160.
- [90] V. Laurent, D. Chatain and N. Eustathopoulos: *Mater. Sci. Eng. A*, **135** (1991) 89–94.
- [91] J. Rams, A. Urena, M. D. Escalera and M. Sanchez: *Composites: Part A*, **38** (2007) 566-575.
- [92] J. M. Molina, M. Rheme, J. Carron and L. Weber: *Scr. Mater.* **58** (2008) 393-396.
- [93] K. Matsugi, Y. B. Choi, K. Arita, O. Yanagisawa, G. Sasaki: *J. Jpn. Inst. Light Met.* **58** (2008) 71-80.

Chapter 2

Fabrication process and microstructure of carbon short fiber and hybrid carbon short fiber-carbon nanofiber reinforced aluminum matrix composites with SiO₂ binder by low pressure infiltration process

2.1	Introduction	42
2.2	Experimental procedure	44
2.2.1	Raw materials	44
2.2.2	Preparation of CSF preform and hybrid CSF-CNF preform	46
2.2.3	Fabrication of CSF/Al and hybrid CSF-CNF/Al composites	48
2.2.4	Evaluation methods and equipment	50
2.2.4.1	Observation of microstructure.....	50
2.2.4.2	X-ray diffraction characterization.....	50
2.3	Results and discussion	51
2.3.1	Microstructures.....	51
2.3.1.1	Microstructures of CSF preform and hybrid CSF-CNF preform	51
2.3.1.2	Microstructures of CSF/Al and hybrid CSF-CNF/Al composites.....	54
2.3.2	Interface structure between CSF and aluminum matrix.....	61
2.4	Summary	65
	References	66

2.1 Introduction

A number of MMCs have been developed for both thermal/electronic and structural applications in the field of automobile [1-5]. Among the family of available MMCs, aluminum is the most dominant matrix for MMCs and aluminum matrix composites (AMCs) possess low-density and excellent thermal and mechanical properties over their unreinforced counterparts are gaining a lot of attentions [6-8]. Carbonaceous materials such as carbon fibers (CFs), carbon nanofibers (CNFs) [9] and carbon nanotubes (CNTs) [10] have appeared to be promising reinforcements due to their high specific surface area (SSA), good elevated temperature stability, profitable electrical conductivity [11, 12]. Therefore, carbon materials system reinforced aluminum matrix composites have the most potential properties such as light weight, low coefficient of thermal expansion (CTE), high electrical/thermal conductivity (TC), high specific strength and well wear resistance [13-16] for using as functional materials and structural materials.

In recent years, research efforts have been made to CF reinforced Al matrix composites [17-19] and Vapor grown carbon fiber (VGCF, CNF) reinforced Al matrix composites [20, 21]. Nevertheless, a variation of microstructure and properties in aluminum matrix composites using carbon short fiber (CSF) and carbon nanofiber (CNF) as reinforcement are rarely investigated. Using CSF and CNF as hybrid reinforcements, the CNFs are expected to be uniformly distributed on the surface of CSFs which can further increase the surface space area to achieve effective stress-transfer across the metal matrix, makes its high bond strength with the matrix. On the other hand, CNFs uniformly distributed on CSF in the matrix which can prevent grain growth during manufacturing. Therefore, the use of hybrid reinforcement (CSF and CNF) is expected to further improve the mechanical properties of AMCs.

Currently, there are several fabrication methods of MMCs, including powder metallurgy, casting methods, in situ routes, chemical synthesis, etc. [22]. Among various techniques, powders metallurgy (PM) and casting techniques are more common than the other methods. PM is one of the useful techniques to achieve uniform distribution of nanoparticles and PM method had been widely used to fabricate composites [23-25].

However, the complex facilities and high energy consumption limit its widely used. As for the casting methods, the stir casting route is considered as a promising route for synthesizing discontinuous reinforcement with metal matrix because of its relative simplicity and easy adaptability. However, due to the poor wetting of the reinforcement by molten alloy, it is different to obtain a uniform dispersion of the reinforcement into the liquid matrix. Furthermore, structural defects, such as interfacial reactions and formation of porosity easily arise from the stir casting process [26].

The liquid metal infiltration process involves the process of using pressure to push the molten metal into the porous preform (fibers or particles) which was fabricated with binder in advance [27, 28]. Low Pressure infiltration (LPI) method belongs to the liquid metal infiltration process is gaining attentions which provides a near net shape fabrication, the shape and size of the composite product can be designed by designing the shape of preform. The LPI method has many advantages such as applying relatively simple facilities, cost-effective and complex shape fabrications by using low pressure [29-31]. For the low-pressure infiltration process of CSF/Al matrix composite, it is often to use inorganic binders such as SiO₂, Al₂O₃ or TiO₂ to retain the integrity and shape of CSF preform [32-34]. The binder prevents the filler fibers or particles from moving during the infiltration process and provides sufficient compressive strength of preform to bear the infiltration pressure. Meanwhile, the binder also acts as a coating material for preventing carbons react with oxygen.

In this study, prior to fabricating composites, the CSF and hybrid CSF-CNF preforms were manufactured with SiO₂ binder. Moreover, CSF and hybrid CSF-CNF reinforced Al matrix composites were fabricated by infiltration of molten Al into porous preform by LPI process. Moreover, the microstructure of CSF and hybrid CSF-CNF preforms, as well as composites, were investigated. The interface structure between CSF and aluminum matrix was analyzed.

2.2 Experimental procedure

2.2.1 Raw materials

A1070 pure Al, A356 alloy and A336 alloy are used as matrix for composites and the chemical compositions of were listed in Table 2-1. Noticing that the three types of matrix contain different kinds and contents of alloying elements. The coal tar pitch based CSFs (K13D2U, Mitsubishi Plastics, Inc. diameter 11 μm , aspect ratio of 230), carbon nanofiber (CNF, Showa Denko Co., Japan) were used as reinforcement, and a SiO_2 sol (ST-ZL, Nissan Chemical Industries, Ltd., Japan) was used as the binder in this study. Table 3-2 shows the properties of the CSF and CNF. Noticed that the CSFs and CNFs have characteristics such as light weight and excellent TC.

Al and its alloys have relatively light weight, good TC, and low CTE in the field of the metal matrix. The A1070 with a purity of 99.7% has a high TC of $237 \text{ W}\cdot\text{m}^{-1}\cdot\text{K}^{-1}$ but low mechanical property, the development of CSF/A1070 composite aims to further improve the TC and mechanical property for use as the heat sink applications for high heat generating electronic components. In addition, the A356 and A336 alloys have relatively low TC but high tensile strength ($\geq 200 \text{ MPa}$) compared to A1070 because of the composition elements of Si and Mg in A356 alloy, and the composition elements of Si, Ni, Cu and Mg in A336 alloy. The development of CSF/A356 and 336 alloys composites aims to both improve the TC and mechanical properties of composite for engine related parts in automobile applications.

Table 2-1 Chemical composition of A1070 aluminum, A336 alloy and A356 alloy (mass%).

Matrix	Si	Cu	Mg	Ni	Fe	Al
A1070	<0.2	<0.04	<0.03	<0.05	<0.25	99.7>
A356 alloy	6.5-7.5	<0.2	0.25-0.45	<0.05	<0.5	Bal
A336 alloy	11-13	0.5-1.5	0.8-1.3	0.8-1.5	<0.7	Bal

Table 2-2 Properties of CSF and CNF.

Material	Density (Mg·m ⁻³)	Mean diameter	Mean length	TC (W·m ⁻¹ K ⁻¹)
CF (K13D2U)	2.21	11 μm	2.5 mm	800
CNF (VGCF)	2.00	150 nm	10-20 μm	1200

2.2.2 Preparation of CSF preform and hybrid CSF-CNF preform

The LPI process involved infiltrating the molten Al into porous CSF preform by using low pressure less than 1 MPa. Therefore, preform needs to be manufactured in advance, the total volume fraction of CSFs and CSFs-CNFs in a preform was 10 vol. %. SiO₂ binder was used to cross-link fibers and surface coating fibers for wettability with Al. CNFs had a high aspect ratio and strong Van der Waals interaction, therefore, CNFs were fascicular winding and agglomeration. CNFs were acid treated by H₂SO₄: HNO₃: 3:1 in ultrasonic for 30 min for dispersion.

Figure 2-1 shows the schematic diagram of CSF preform and hybrid CSF-CNF preform fabricating process. CSFs with 10 vol. % or CSFs-CNFs total with 10 vol. % were poured into distilled water mixed with 8 wt% SiO₂ binder, after stirring for 8 min then poured into the acrylic mold to eliminate the distilled water and press to height 20 mm. Afterwards, the preform was dried at 403K for 2h and then sintering at 1433K for 6h in Argon for retaining the integrity and providing the strength of preform. The final size of the preform is $\phi 30 \times h20$ mm. Prior to fabricating hybrid CSF-CNF composite, it is essential to analyze a suitable condition that CNFs were well dispersed in the preform. Therefore, a different ratio of CSF: CNF (5:5, 7:3, 9:1 and 9.5:0.5) was carried out to investigate the best CNF dispersion condition.

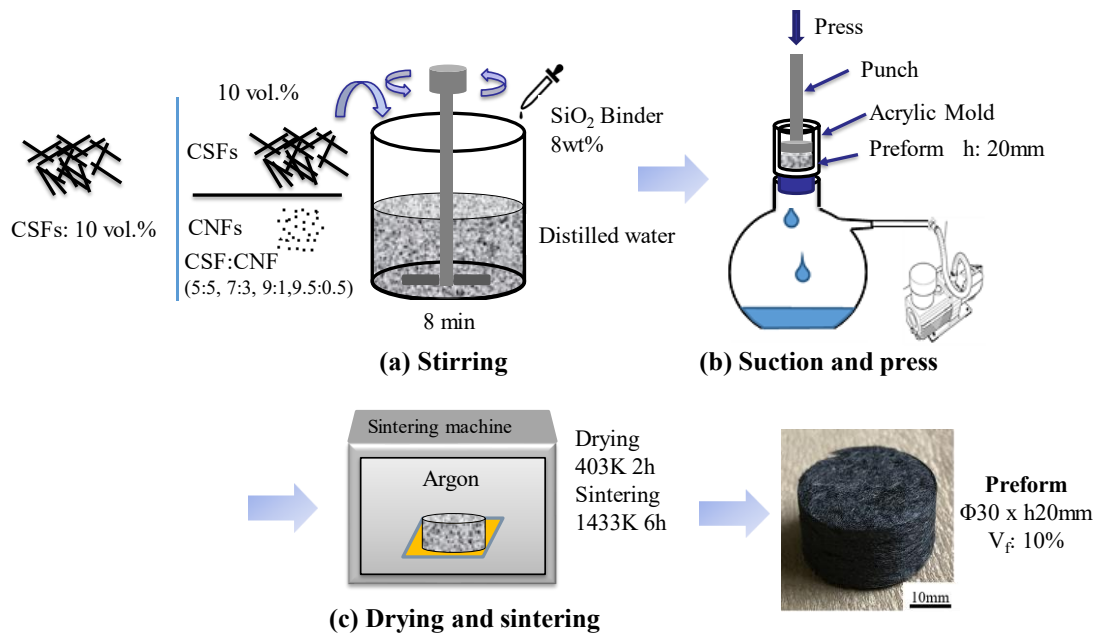


Fig. 2-1 Schematic diagram of CSF preform and hybrid CSF-CNF preform fabricating process.

2.2.3 Fabrication of CSF/Al and hybrid CSF-CNF/Al composites

Al matrix composites were fabricated with infiltrating Al and Al alloys into the preform by low pressure infiltration process. Figure 2-2 shows the schematic illustration of LPI equipment. The manufactured CSF preform or hybrid CSF-CNF preform was put into the cylindrical graphite mold, Al was placed on the preform, then the total mold was put into LPI equipment and heating up to the temperature of 1073K to melt Al. Noticed that the higher infiltration temperature than Al melting point (933 K) was aimed to promote the molten Al easily infiltrating into the preform. Subsequently, the pressure was applied by the iron weight with a lever to infiltrate molten Al into the preform. The parameters of LPI process were shown in Table 2-3. The infiltration pressure was 0.4 MPa, the environment was Argon in order to avoid the oxidation of Al. Finally, holding for 1h after infiltration and then furnace cooling.

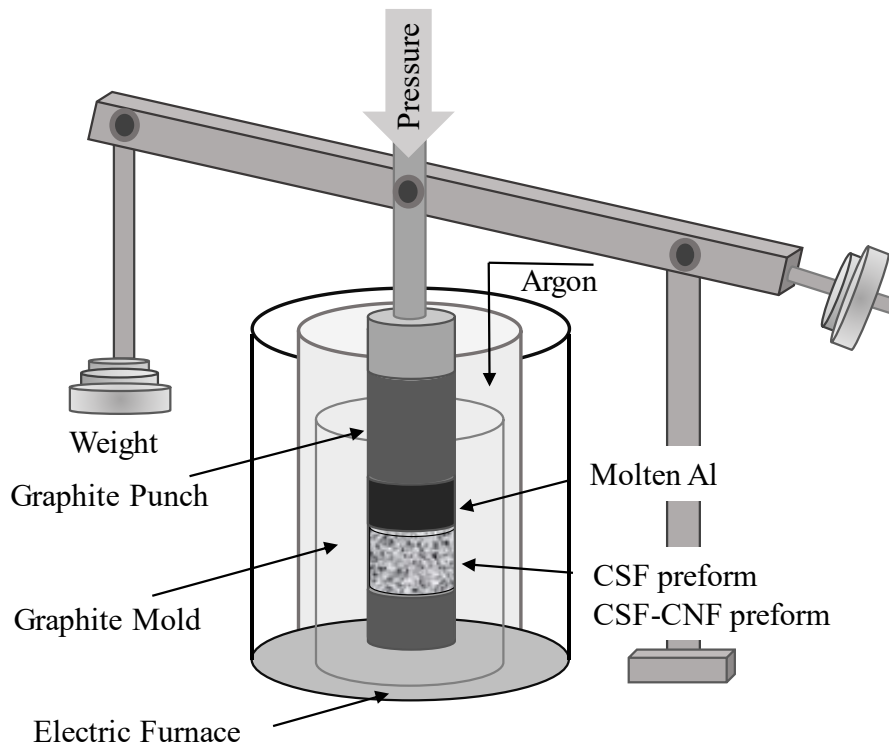


Fig. 2-2 Schematic illustration of low-pressure infiltration equipment.

Table 2-3 Conditions of low-pressure infiltration

Conditions	Parameter
Applied pressure (MPa)	0.4
Infiltration temperature (K)	1073
Holding time (Ks)	3.6
Atmosphere	Argon
Cooling rate	Furnace cooling

2.2.4 Evaluation methods and equipment

2.2.4.1 Observation of microstructure

The samples for metallographic observation were cut from the composite along its transverse direction. The samples were carefully polished using waterproof abrasive SiC paper (#200, #600, #1000, #1500, #2000). The microstructures of the preforms and composites were observed by Optical Microscope (Metal Microscope OPTIPHOT-2, Nikon Corporation, Japan), Electron Probe Micro-Analyzer (EPMA, JXA-8900RL) and Field Emission Scanning Electron Microscope (FE-SEM, Hitachi S-5200, Japan). The interface between CSF and matrix was analyzed by Transmission Electron Microscope (TEM, JEOL JEM-2010, Japan). The elemental analysis was carried out by energy dispersive X-ray spectroscopy (EDS, EDAX JAPAN Genesis XM2).

2.2.4.2 X-ray diffraction characterization

X-ray diffraction (XRD) was carried out with a D/max-2500/PC, Japan. Using Cu K α radiation at 40 kv and 0.1A, a scan speed of 2°/min was used in the range of 20-80° to identify the presence of phases in the composites.

2.3 Results and discussion

2.3.1 Microstructures

2.3.1.1 Microstructures of CSF preform and hybrid CSF-CNF preform

Figure 2-3 shows SEM images of as-received CSFs, as-received CNFs and CNFs after acid treatment. Fig. 2-3 (a) shows the as-received CSFs presented a clean and smooth surface without impurities. The as-received CNFs are easily agglomerated due to the Van der Waals interaction as shown in Fig. 2-3 (b). Therefore, as a filler material of composite, CNFs should be dispersed uniformly to be better distributed in the matrix. In this study, acid treatment was adopted to improve the dispersion of CNFs. Fig. 2-3 (c) shows the agglomeration of CNF was reduced fairly after acid treatment, which allows the CNF could be used as reinforcement in the composite.

Figure 2-4 shows the SEM images of hybrid CSF-CNF preforms depending on the different ratios of CSF to CNF. It could be found that with decreasing the content of CNFs, CNFs agglomeration in preform was weakening accordingly. In Figs. 2-4 (a) and (b), when the CNFs were at a high content, CNFs were prone to entangle together and attached at the corner of CSFs by SiO₂ binder. As decreasing the ratio of CNF in Figs. 2-4 (c) and (d), CNFs agglomeration was significantly weakened, CNFs were dispersed more loosely. It was observed that the condition of CSF: CNF by 9.5:0.5, CNFs were presented the best distribution, therefore, the hybrid preform contained CSF: CNF-9.5:0.5 was used to fabricate composite.

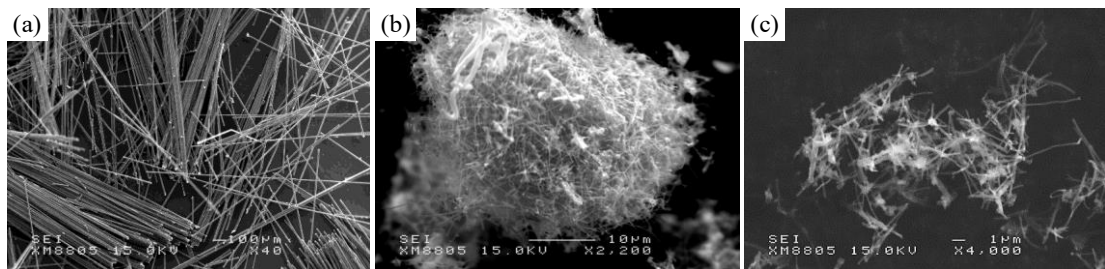


Fig. 2-3 SEM images of (a) as-received CSF, (b) as-received CNF and (c) CNF after acid treatment.

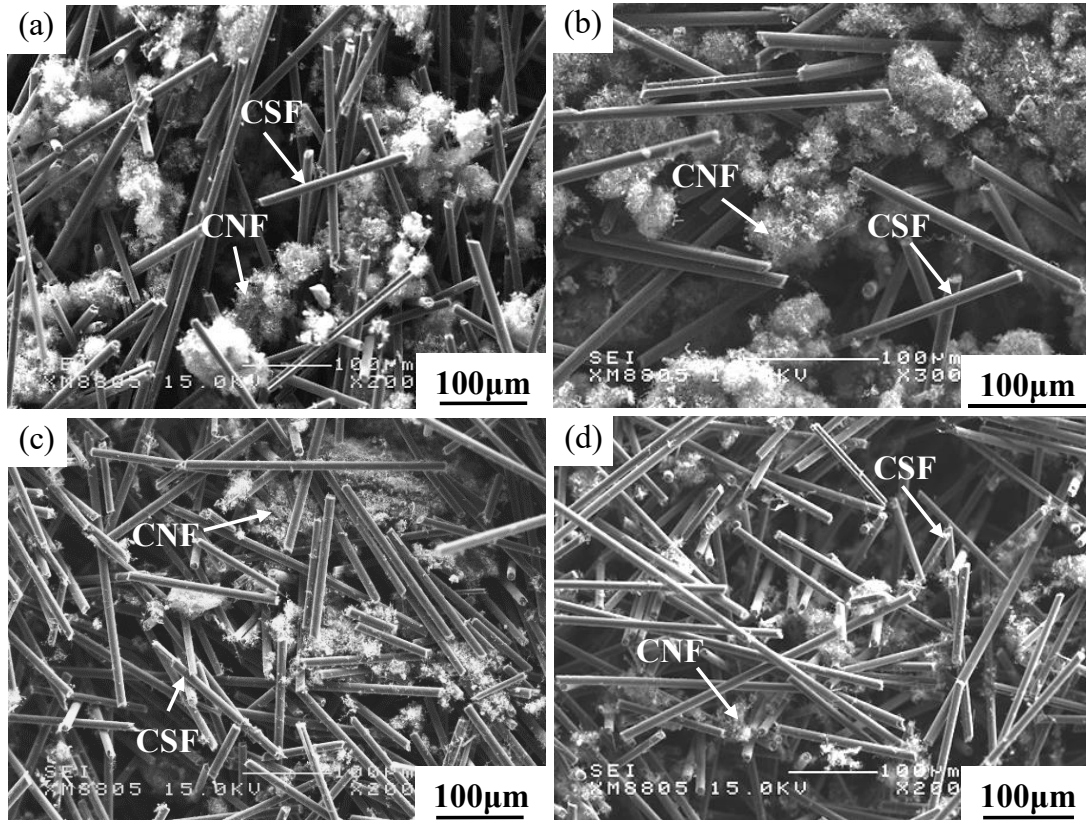


Fig. 2-4 SEM images of hybrid preforms, different ratio of CSF: CNF (a) 5:5, (b) 7:3, (c) 9:1 and (d) 9.5:0.5.

Figure 2-5 represents the SEM images of obtained CSF preform and CSF-CNF hybrid preform with SiO₂ binder. Fig.2-5 (a) exhibits the thick SiO₂ binder layer was coated on the surface of CSFs. Fig. 2-5 (b) shows that the CSFs were cross linked and clustered together by SiO₂ binder, a narrow space region was also observed at the corner of CSFs intersecting parts. Fig. 2-5 (c) shows much of CNFs were stuck together at the corner of CSFs bridges due to the role of SiO₂ binder, the partial enlargement shown in Fig. 2-5 (d) presented that some CNFs were dispersed on the surface of CSF. The purpose of SiO₂ binder was the surface coating of fibers for wettability with Al and ensure preform exhibits large fiber adhesion at intersecting parts. The addition of SiO₂ binder could be a cause of preform strength improvement and enhance the preforms fracture resistance to the applied infiltration pressure.

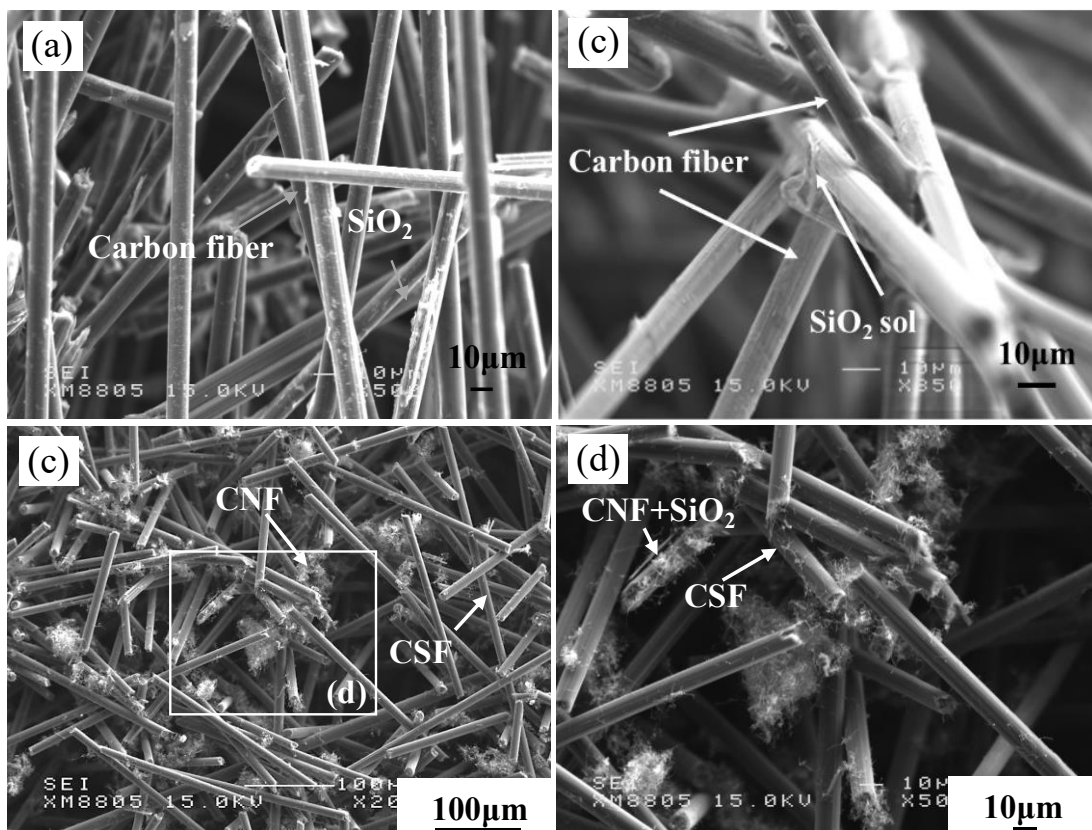


Fig. 2-5 SEM images of preforms: (a), (b) CSF inside preform, (c) CSF-CNF hybrid preform (9.5:0.5) and (d) partial enlargement of (c).

2.3.1.2 Microstructures of CSF/Al and hybrid CSF-CNF/Al composites

To investigate the dispersion of fibers in the matrix, OM and SEM images of composites are shown in Fig. 2-6. Figs. 2-6 (a), (b) and (c) showed that most CSFs were well and evenly distributed as short fibers in the Al and Al alloys matrix, while some CSFs were presented as clusters due to CSFs were agglomerated in the preform. In Fig. 2-6 (d), CNFs cluster was found in the composite. Fig. 2-6 (e) shows the enlargement of CNFs cluster, it was observed that the CNFs cluster was indeed gathered at the corner of CSFs bridge which would cause large defects between fibers.

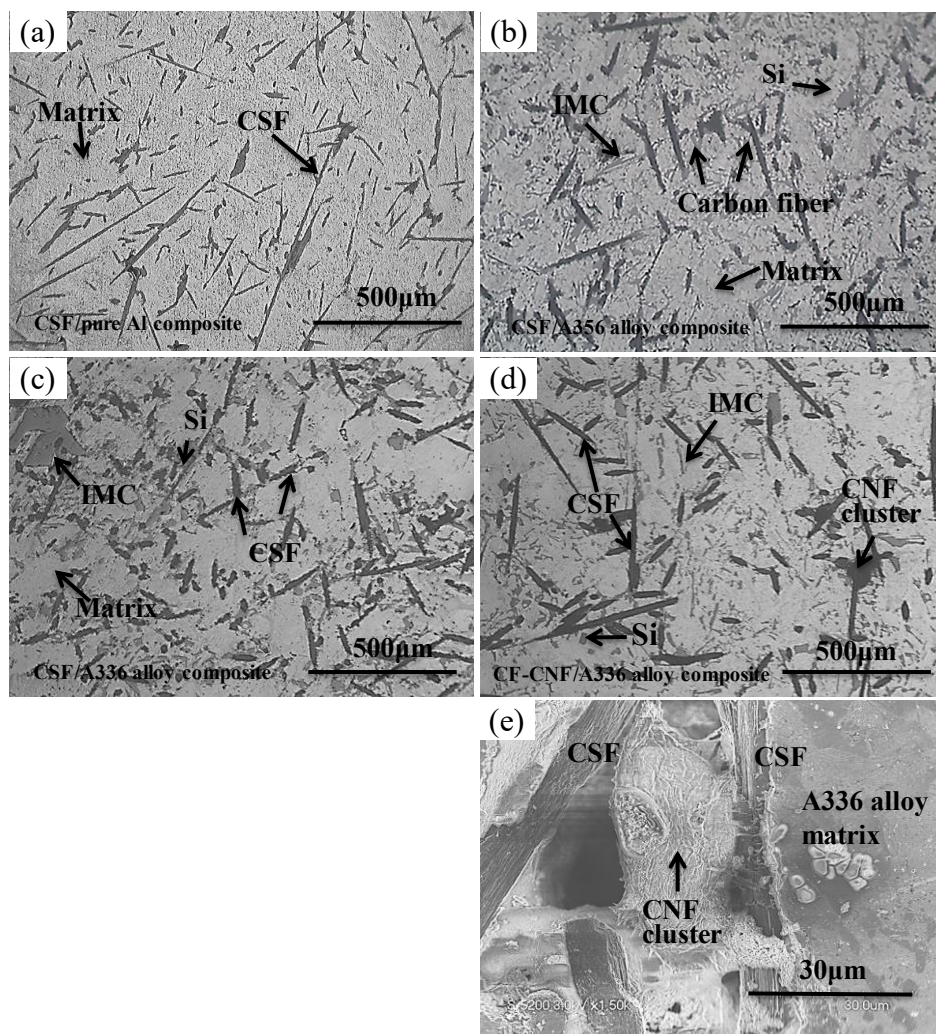


Fig. 2-6 OM and SEM images of the composites: (a) CSF/A1070 composite (OM), (b) CSF/A356 alloy composite (OM), (c) CSF/A336 alloy composite (OM), (d) CSF-CNF/A336 alloy composite (OM) and (e) enlargement of CNF cluster (SEM).

Figure. 2-7 shows the microstructure of the CSF/Al matrix composites with SiO₂ binder. Figs. 2-7 (a) - (a'') are SEM images of CSF/A1070 composite. Figs. 2-7 (b) - (b'') are SEM images of CSF/A356 alloy composite. Figs. 2-7 (c) - (c'') are SEM images of CSF/A356 alloy composite. Figs. 2-7 (d) - (d'') are SEM images of hybrid CSF-CNF/A336 alloy composite. Figs. 2-7 (a), (b), (c) and (d) show the low magnification microstructures of composites, which displayed an overall morphology of composites. Fig. 2-7 (a) shows that many large defects were generated inside CSF clusters and between CSF/matrix. Figs. 2-7 (b), (c) and (d) show that Si phase and intermetallic compound (IMC) were generated in the matrix, also, defects existed. Noticed that Figs. 2-7 (c) and (d) showed more content of IMCs due to a higher content of Ni element of A336 alloy. In Fig. 2-7 (a'), it can be clearly seen the morphology of defects which were caused by the poor fluidity of A1070 Al. It was obviously discovered that the amount and size of defects were decreased due to the Si element of A356 alloy and A336 alloy which effectively increased the fluidity of alloys as shown in Figs. 2-7 (b') and (c'). EDS analysis was conducted to analysis the IMC in composite In Fig. 5 (c'). EDS analysis result of point A (white phase) is shown in Table 2-4, which proved the existence of the Al₃Ni phase. The Al₃Ni phase formation sequence was described as the following equation [35]:

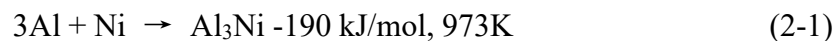


Fig. 2-7 (d') shows that CNFs were agglomerated at the corner of CSFs. Defects would arise from entrapped gases at the corner of the CNFs cluster, the alloy was hard to infiltrate into the corner and finally generated defects. Figs. 2-7 (a'') - (d'') shows the high magnification microstructures of composites, which all showed the interface layers emerged between CSF and matrix which supposed to be caused by the reaction between SiO₂ binder and Al matrix.

Table 2-4 EDS point analysis result of IMC of CSF/A336 alloy composite in Fig. 2-7 (b'), white phase.

Element	Wt.%	At%
Al	73.42	57.87
Ni	26.58	42.13

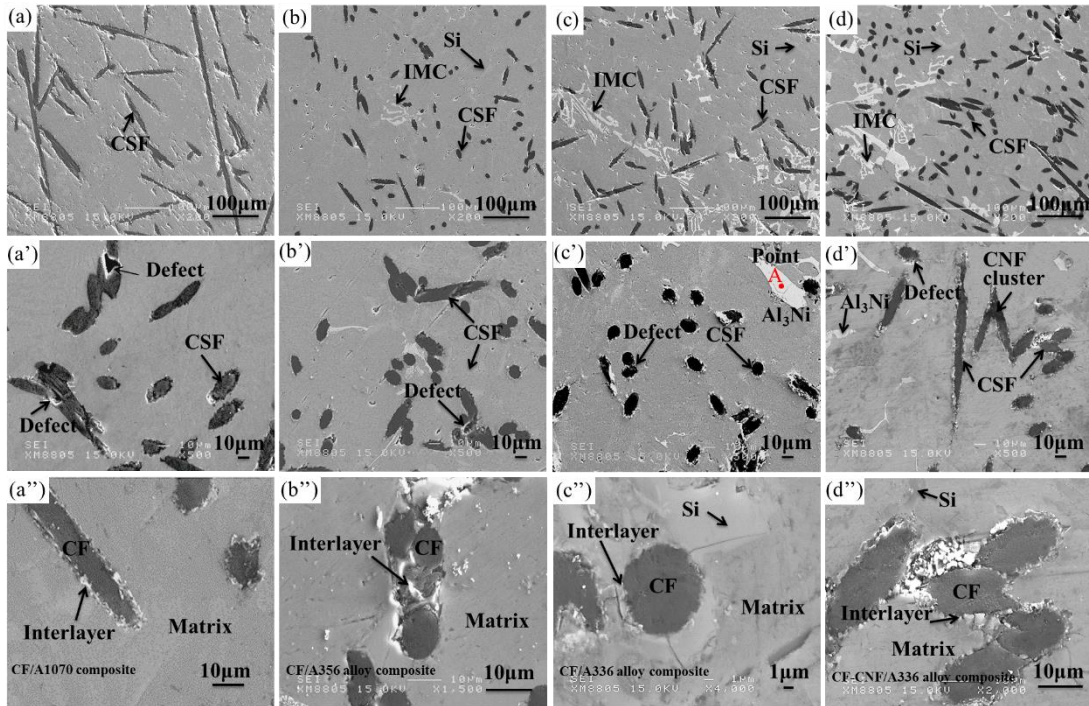


Fig. 2-7 SEM images of composites: (a), (a'), (a'') CSF/A1070 composite, (b), (b'), (b'') CSF/A356 alloy composite, (c), (c'), (c'') CSF/A336 alloy composite and (d), (d'), (d'') CSF-CNF/A336 alloy composite.

Figure 2-8 shows the results of area elemental mapping and point analysis of CSF/A336 alloy composite. The elemental mapping shows an obvious oxide layer were generated at the interface between CSF and matrix caused by the interfacial reaction (equation 2-2) between Al and SiO₂ binder. The dark phase was Si phase which precipitated from the matrix during solidification and the gray phase was Al₃Ni IMC. The point analysis of point A revealed that the oxide layer consisted of Al₂O₃ and SiO₂. The introduction of SiO₂ binder was expected to promote the wettability between fibers and molten Al. Laurent et al [36]. investigated the wettability of SiO₂-Al system and concluded that the SiO₂-Al system transformed from nonwetting system of 150° to a wetting system of 68° at melting temperature of 1073K. Therefore, the SiO₂ binder which coating on the fiber surface encouraged the molten Al to infiltrate into preform by reaction with molten Al alloy to accomplish densification of the composites. The reaction between the Al and SiO₂ binder can be presented as following [36]:



Furthermore, the reaction between Al and SiO₂ binder was also contributed to increasing the relative density of the CSF/Al matrix composites.

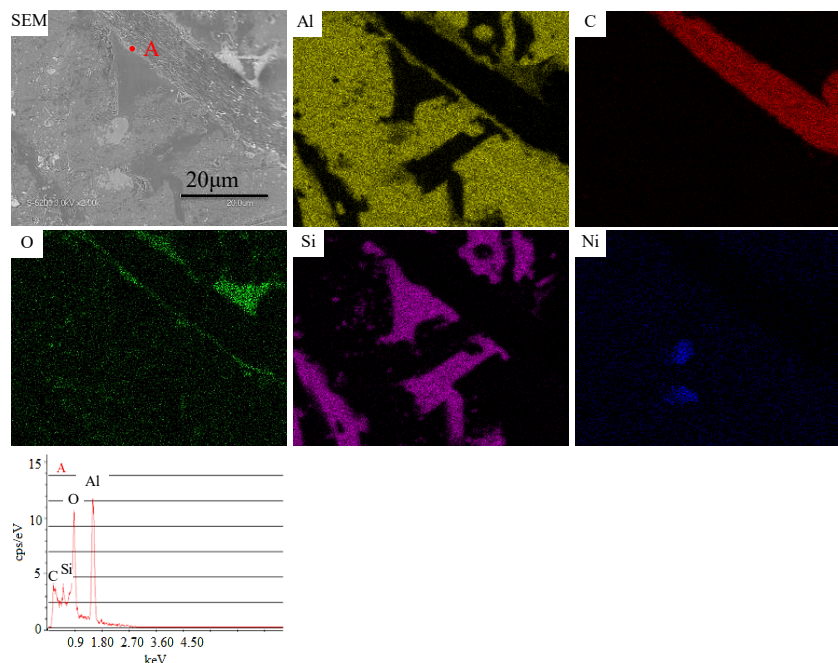


Fig. 2-8 Results of area elemental mapping and point analysis of CSF/A336 alloy composite.

For analyzing the imperfect penetration phenomenon of CSF/Al matrix composites, the microstructure of defects and area elemental mapping of CSF /Al matrix composites and CSF-CNF /A336 alloy composite were shown in Fig. 2-9 (a) – (d). CSF /A1070 composite exhibited large size defects in the region of CSF clusters with a size of about 25 μm as shown in Fig. 2-9 (a). These defects manifested because of the agglomeration of CSFs by the SiO_2 binder and the poor fluidity of A1070 resulted in molten Al could not infiltrate into the narrow space between CSFs cluster. Meanwhile, besides the oxides layer at the interface between CSF and matrix, oxides were also observed at the edge of defects from the area elemental mapping, which meant air cannot be removed in the region of CSFs agglomeration, causing pores to remain in the composite and oxidizing the matrix at the edge of the defect. For the CSF/A356 and A336 alloy composites of Figs. 2-9 (b) and (c), the defects were generated at the region of CSFs cluster similar to CSF /A1070 composite, defect size was approximately 20 μm and 10 μm , respectively. The existence of Si element in Al alloys promoted the metal fluidity for better infiltration and helped to realize a much denser composite. Especially, Fig. 2-9 (c) possessed the smallest defect size due to the highest amount of Si element (13 mass%) of A336 alloy. The smallest defect would contribute to the highest relative density of CSF/A336 alloy composite.

Fig. 2-9 (d) shows the defect of CSF-CNF/A336 alloy composite, CNFs were stuck and gathered at the intersection of CSFs by SiO_2 binder which can be concluded from the distribution of C and O elements in area elemental mapping. It can be found that there existed imperfect infiltration defects at the CSF-CNF agglomeration place in the composite, defect size was approximately 60 μm . The imperfect infiltration defects were related to the structure of CSF-CNF hybrid preform, some CNFs were attached on the surface of CSFs, while, most CNFs were entangled at the intersection of CSFs. During infiltration, the molten Al preferentially infiltrated into the large area of the preform, the narrow space in the region of CSF-CNF coexisted place was hard to be infiltrated because of the existence of extra capillary resistance which obstructed the smooth infiltration.

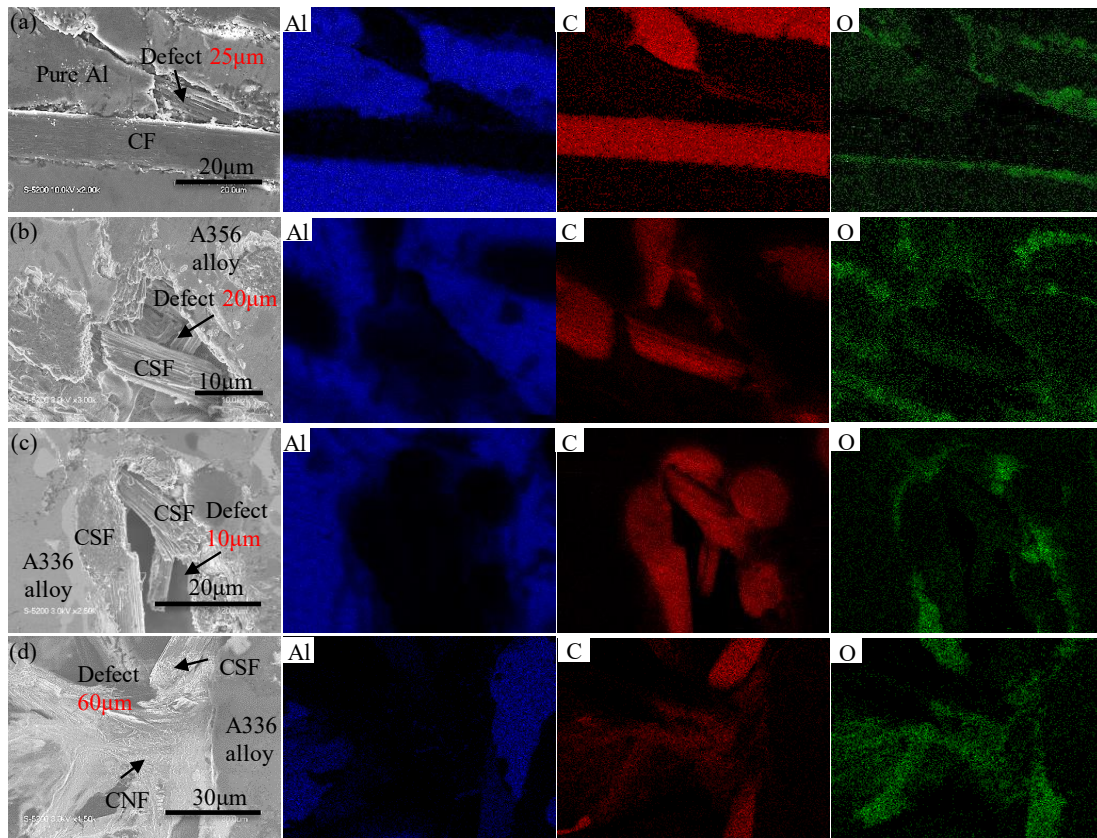


Fig. 2-9 Defects and area elemental mapping of CSF/Al matrix composites:
(a) CSF/A1070 composite, (b) CSF/A356 alloy composite, (c) CSF/A336 alloy composite and (d) CSF-CNF/A336 alloy composite.

It has been known that Al_4C_3 is prone to be formed at the CF/Al interface at temperatures above 773 K and it deteriorates the mechanical property and TC of composites. The LPI process was carried out at a temperature of 1073 K in the present study, Al_4C_3 may have formed in the composite. Therefore, in order to investigate the existence of Al_4C_3 and analyze the infiltration mechanism due to the presence of SiO_2 binder, XRD analysis was performed.

Figure 2-10 represents the X-ray diffraction (XRD) result of CSF/A336 alloy composite with SiO_2 binder. The XRD result indicated that the A336 alloy matrix reacted with SiO_2 binder according to the equation 2-2, which was confirmed by the presence of the $\gamma-Al_2O_3$. That is the SiO_2 binder coating on fibers reacted with the A336 alloy matrix and generated Al_2O_3 as well as Si, the interaction would improve the wettability of CSF and Al, the Al_2O_3 reactant can contribute to the enhancement of mechanical properties of the composite. MgO was produced by the interfacial reaction between A336 alloy and SiO_2 binder as $2Mg + SiO_2 \rightarrow 2MgO + Si$, and $MgAl_2O_4$ was also detected which was generated by the interfacial reaction between $\alpha-Al_2O_3$ and MgO as i.e. $\alpha-Al_2O_3 + MgO \rightarrow MgAl_2O_4$. It is noticed that the generation of MgO and $MgAl_2O_4$ could improve interfacial wettability [37].

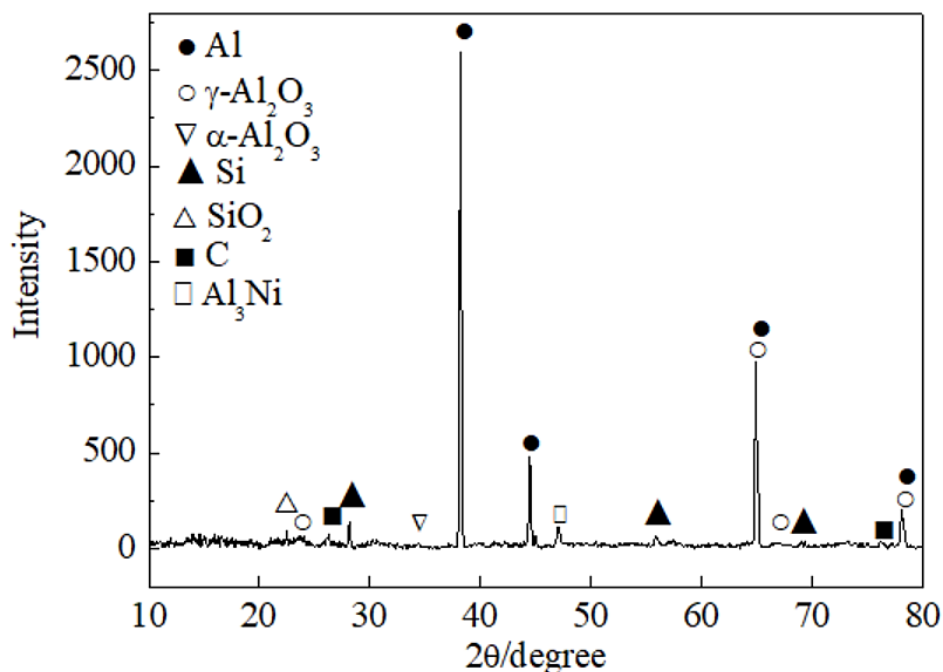


Fig. 2-10 Results of X-ray diffraction spectra of CSF/A336 alloy composite.

2.3.2 Interface structure between CSF and aluminum matrix

Figure 2-11 shows the typical transverse microstructure of pitch-based CF and K13D2U pitch based CF used in this study. It was summarized the main microstructure of pitch-based CF contained radial, random and onion skin forms [38]. The pitch based (K13D2U) CF derived from an anisotropic pitch exhibited zigzag micro texture as shown in Figs. 2-11 (a) and (b). Figs. 2-11 (c) and (d) show the structure of CF by TEM, two kinds of structures were observed which presented stacking structure marked as A and short curved structure marked as B. The two types of domains formed a zigzag nanostructure. This domain structure was known as pitch structure. The different forms of structure were supposed to have different effects on the interfacial reaction between CF and the Al matrix.

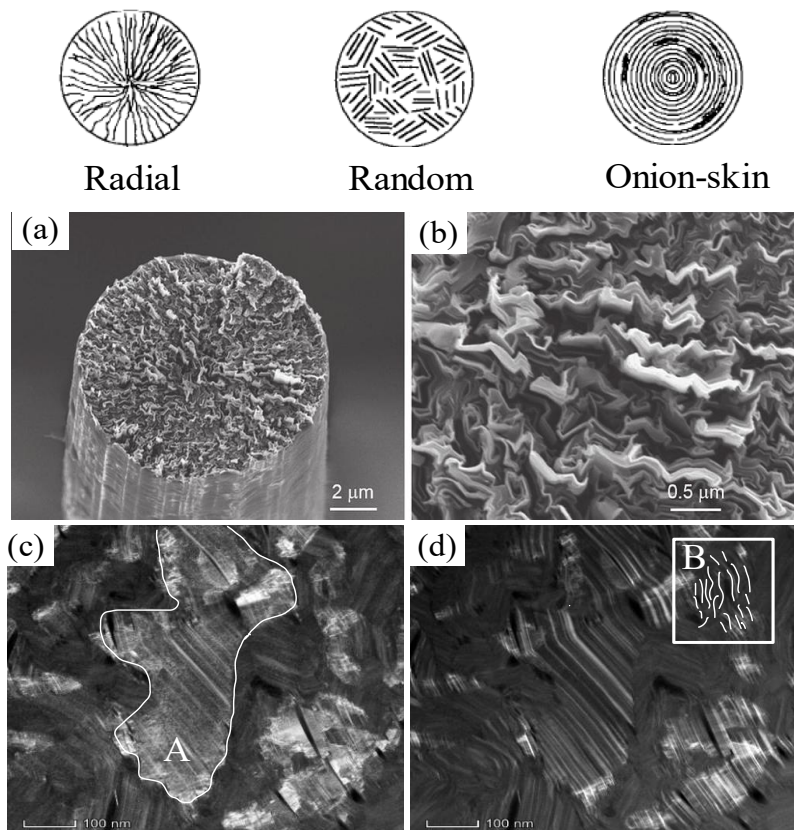


Fig. 2-11 Typical transverse microstructure of pitch based and K13D2U pitch CSF used in this study. (a), (b) SEM images of CF, (c), (d) TEM images of CF.

Figure 2-12 shows HAADF image and area elemental mapping of CSF/A336 alloy composite by TEM. It demonstrated that there were Al_2O_3 oxides existed at the interface between CSF and matrix, while, the thickness of the interface layer was not uniform. Therefore, it is essential to analyze the effect of structure of CF on interfacial reaction and the interface structure between CF and Al matrix. Figure 2-13 shows the TEM images of interface and interfacial reactions between CF and Al of CSF/A336 alloy composite. Fig. 2-13 (b) shows the interface was continuous, no microscopic holes, cracks or other defects were found at the interface which indicated that good metallurgical bonding between CF and matrix was achieved. Figs. 2-13 (c) and (d) indicate the Al_2O_3 was generated at the interface according to the equation 2-2, the shape and thickness of the Al_2O_3 layer varied with CF structure. Meanwhile, no Al_4C_3 was generated at the interface, which meant the SiO_2 binder coating on the surface of CSF prevented the formation of Al_4C_3 . Fig. 2-13 (e) shows the TEM image of high magnification of interface, it was observed the interface presented an amorphous structure, and the thickness of interface was not uniform. CF behaved short curved structure and stacking structure which formed a thin or thick interface layer.

Figure 2-14 shows the schematic diagram of interface formation with different structure of CF. As for the structure of CF which contained two types of structures of stacking structure and short curved structure. The stacking structure presented a smooth laminar structure with the carbon layers oriented parallel within each crystallite in the fiber lattice unit. The short curve structure had the carbon layers in the form of small curved crystallites with exposed carbon atoms and interstices within each crystallite. During the preform manufacturing process with SiO_2 binder, lot of SiO_2 binder molecular was prone to attach to the interstices of short curved structure, therefore, a thick interface layer was tended to form where short curved structure existed.

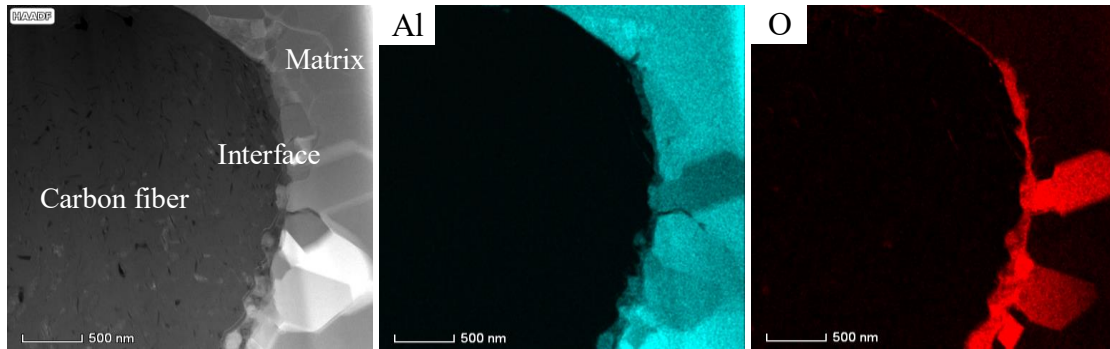


Fig. 2-12 TEM image and area elemental mapping of CSF/A336 alloy composite.

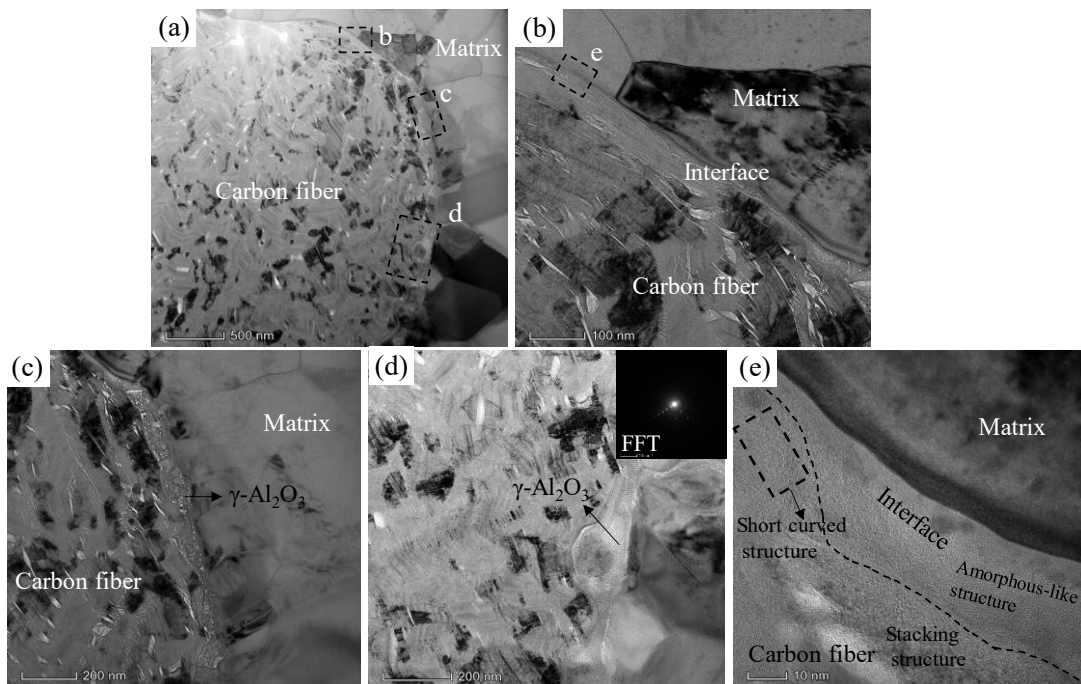


Fig. 2-13 TEM images of interface and interfacial reactions between CF and Al of CSF/A336 alloy composite: (b) interface and (c), (d), (e) interfacial reactions.

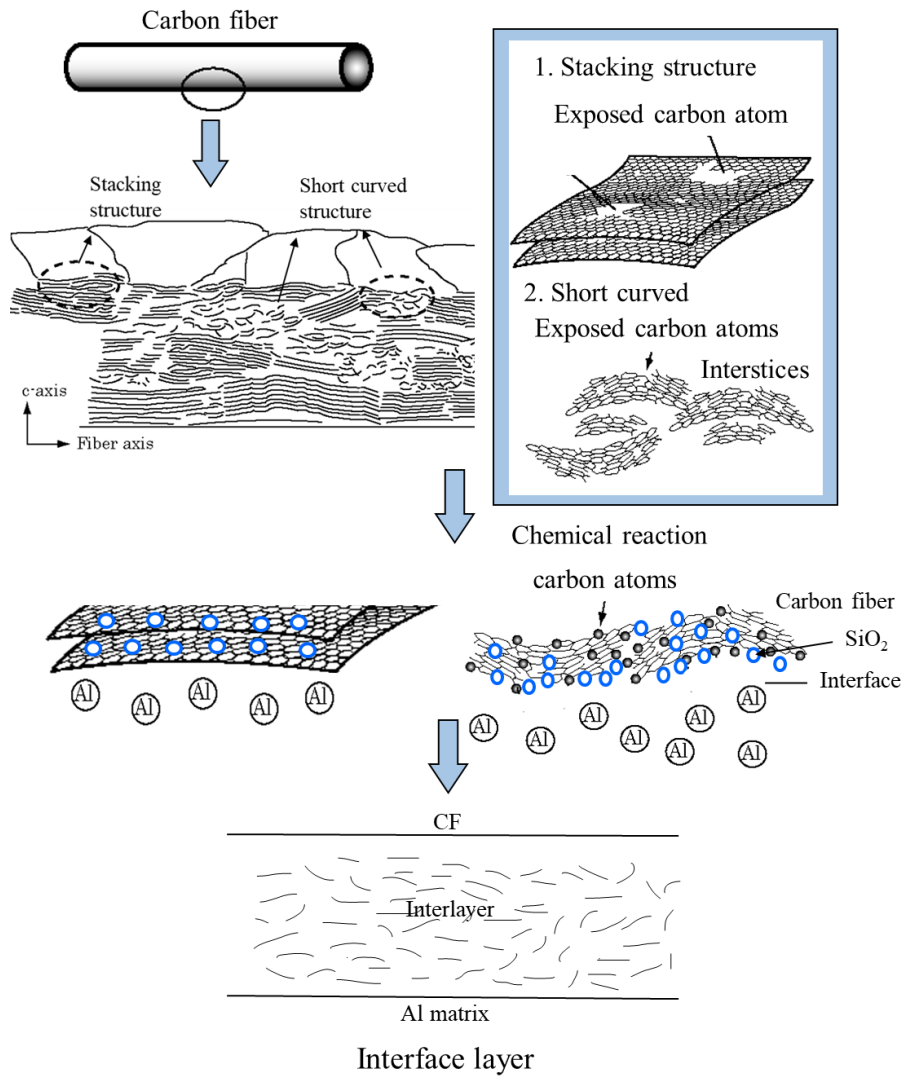


Fig. 2-14 Schematic diagram of interface formation with different structure of CF.

2.4 Summary

(1) CSF preform and CSF-CNF hybrid preform were prepared with SiO₂ binder. SiO₂ binder layer was coated on the surface of CSFs and CSFs were cross linked and clustered together by SiO₂ binder. CNFs were attached on the surface of CSF as well as mostly agglomerated together at the corner of CSFs bridges.

(2) The CSF/Al matrix composites and CSF-CNF/A336 alloy composite were fabricated in conjunction with LPI process. In all CSF/Al matrix composites, CSFs were random distributed in the matrix, CNFs were observed at the corner of cross-linked CSFs. An obvious oxide layer was discovered between CSF and Al matrix, which was proved to be γ -Al₂O₃, generated by the interfacial reaction of SiO₂ binder and Al matrix.

(3) The pitch-based CF possessed two types of structure, stacking structure and short curved structure. The interface thickness between CSF and Al matrix was not uniform, the stacking structure formed a thin interface and the short curved structure formed a thick interface.

References

- [1] P. K. Schelling, L. Shi and K. E. Goodson: *Mater. Today*, **8** (2005) 30-35.
- [2] K. Mizuuchi, K. Inoue, Y. Agari, T. Nagaoka, M. Sugioka, M. Tanaka, T. Takeuchi, J. Tani, M. Kawahara and Y. Makino: *Compos. Part. B. Eng.* **43** (2012) 2012-2019.
- [3] B. G. Kim, S. L. Dong and S. D. Park: *Mater. Chem. Phys.* **72** (2001) 42-47.
- [4] A. Rape, S. Chanthapan, J. Singh and A. Kulkarni: *J. Mater. Sci.* **46** (2011) 94-100.
- [5] L. Duan, W. Lin, J. Wang and G. Yang: *Int. J. Refract. Met. H.* **46** (2014) 96-100.
- [6] G. B. V. Kumar, C. S. P. Rao, N. Selvaraj, *J. Miner. Mater. Charact. Eng.* **10** (2011) 59–91.
- [7] H. Guo and Z. Zhang: *Met. Powder Rep.* **73** (2018) 62-67.
- [8] M. Li, K. Ma, L. Jiang, H. Yang, E. J. Lavernia, L. M. Zhang and J. M. Schoenung: *Mater. Sci. Eng. A.* **656** (2016) 241-248.
- [9] O. Lee, M. H. Lee, Y. B. Choi, K. Sugio, K. Matsugi and G. Sasaki: *Mater. Trans.* **55** (2014) 827- 830.
- [10] A. Esawi and K. Morsi: *Compos.* **38** (2007) 646-650..
- [11] H. Lu, F. Liang, Y. Yao, J. Gou and D. Hui: *Compos.* **59** (2014) 191-195.
- [12] M. Yang, L. Weng, H. X. Zhu, F. Zhang, T. X. Fan and D. Zhang: *Scr. Mater.* **138** (2017) 17-21.
- [13] M. K. Akbari, H. R. Baharvandi and O. Mirzaee: *Compos.* **55** (2013) 426-432.
- [14] J. Park and M. Oh: *Scr. Mater.* **133** (2017) 54-58.
- [15] F. P. M. Geffroy, T. Chartier and J. F. Silvain: *J. Eur. Ceram. Soc.* **27** (2007) 291-299.
- [16] E. Neubauer, M. Kitzmantel, M. Hulman and P. Angerer: *Compos. Sci. Technol.* **70** (2010) 2228-2236.
- [17] J. J. Zhang, S. Ch. Liu, Y. P. Lu, L. Jiang, Y. B. Zhang, T. J. Li: *J. Mater. Sci. Technol.* **33** (2017) 623-629.
- [18] X. Cao, Q. Y. Shi, D. M. Liu, A. L. Feng, Q. Liu and G. Q. Chen: *Compos.* **139** (2018) 97-105.

- [19] A. Daoud: Mater. Sci. Eng. A. **391** (2005) 114-120.
- [20] E. Sato, T. Takahashi, T. Natsume and K. Koyama: Tanso. **109** (2003) 159–164.
- [21] Z. F. Xu, Y.B. Choi, K. Matsugi, D.C. Li and G. Sasaki: Mater. Trans. **50** (2009) 2160-2164.
- [22] S. Ghanaraja, K. L. V. Kumar, H.P. Raju and K. S. Ravikumar: ELSEVIER, Science Direct Materials Today: Proceedings, **2** (2015) 1291-1300.
- [23] M. Oghbaei and O. Mirzaee: J. Alloy. Comp. **494** (2010) 175-189.
- [24] Z. F. Xu, Y. B. Choi, K. Matsugi, D. C. Li and G. Sasaki: Mater. Trans. **50** (2009) 2160-2164.
- [25] K. Fukuchi, K. Sasaki, K. Katagiri, T. Imanishi and A. Kakitsuji: Procedia Engineering, **10** (2011) 912–917.
- [26] Vinitha and B. S. Motgi: International Journal for Scientific Research and Development, **2** (2014) 190-193.
- [27] S. Lai and D. D. L. Chung: J. Mater. Sci. **29** (1994) 3128-3150.
- [28] X. F. Yang and X. M. Xi: J. Mater. Res. **10** (1995) 2415-2417.
- [29] Y. B. Choi, K. Matsugi, G. Sasaki, K. Arita and O. Yanagisawa: Mater. Trans. **47** (2006) 1227–1231.
- [30] Y. B. Choi, G. Sasaki, K. Matsugi, N. Sorida, S. Kondoh, T. Fujii and O. Yanagisawa: JSME A, **49** (2006) 20-24.
- [31] K. Matsugi, Y. B. Choi, K. Arita, O. Yanagisawa, G. Sasaki: J. Jpn. Inst. Light Met. **58** (2008) 71-80.
- [32] J. Kaczmar, K. Naplocha and J. Morgiel: J. Mater. Eng. Perform, **23** (2014) 2801-2808.
- [33] Q. B. Zeng: J. Appl. Polymer Sci. **70** (1998) 177-183.
- [34] T. P. D. Rajan, R. M. Pillai and B. C. Pai: J. Mater. Sci. **33** (1998) 3491-3503.
- [35] Y. B. Choi, T. Motoyama, K. Matsugi and G. Sasaki: Met. Mater. Inter. **20** (2014) 741-745.
- [36] V. Laurent, D. Chatain and N. Eustathopoulos: Mater. Sci. Eng. A. **135** (1991) 89–94.
- [37] Z. Q. Yu, G. H. Wu, D. L. Sun and L. T. Jiang: Mater. Lett. **57** (2003) 3111-3116.
- [38] D. D. Edie: Carbon, **36** (1998) 345-362.

Chapter 3

Fabrication process and microstructure of nickel plated carbon short fiber reinforced aluminum matrix composites by low pressure infiltration process

3.1	<i>Introduction</i>	70
3.2	<i>Experimental procedure</i>	72
3.2.1	<i>Raw materials and electroless Ni plating process</i>	72
3.2.2	<i>Electroless Ni plating of CSFs</i>	73
3.2.3	<i>Fabrication of Ni plated CSF reinforced aluminum matrix composites without preform manufacturing</i>	76
3.2.4	<i>Evaluation methods and equipment</i>	78
3.2.4.1	<i>Observation of microstructure</i>	78
3.2.4.2	<i>Measurement of thickness of Ni layer</i>	78
3.2.4.3	<i>X-ray diffraction characterization</i>	78
3.3	<i>Results and discussion</i>	79
3.3.1	<i>Microstructures</i>	79
3.3.1.1	<i>Microstructures of Ni plated CSFs</i>	79
3.3.1.2	<i>Microstructures of Ni plated CSF/Al matrix composites</i>	84
3.3.2	<i>Wetting and dispersion behavior of Ni plated CSF in composites</i>	93
3.4	<i>Summary</i>	96
	<i>References</i>	97

3.1 Introduction

AMCs are among the most popular of MMCs due to major advantages in both processing and final properties. Al matrix reinforced with CFs can show superior specific stiffness, high strength, high TC, low CTE, and good wear resistance compared to their conventional polymer matrix composite and unreinforced aluminum alloy counterparts [1-3]. Because of the high-temperature strength and the self-lubrication effect of the CFs [4], CFs have attracted a lot of attention in various fields and have been considered as an ideal candidate for the reinforcement of multifunctional composites and structural applications. Recent studies on the use of CFs in Al matrix composites have mainly involved the enhancement of the mechanical properties [5, 6], along with the improvement of the TC [7] and the reduction of coefficient of thermal expansion of the composites [8].

A variety of manufacturing processes have been introduced in the field of discontinuous reinforcement metal matrix composites in order to obtain the high-performance materials. The fabrication of MMCs was divided into two main routes: solid state process such as powder metallurgy (PM) [9, 10] and liquid state process: casting methods [11, 12]. In case of PM, the complex equipment and high energy consumption limit its widely used. The conventional casting processes such as squeeze casting has some disadvantages contain the limiting degree of freedom in shape of productions, fiber fracture and deformation of the fiber preform by applying high pressure of composites [13]. LPI process which is belonged to the casting method is easily adaptable and economically viable [14]. The LPI process enabled complex or large shape fabrication with relatively simple facilities, cost-effective fabrication by applying low pressures ($\cong 1$ MPa). For the liquid-metal-infiltration process of the CSF/Al based composite, inorganic binders are commonly used for the CSF preform manufacturing. However, the preform with an inorganic binder is complicated which requires sintering at high temperatures for a long duration, necessitating large energy inputs and preparation time. Therefore, a new manufacturing process is the need of the hour for manufacturing CSF/Al composite

The problem associated with the fabrication of CF/Al matrix composites is the poor

wettability between CFs and molten Al. It is noted that the highest wettability exists between the liquid metals and solid metals in case of mutual solubility or the formation of inter-metallic compounds. Therefore, the infiltration is much easier by the desorption of a metallic coating on the surface of the reinforcement ^[15]. Ni is frequently used for coating reinforcements to facilitate the wetting with Al matrix ^[16, 17]. It has been found that nickel coatings can improve the wetting behavior of CFs by molten Al and effectively avoid the interaction of CF and Al to prevent the generation of Al₄C₃ ^[18].

In this study, a novel alternative fabrication process without preform manufacturing was developed for CSF/Al matrix composite by LPI method. Especially, in order to improve the wettability and prevent the chemical reaction between CSF and Al matrix, electroless Ni plating process was adopted and conducted on CSFs. Moreover, the microstructure of Ni plated CSFs, the effects of Ni plated CSFs and the applied pressure on microstructures of composites were investigated.

3.2 Experimental procedure

3.2.1 Raw materials

A1070 pure Al, A356 alloy and A336 alloy are used as the matrix for composites and used for performance comparison with composites. The chemical compositions of A1070, A356 alloy, and A336 alloy are listed in Table 3-1. Noticing that the three types of matrix contain different kinds and contents of alloying elements. The coal tar pitch based CFs (K13D2U, Mitsubishi Plastics, Inc. diameter 11 μm , the aspect ratio of 230) were used as reinforcement in this study. Table 3-2 shows the physical and mechanical properties of the CSF and the Al matrix. The CFs have light weight, high tensile strength and low CTE with excellent TC [19].

The Al and its alloys have relatively good TC, low CTE and light weight in the field of metal. The A1070 with the purity of 99.7% has a high TC of $237 \text{ W}\cdot\text{m}^{-1}\cdot\text{K}^{-1}$. In addition, the A356 and A336 alloys have relatively low TC but high tensile strength compared to A1070 because of the composition elements of Si and Mg in A356 alloy, and the composition elements of Si, Ni, Cu and Mg in A336 alloy.

Table 3-1 Chemical composition of A1070, A336 alloy and A356 alloy (mass%).

Matrix	Si	Cu	Mg	Ni	Fe	Al
A1070	<0.2	<0.04	<0.03	<0.05	<0.25	99.7
A356 alloy	6.5-7.5	<0.2	0.25-0.45	<0.05	<0.5	Bal
A336 alloy	11-13	0.5-1.5	0.8-1.3	0.8-1.5	<0.7	Bal

Table 3-2 Properties of CSF and Al matrix for CF/Al matrix composites.

Material	Density (Mgm^{-3})	Tensile strength (MPa)	CTE ($\times 10^{-6}\text{K}^{-1}$)	TC ($\text{Wm}^{-1}\text{K}^{-1}$)
CF (K13D2U)	2.21	3700	-1.2	800
Al (A1070)	2.70	70	24	234
A356 alloy	2.68	200	21.5	159
A336 alloy	2.70	220	20	125

3.2.2 Electroless Ni plating of CSFs

In order to infiltrate the molten Al into porous CF easily by the LPI process, a good wettability between CFs and molten Al is required. Electroless Ni plating was conducted on the CSFs for improving wettability. Electroless Ni plating possesses some distinct collection of properties such as high hardness, excellent corrosion and wear resistance, fast plating rate, good deposit uniformity [20]. For this reason, electroless Ni has found wide applications in aerospace, automobile, electrical and chemical industries. The incorporation of additional metal elements into the electroless deposits can be an important way of enlarging the range of chemical and mechanical properties attainable. For Ni plating, the main binary alloys have been used such as Ni-P [21, 22] and Ni-B binary alloys [23, 24]. The properties of electroless Ni-B plating is often superior to those of deposits with other boron compounds or with sodium hypophosphite. The principal advantages of Ni-B electroless Ni deposits are its hardness and superior wear resistance in the as-deposited condition.

The electroless Ni plating process consisted of three well defined stages: sensitization, activation, and metallization. Table 3-3 summarizes the working procedure that had been used in this study [25]. Prior to plating, the CSFs were pre-heated in an air furnace for 10 min at 500 °C, then CSFs were ultrasonically degreased in acetone for 10 min followed by a rinse with distilled water. To catalyze the fibers, a two-step pretreatment of sensitization and activation was done. They were sensitized in SnCl₂/HCl solution for 15 min and then activated in PdCl₂/HCl solution for 15 min with ultra-sonication at room temperature. Finally, after filtration and rinsing, the CSFs were immersed in a Ni electroless plating solution (Okuno Chemical Industries Co., LTD Top Chem Alloy B-2.8 at.%). For obtaining the uniform, continuous and well-adhered Ni plated layer, plating was carried out under ultrasonic treatment by 60s, 90s, 120s and 180s irrespective of the deposition rate, the pH and temperature of the electroless plating bath were 6.5 and 313 K, respectively. After filtration and rinsing with distilled water, the electroless-plated CSFs were dried for 120 min at 333 K and stored for characterization.

The CSFs deposited by the electroless Ni plated was then observed by an electron probe micro-analyzer (EPMA, JXA-8900RL). EDS analysis was conducted by EDAX

Japan Genesis XM2 equipment. The thickness, hardness, structure, and morphology of the Ni deposit are greatly affected by the heat treatment [26]. Fig. 3-1 shows the variation of hardness of Ni-B films after heat treatment at various temperatures for 1h [27]. It is noted that the electroless Ni plated layer has a hardness of about Hv 600 when it is deposited. By performing an appropriate heat treatment, the electroless Ni plated is possible to exceed Hv1000 by the process of transformation of the amorphous phase to crystalline Ni and Ni boride (Ni₃B and Ni₂B) phases. The optimal heat treatment regime is 350 °C as it results in maximal hardness of the electroless Ni plated layer due to the growth of crystalline nickel and conversion of Ni₂B phase to the more stable Ni₃B phase [28].

Table 3-3 Solutions used for the different stages in the Electroless Ni plating process.

Stage	Solution
Sensitization	12g/l SnCl ₂ · 2H ₂ O
	40ml/l HCl
Activation	0.2g/l PdCl ₂ · 2H ₂ O
	2.5ml/l HCl
Metallization	24g/l NiSO ₄ · 6H ₂ O
	4.5g/l NiCl ₂ ·6H ₂ O
	3g/l H ₃ BO ₃
	HCl to control the pH

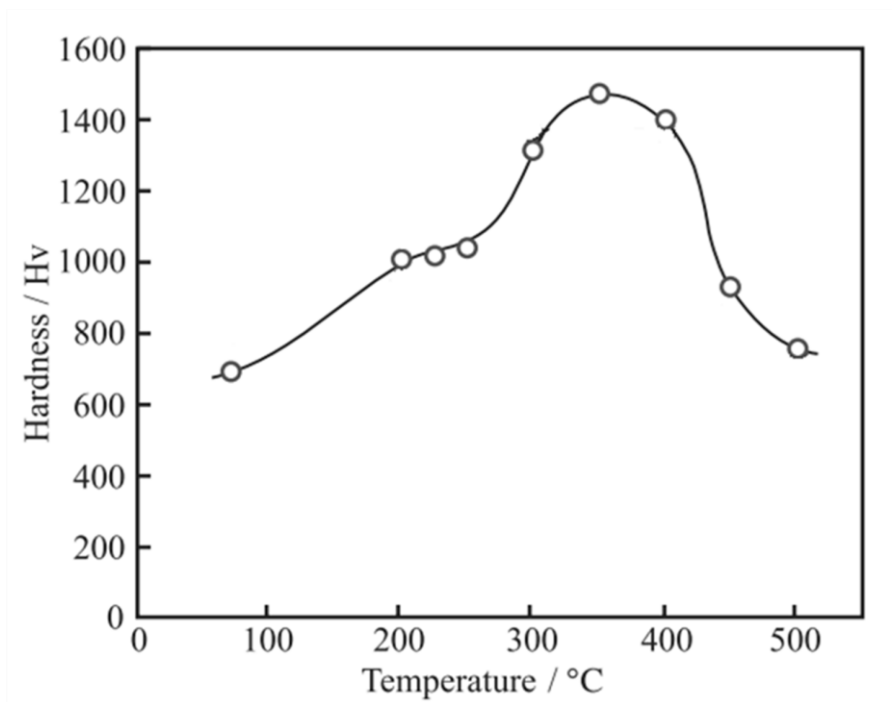


Fig. 3-1 Variation of hardness of Ni-B films after heat treatment at various temperatures.

3.2.3 Fabrication of Ni plated CSF reinforced aluminum matrix composites without preform manufacturing

Electroless Ni plated CSFs (plating time, 120s) were used as reinforcement for fabricating composites, wherein, the volume fraction of CSFs is 10 vol. %. Fig. 3-2 shows the schematic illustration of the new fabrication process without preform manufacturing by low-pressure infiltration method. The Ni plated CSFs were put into a graphite mold of diameter 10 mm with adjustable height. To achieve a volume fraction of 10 vol. %, the height was adjusted to 10 mm. Al ingot was placed on the fibers, then the total mold was put into LPI equipment and heating up to the temperature of 623K holding for 2h. (for better Ni deposit recrystallization, heat-treatment time was prolonged to 2h). Thereafter, the temperature was rise to 1073K for melting Al, the higher infiltration temperature than Al melting point (933 K) is able to lead the molten Al to be easily infiltrated with CSFs. The Ni plated CSFs/Al matrix composites were fabricated under the LPI process by means of the infiltration of molten Al and Al alloys into the Ni plated CSFs. The infiltration pressure was applied by the iron weight with a lever. The infiltration pressure of LPI process was 0.4 and 0.8 MPa, respectively. The environment for LPI process was argon in order to avoid the oxidation of Al and Ni plated CSFs. Finally, holding for 1h after infiltration and then furnace cooling.

For comparison of microstructure and properties of the composites, the manufacturing conditions and process of the preform with SiO₂ binder were procedures and conditions followed were those put forth by Choi et al ^[29] as mentioned in Fig. 2-1. CSFs with 10 vol. % were poured into distilled water mixed with 8 wt% SiO₂ binder, after stirring for 8 min then poured into the acrylic mold to eliminate the distilled water and press to height 20 mm. Afterwards, the preform was dried at 403K for 2h and then sintering at 1433K for 6h.

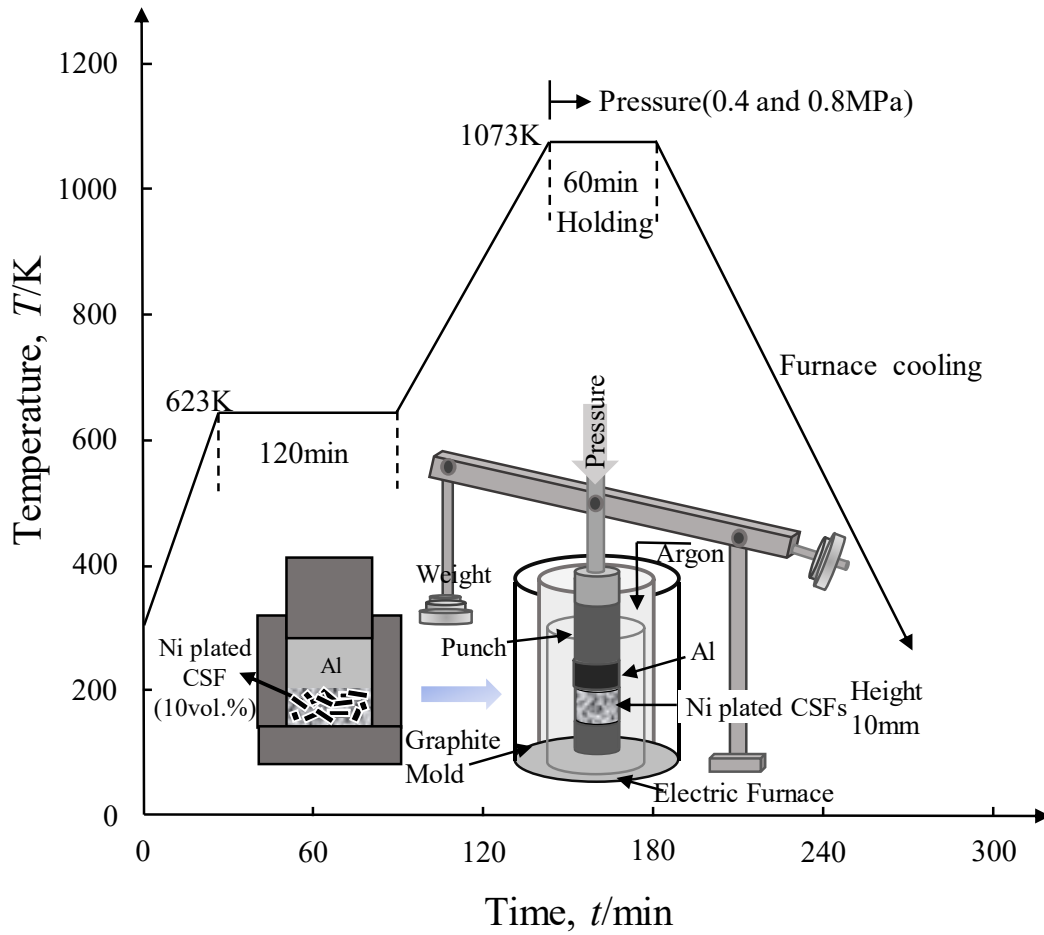


Fig. 3-2 Schematic illustration of the new fabrication process without preform manufacturing by low-pressure infiltration method.

3.2.4 Evaluation methods and equipment

3.2.4.1 Observation of microstructure

Samples for metallographic observation were cut from the composite along its transverse direction. The samples were carefully polished using waterproof abrasive SiC paper (#200, #600, #1000, #1500, #2000). The microstructures of the Ni plated CSF and composites were observed using an Electron Probe Micro-Analyzer (EPMA, JXA-8900RL). The elemental analysis was carried out by energy dispersive X-ray spectroscopy (EDS, S-5200 Energy Dispersive X-ray Analyzer, Hitachi, Japan). The image analysis was carried out by an image analyzer (Media Cybernetics Image-Pro Plus 5.0, Inc., USA).

3.2.4.2 Measurement of thickness of Ni layer

Thickness of Ni plated layer under different plating time by electroless plating process was measured by subtracting the diameter of Ni plated CSFs and as- received CSFs, then divided by two. The diameter of Ni plated CSFs is calculated by Image-Pro Plus 5.0 software.

3.2.4.3 X-ray diffraction characterization

X-ray diffraction (XRD) was carried out with a Rigaku Smart Lab, Japan. Using Cu K α radiation at 40 kv and 0.1A, a scan speed of 2°/min was used in the range of 20-80°.

3.3 Results and discussion

3.3.1 Microstructures

3.3.1.1 Microstructures of Ni plated CSFs

Fig. 3-3 shows SEM images of as received CSFs and electroless nickel plated CSFs by 60 to 180s plating time (pH of 6.5 and temperature of 313 K). As-received CSF presented a clean and smooth surface in Fig. 3-3 (a). In Figs. 3-3 (b), (c) and (e), CSFs were not uniformly plated with Ni layer, while left some unplated parts (Fig. 3-3 (b), (c)) and excessive nickel particles (Fig. 3-3 (e)) as pointed by arrows due to inappropriate (short or too long) plating time. In Fig. 3-3 (d), a perfect uniformly Ni-plated layer was obtained over the CSFs. In case of CSFs plating for 120s that the Ni particles on fiber surface grew gradually, met each other particles and formed a uniform metallic layer by the process of “layer formation”, which provided uniform wettability and protection over CSFs. Fig. 3-3 (f) shows that there was no oxygen or other atoms atomic peak which meant the surface of CSF (plating time, 120s) was wholly even covered by nickel layer. Therefore, Ni plated CSFs (plating time, 120s) were selected for fabrication composites. Figure. 3-4 shows the SEM images of surface view of the Ni plated CSFs and cross section view of the Ni plated CSFs. The average diameter of as-received CSF was 9.20 μm which is slightly smaller than the diameter data provided by the company as shown in Fig. 3-4 (a). Figs. 3-4 (b)- (e) show the diameters of Ni plated CSFs by different plating time, diameters were calculated by Image-Pro Plus 5.0 which were marked in the images. The average Ni plated layer thickness was also shown in the images. Figs. 3-4 (b’)- (e’) shows the cross-section view of Ni plated CSFs, the Ni plated layer on the surface of CSFs could be clearly observed.

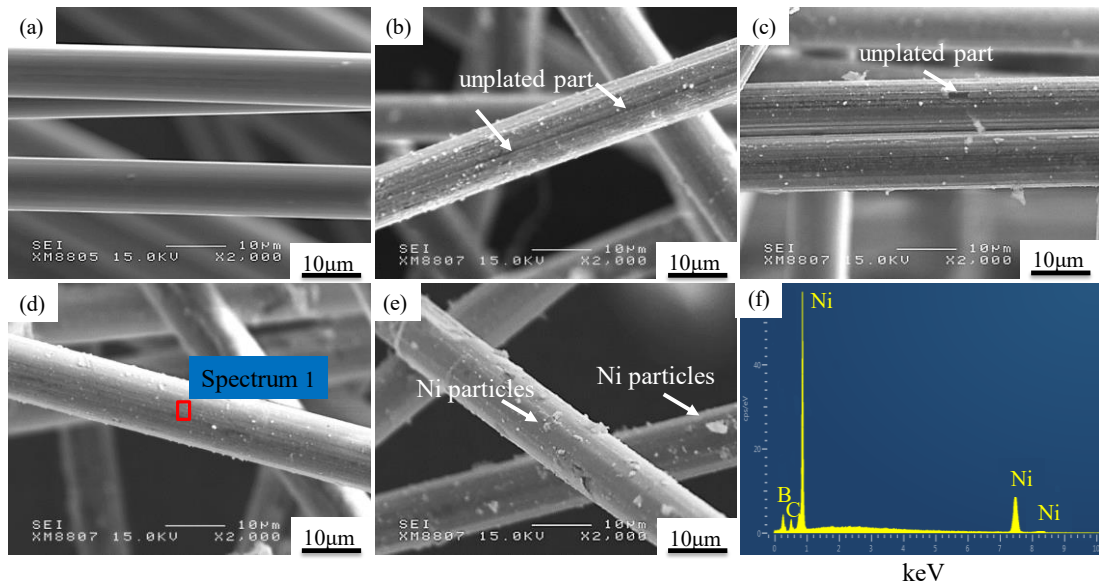


Fig. 3-3 SEM images of (a) as-received CSF, (b) Ni plated CSF (60s), (c) Ni plated CSF (90s), (d) Ni plated CSF (120s), (e) Ni plated CSF (180s) and (f) EDS data of Ni plated CSF (120s).

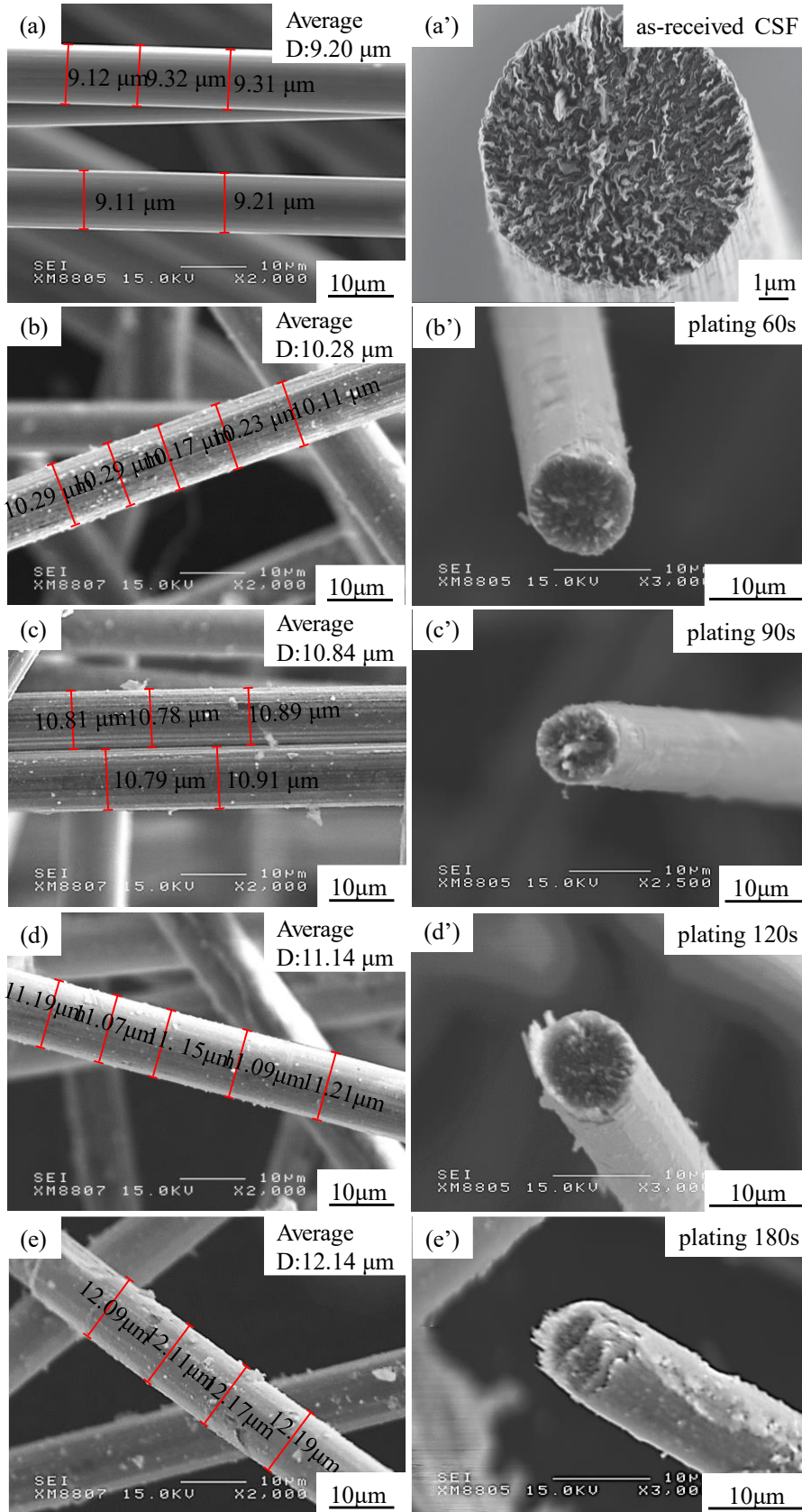


Fig. 3-4 SEM images of (a-e) surface view of the Ni plated CSFs, (a'-e') cross section view of the Ni plated CSFs.

Volume fraction of electroless plated Ni to CSF, the density of Ni plated CSF and the Ni plated thickness are summarized in Table 3-4. Fig. 3-5 and Fig. 3-6 show the effect of plating time on the volume fraction of Ni/CSF and the density of Ni plated CSFs. It can be noticed that the volume fraction of Ni/CSF and the density of Ni plated CSFs increased with increasing plating time. The trend line could provide a prediction for the nickel/CSF volume fraction and nickel-plated CSF density at the condition of further plating.

Table 3-4 Results of Electroless Ni plated CFs with different plating time.

Plating time (s)	Ni/CSF (Vol. %)	Ni/CSF (Wt. %)	Density of Ni plated CSF (g/cm ³)	Ni plated thickness (μm)
Ni-0	—	—	—	—
Ni-60	2.8	11.5	2.37	0.54 ^{+0.05} _{-0.02}
Ni-90	4.3	17.5	2.47	0.82 ^{+0.03} _{-0.13}
Ni-120	5.3	22.5	2.53	0.97 ^{+0.11} _{-0.02}
Ni-180	7.9	32.0	2.70	1.45 ^{+0.12} _{-0.01}

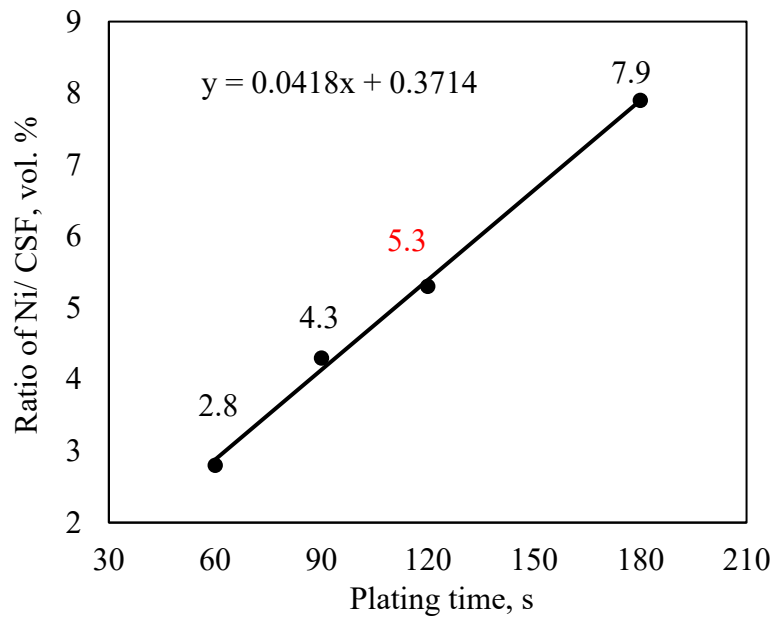


Fig. 3-5 Effect of plating time on volume fraction of Ni/CSF.

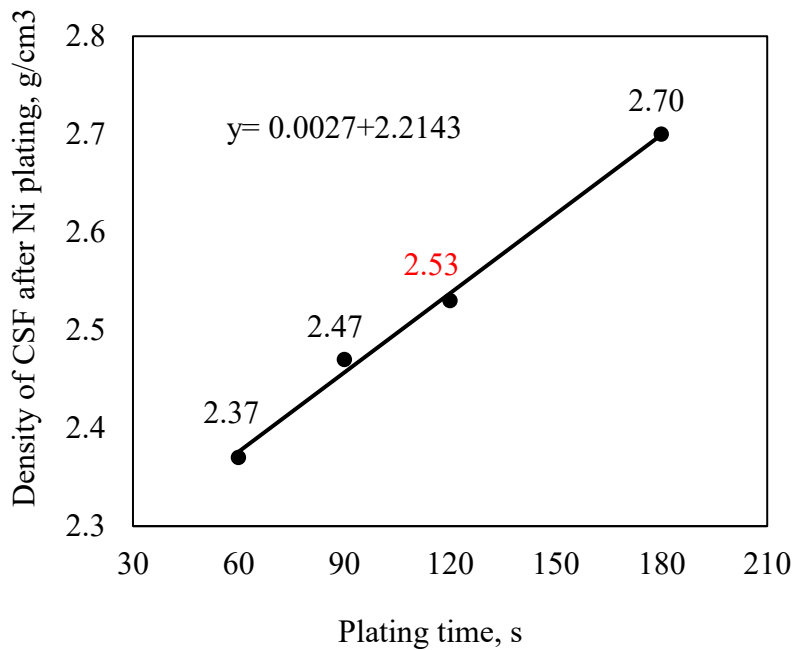


Fig. 3-6 Effect of plating time on the density of CSF.

3.3.1.2 Microstructures of Ni plated CSF reinforced aluminum matrix composites

Figure. 3-7 shows the microstructure of the Ni plated CSF/Al matrix composites fabricated under 0.4 MPa and 0.8 MPa, respectively. In Figs. 3-7 (a)-(c) fabricated by 0.4 MPa, and (d)-(f) fabricated by 0.8 MPa, it is observed that the CSFs were random distributed in the composites, white phases were formed around CSFs and some were dispersed in the matrix. The white phases were supposed to be Al-Ni compounds which were generated by not only the Ni plated layers dissolving and reacting with the Al matrix, but also the Ni element in the matrix promoted the formation of compounds. Therefore, the content of Al-Ni compound in Ni plated CSF/A336 alloy composites in Figs. 3-7 (c) and (f) was much higher than the other two composites due to a higher amount of Ni element of A336 alloy. Si phases were observed in Figs. 3-7 (b) and (c), (e) and (f) due to the existence of Si element in A356 and A336 alloys. In Figs. 3-7 (a) and (d), (b) and (e), (c) and (f), by comparison of the same kind of composite fabricated under 0.4 MPa and 0.8 MPa, CSFs have presented a relative aggregation in Figs. 3-7 (d), (e) and (f) due to a higher pressure of 0.8 MPa than 0.4 MPa.

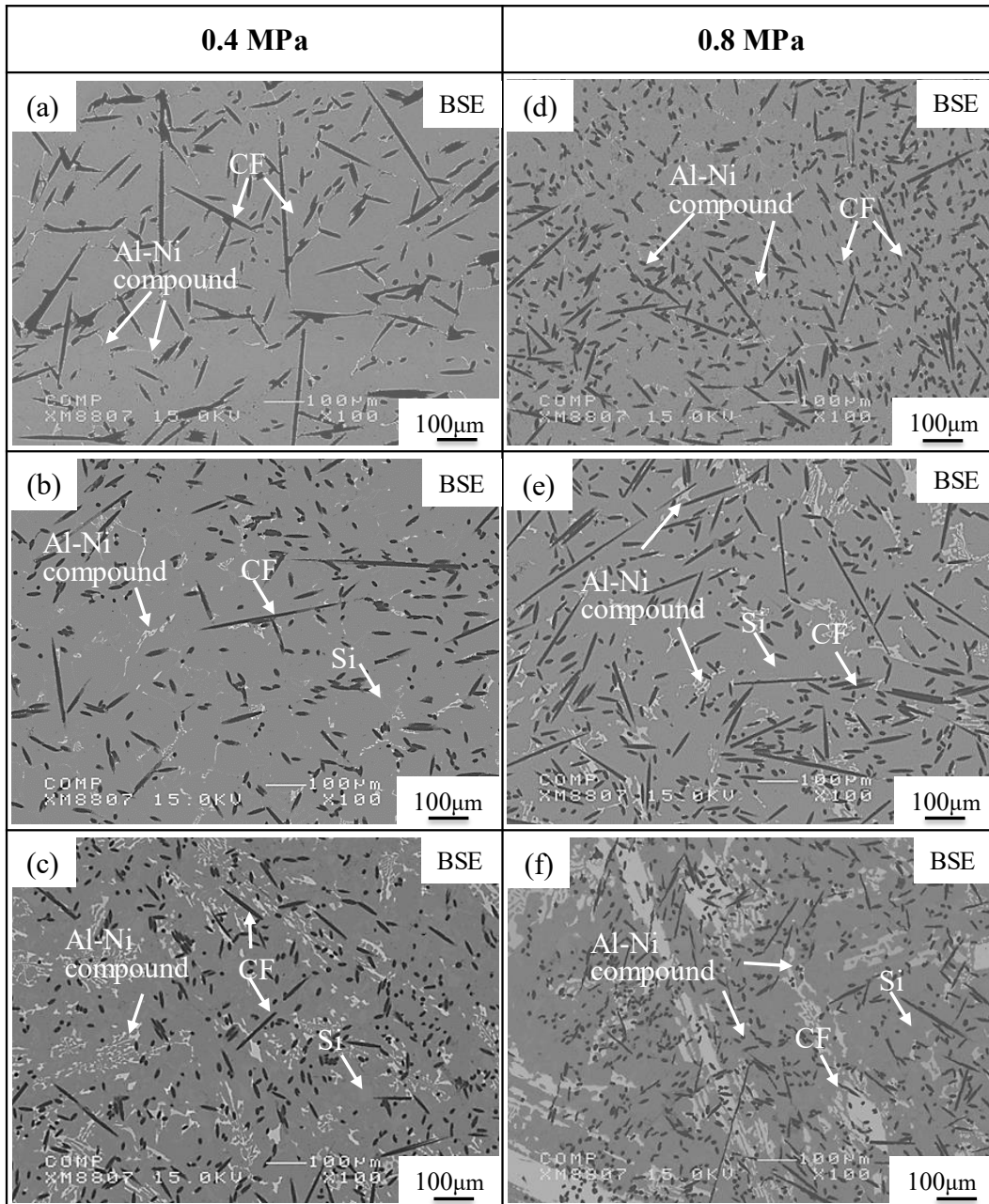


Fig. 3-7 Microstructures of composites (0.4 MPa and 0.8 MPa): (a), (d) Ni plated CSF/A1070 composite, (b), (e) Ni plated CSF/A356 alloy composite, and (c), (f) Ni plated CSF/A336 alloy composite.

Figure. 3-8 shows the image analysis of the Ni plated CSF/Al matrix composites fabricated under 0.4 MPa and 0.8 MPa, respectively. It is seen that the CSFs in Ni plated CSF/Al matrix composites (0.4 MPa) showed a volume fraction varied from 10.1% to 10.3% that was corresponding to the initially 10 vol. % CSFs. However, CSFs in composites (0.8 MPa) showed a relative higher volume fraction varied from 13.0% to 13.7%. The relatively higher pressure of 0.8 MPa than 0.4 MPa reduced the height of the CSFs, resulting in an increase in the volume fraction of CSFs in the composites.

Table 3-5 indicates the volume fraction of CSFs, Al-Ni compounds and Si phases of the Ni plated CSF/Al matrix composites fabricated under 0.4 MPa and 0.8 MPa, respectively. Ni plated CSF/1070 and A356 alloy composites (0.4 MPa) exhibited 2.4 and 2.5 vol.% of Al-Ni compounds generated by the reaction of Ni plated layer and Al matrix. Ni plated CSF/A336 alloy composite (0.4 MPa) exhibited a higher of 5.8 vol.% of Al-Ni compounds generated by not only the reaction of Ni plated layer and matrix, but also the high amount of Ni element (1.5 mass%) in A336 alloy matrix. In comparison, the Ni plated CSF/1070 and A356 alloy composites (0.8 MPa) exhibited 3.6 vol. % of Al-Ni compounds, Ni plated CSF/A336 alloy composite (0.8 MPa) exhibited 8.4 vol. % of Al-Ni compounds. The higher pressure of 0.8 MPa lead to an increase of volume fraction of Ni plated CSFs in composite, which introduced more Ni plated layer, resulted in an extra increase of Al-Ni compounds. The amount of Si phases in A356 and A336 alloys composites was about 8.0 vol.% and 15.0 vol.%, respectively, which was caused by 7 mass% and 12 mass% Si content in A356 and A336 alloys. The amount of Si phase did not change with changing the applied pressure.

Table 3-5 Volume fraction of CSFs, Al-Ni compounds and Si phases in Ni plated CSF/Al matrix composites fabricated under 0.4 MPa and 0.8 MPa.

	Ni plated CSF/A1070 composite		Ni plated CSF/A356 alloy composite			Ni plated CSF/A336 alloy composite		
	CSFs Vol.%	Al-Ni compounds Vol.%	CSFs Vol.%	Al-Ni compounds Vol.%	Si Vol.%	CSFs Vol.%	Al-Ni compounds Vol.%	Si Vol.%
0.4 MPa	10.3	2.4	10.1	2.5	7.8	10.3	5.8	15.0
0.8 MPa	13.7	3.6	13.0	3.6	8.0	13.5	8.4	15.2

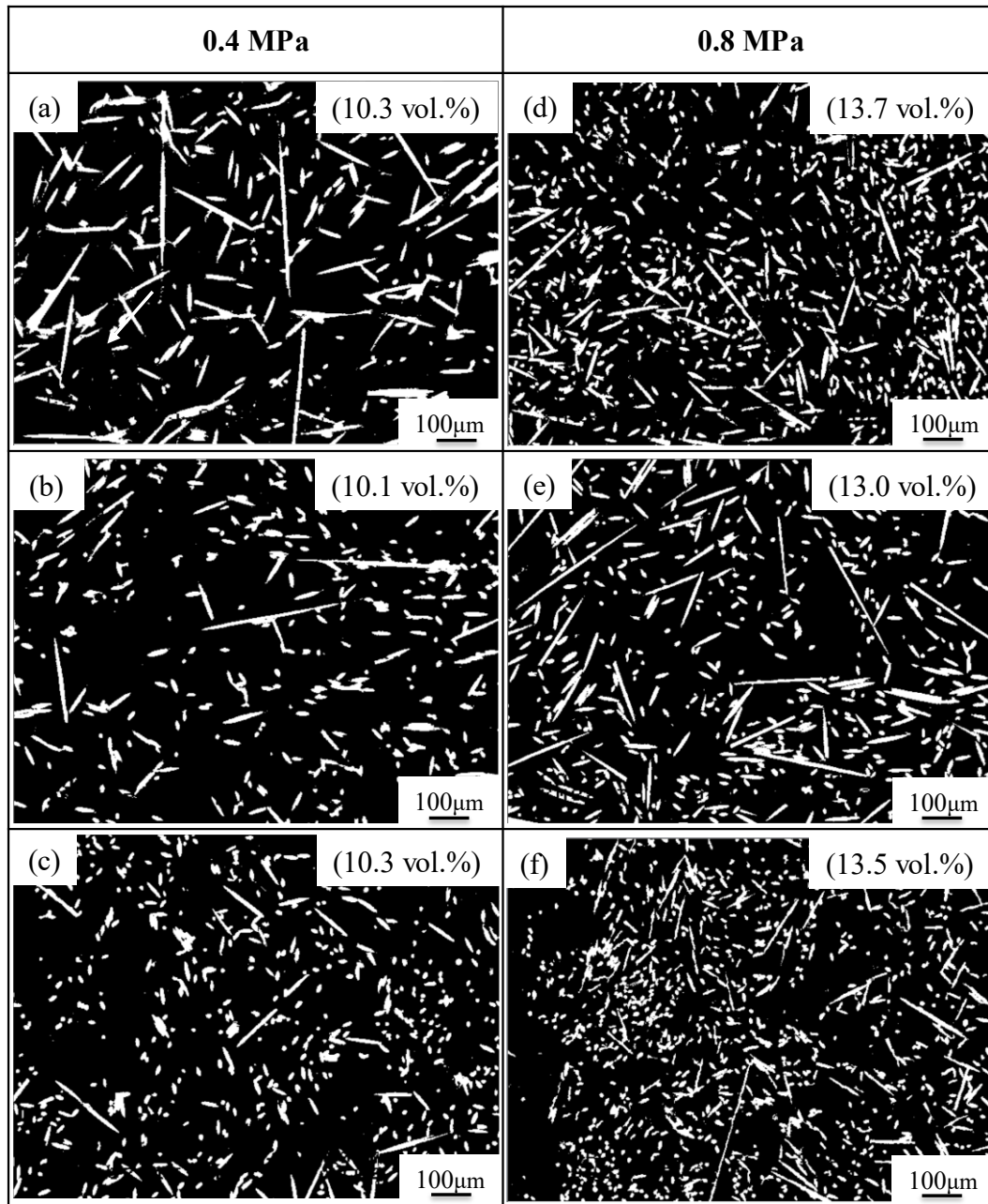


Fig. 3-8 Image analysis of composites (0.4 MPa and 0.8 MPa): (a), (d) Ni plated CSF/A1070 composite, (b), (e) Ni plated CSF/A356 alloy composite, and (c), (f) Ni plated CSF/A336 alloy composite.

Figure. 3-9 shows the SEM images and size of defects of the Ni plated CSF/Al matrix composites fabricated under 0.4 MPa and 0.8 MPa, respectively. It can be found that there existed some imperfect infiltration regions such as infiltration defects between CF/CF and CF/matrix in all composites. It is supposed that the molten Al preferentially infiltrated to a largely spaced region of the adjacent CSFs. At the same time, the narrow space between CSFs was hard to be infiltrated because of the existence of capillary resistance. Meanwhile, the fluidity of metals also had a great impact on infiltration. At the condition of 0.4 MPa, some large size defects were observed in Fig. 3-9 (a) in the region of CF/CF (8.3 μm) and CF/matrix (2.5 μm) because there is no alloying element in 1070 Al lead to a poor metal fluidity, the CSFs cannot be fully infiltrated result in large defects between CF/CF and CF/matrix. Figs. 3-9 (b) and (c) showed an apparent decrease in the size of defect than 1070 composite due to the existence of Si element in Al alloys which could increase the metal fluidity. Especially, Fig. 3-9 (c) possessed the smallest defect size compared to Figs. 3-9 (a) and (b) due to the highest amount of Si element (13 mass%) of A336 alloy. Compared with Figs. 3-9 (a)-(c), Figs. 3-9 (d)-(f) showed an obvious decrease of defects size in the region between CF/CF and CF/matrix of each composite by a relatively higher applied infiltration pressure of 0.8 MPa. It meant that the pressurized Al contacted both sides of CSFs which further enhanced the wettability, and the relatively high applied pressure encouraged molten Al infiltrated into some quite narrow space between CSFs to achieve a much denser microstructure.

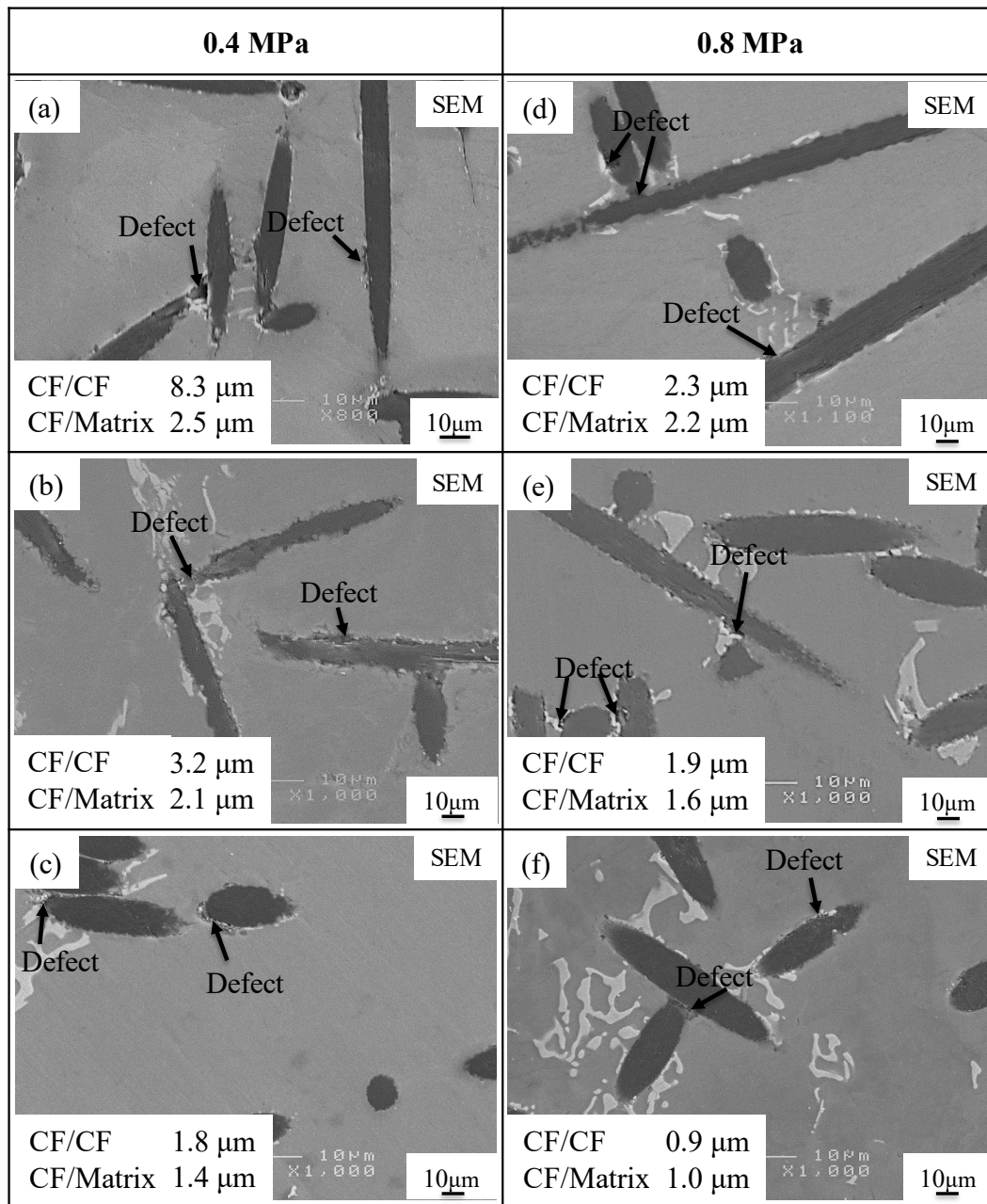
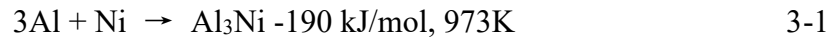


Fig. 3-9 SEM images of defects of composites (0.4 MPa and 0.8 MPa): (a), (d) Ni plated CSF/A1070 composite, (b), (e) Ni plated CSF/A356 alloy composite, and (c), (f) Ni plated CSF/A336 alloy composite.

For analyzing the kind of Al-Ni compound, element mapping and EDX analysis were conducted to Ni plated CSF/A1070 composite as shown in Fig. 3-10 and Table 3-6. In Fig. 3-10, it indicated that the compound indeed consisted of Al and Ni elements which proved the IMCs were Al-Ni compound. The EDX analysis data of compound showed the ratio of Al to Ni was 3:1 which confirmed Al-Ni compound was Al₃Ni phase. The phase-formation sequence was described in the following equation ^[30]:



The Al₃Ni phase was generated as the following process: the infiltration temperature was 1073K which was higher than 973K, during the infiltration process, Ni layer on the surface of CSFs was in contact with molten aluminum and reacted with aluminum directly. It was observed that the Al₃Ni phases were separated from the CSFs surface and distributed around the CSFs in Fig. 3-10, in light of the densities of the Ni and Al₃Ni, i.e. 8.9 and 4.0 kg/m³, the formation of Al₃Ni was thought to be an expansion reaction and finally the fine Al₃Ni phases were dispersed into the matrix which was separated from the CSFs surface.

Table 3-6 EDX analysis of the Al-Ni compound.

Position	Composition (at%)		Al:Ni	Al-Ni phase
	Al	Ni		
1	72.45	23.36	3:1	Al ₃ Ni
2	74.86	22.58		

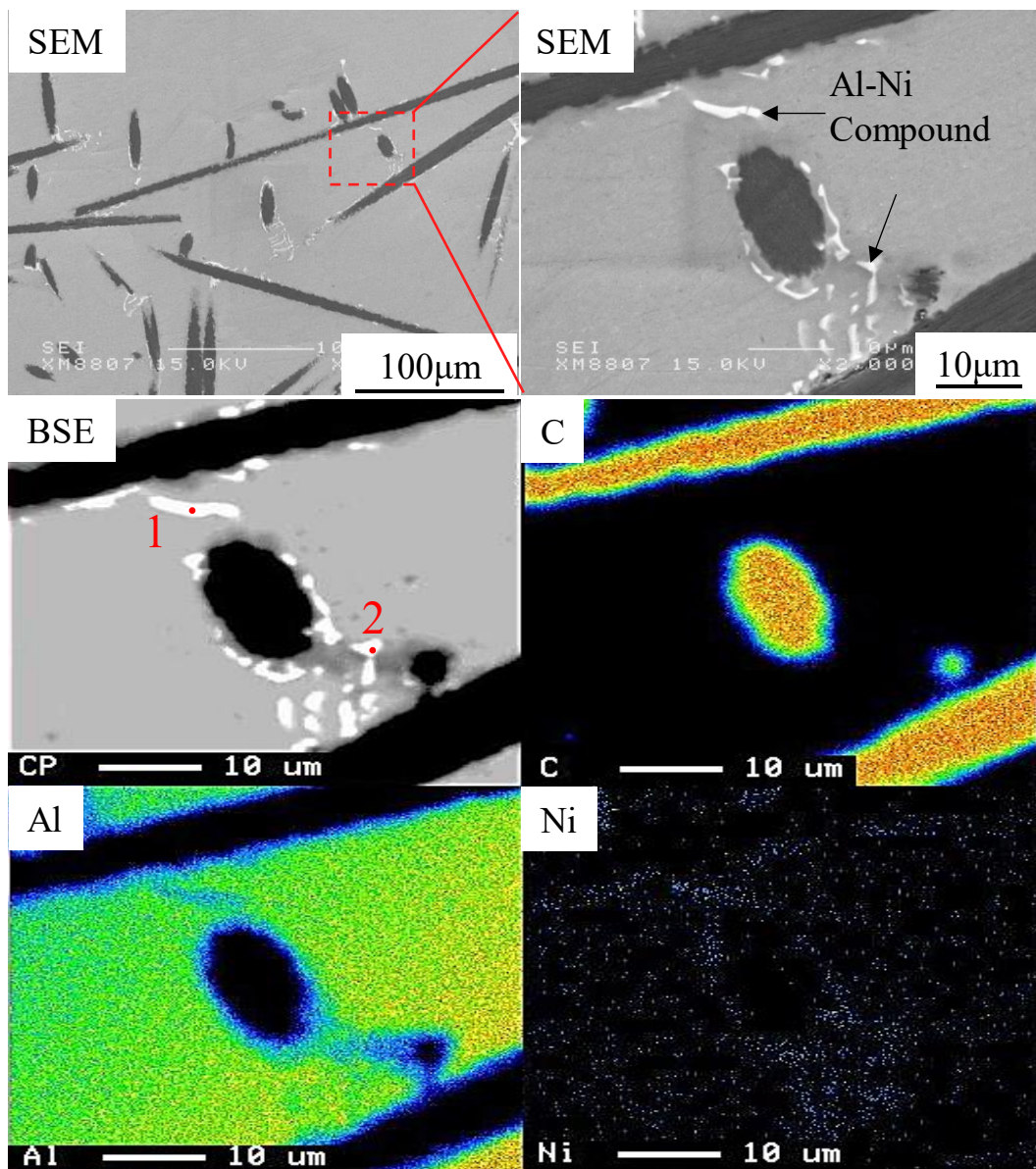


Fig. 3-10 Element mapping analysis of Ni plated CSF/A1070 composite.

It has been known that Al_4C_3 forms at the CF/Al interface at temperatures above 773 K and it deteriorates the mechanical property and TC of composites [31]. Since the LPI process temperature in the present study was set at 1073 K, Al_4C_3 may have formed in the composite. In order to investigate the existence of Al_4C_3 , XRD analysis was performed.

Figure 3-11 depicts the X-ray diffraction results of electroless Ni plated CSF/Al matrix composites. The detected crystals are only Al, C, Al_3Ni , Mg_2Si and Si. It is worth noting that no peaks for Al_4C_3 were detected in all electroless Ni plated CSF/Al matrix composites which indicated that the Ni plated layer acted as a barrier layer to effectively prevent the matrix from chemically reacting with the CSFs to cause damage to the strength of the fibers. The peak of Al_3Ni , Mg_2Si and Si phase in Fig. 3 -11 (c) is higher than that of other composites which meant a higher content of IMCs and precipitate in electroless Ni plated CSF/A336 alloy composite.

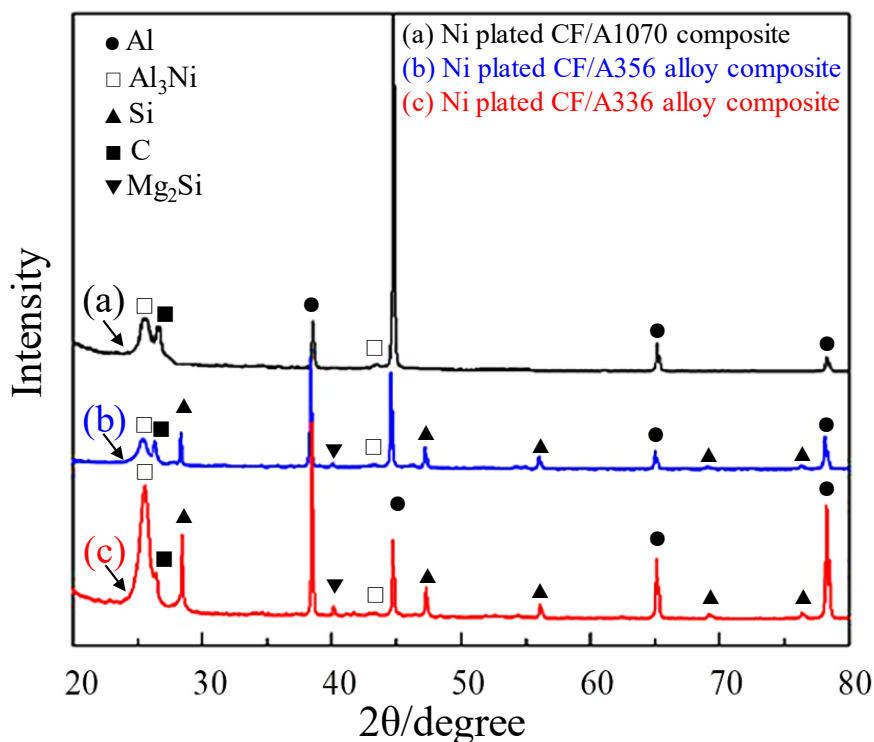


Fig. 3-11 Results of X-ray diffraction spectra of composites: (a) Ni plated CSF/A1070 composite, (b) Ni plated CSF/A356 alloy composite, and (c) Ni plated CSF/A336 alloy composite.

3.3.2 Dispersion behavior of Ni plated CSF inside matrix

Figure 3-12 shows the dispersion of CSFs inside the A1070 and A336 alloy matrix. Figs. 3-12 (a)- (c) shows the microstructure of CSFs/A1070 composite, Figs. 3-12 (a) and (b) revealed that the CSFs were randomly dispersed inside the matrix, seldom obvious fibers aggregation was observed. Fig. 3-12 (c) shows the enlargement of microstructure which proved that the Al_3Ni compounds with small size were generated and distributed near CSFs. Figs. 3-12 (d)- (e) shows the microstructure of CSFs/A336 alloy composite, Figs. 3-12 (a) and (b) revealed that CSFs were narrowly dispersed inside the matrix, large and long strip Al_3Ni phase was generated which caused a squeezing effect on fibers, fibers rarely exist where the large size compounds were presented. Fig. 3-12 (f) shows the enlargement of microstructure which revealed that the CSFs were crowded dispersed between large size Al_3Ni compounds.

Therefore, the CSFs dispersion behavior was analyzed and the pattern diagram of the dispersion behavior of Ni plated CSF inside matrix was shown in Fig. 3-13. Figs. 3-13 (a)- (c) show the CSFs dispersion behavior in A1070 matrix. It was observed during the infiltration process, the Ni plated layers were dissolved into the A1070 matrix (Fig. 3-13 (b)) which improved the wettability of CSFs by the Al matrix. Then, the dissolved Ni plated layer reacted with A1070, as a result, Al_3Ni intermetallic compounds were formed (Fig. 3-13 (c)). Since A1070 possesses no alloying elements, the Ni that reacted with Al was provided only by the Ni plated layer. Therefore, small size Al_3Ni compounds were dispersed near fibers. Figs. 3-13 (d)- (f) shows the CSFs dispersion behavior in the A336 alloy matrix. It is observed small size Al_3Ni compounds were dispersed near fibers, large size Al_3Ni compounds were dispersed in the matrix (Fig. 3-13 (f)). It is noticed that A336 alloy possesses a higher content of Ni element (1.5 mass%) than A1070 matrix, which contributed to the large size Al_3Ni compounds in the matrix. As a result, a higher amount of Al_3Ni compounds were generated in the Ni plated CSF/A336 alloy composite. However, the generated large and long strip Al_3Ni phases produced a pressing force to the nearby CSFs, fibers were more densely distributed in the matrix.

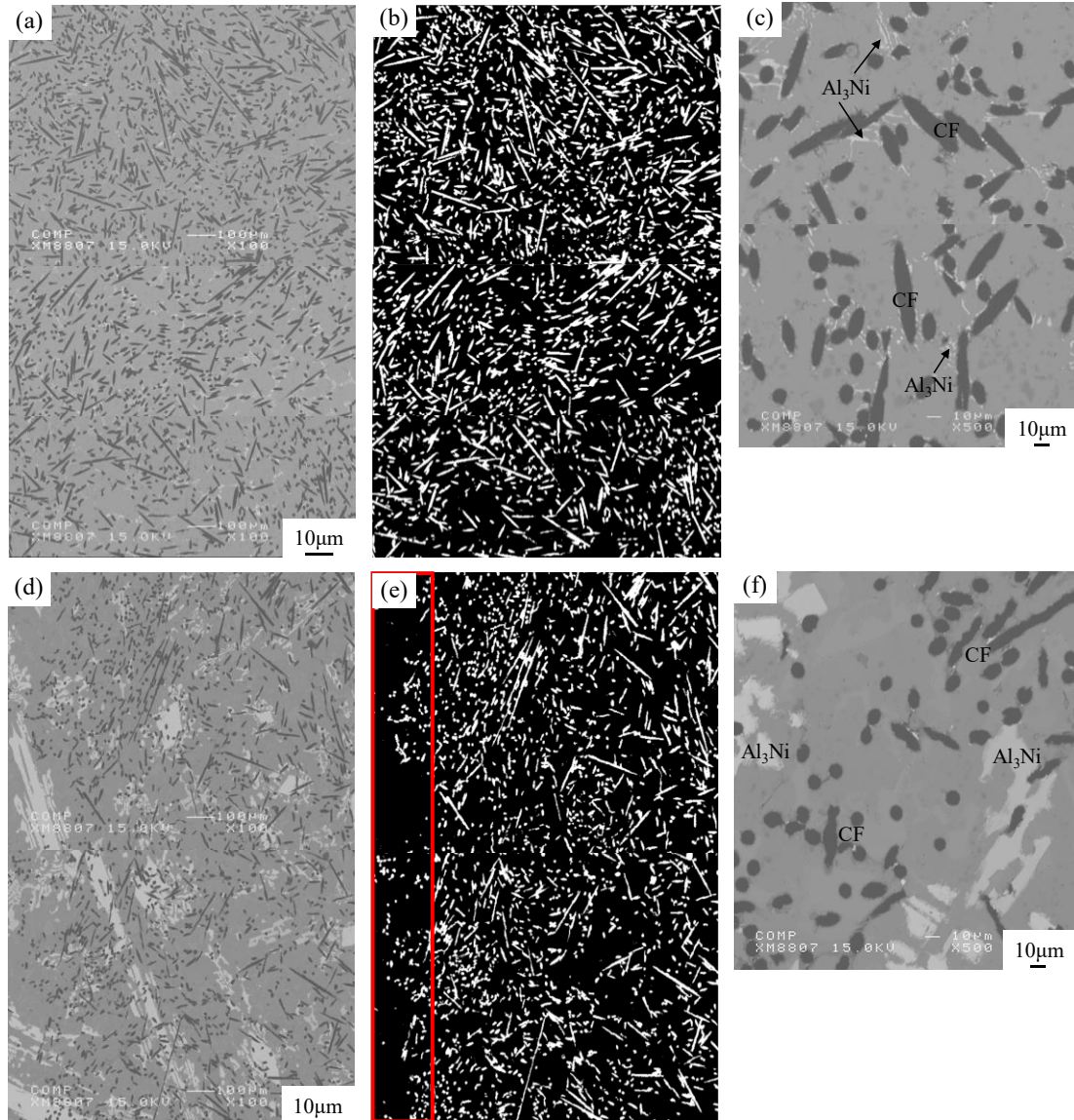


Fig. 3-12 Dispersion of CSFs inside the matrix: Ni plated CSF/A1070 composite (0.8 MPa) (a), (b) microstructure of composite, (c) enlargement of microstructure. Ni plated CSF/A336 alloy composite (0.8 MPa) (d), (e) microstructure of composite, (f) enlargement of microstructure.

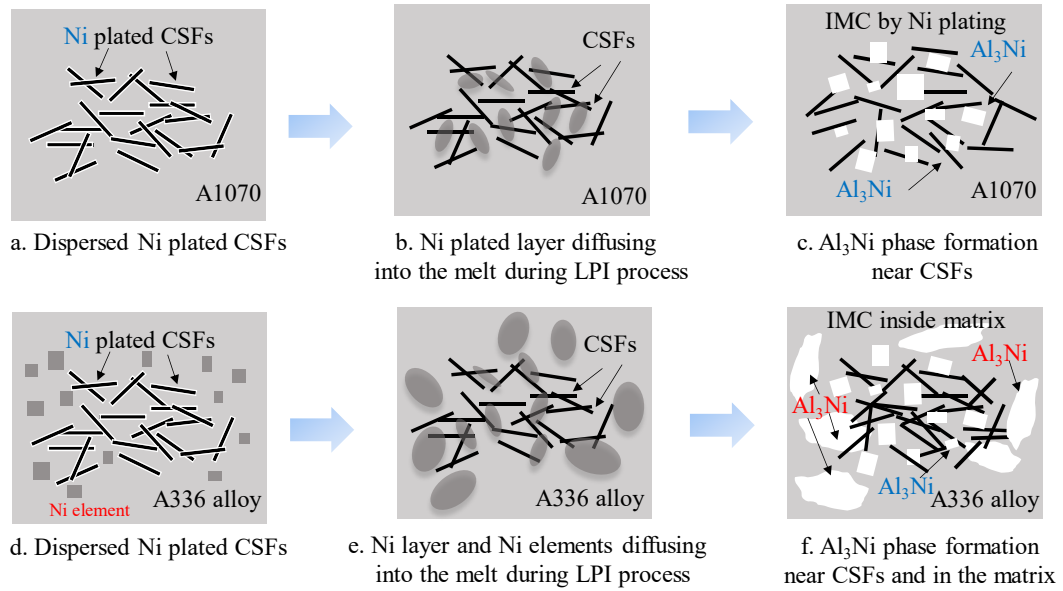


Fig. 3-13 Pattern diagram of dispersion behavior of Ni plated CSF inside matrix.

3.4 Summary

(1) A new fabrication process without preform manufacturing has been developed for CSF/Al based composites. Nickel plated CSFs were prepared using an electroless plating process, various plating time was carried out on CSFs for obtaining uniform Ni plated layer on the surfaces of CSFs. With plating for 120s, the nickel was homogeneously deposited on the CSFs.

(2) The Ni plated CSF/Al matrix composites were fabricated by the LPI process, in conjunction with the applied 0.4 MPa and 0.8 MPa infiltration pressure. In all Ni plated CSF/Al matrix composites, groups of Al_3Ni compounds were generated in the matrix and near the surface of CSFs, no Al_4C_3 was generated. The Ni plated CSF/A336 alloy composite possessed the highest content of Al_3Ni compounds due to the highest content of Ni element of A336 alloy promoted the generation of Al_3Ni compound. Meanwhile, the smallest defect size was presented in Ni plated CSF/A336 alloy composite due to the highest Si element of A336 alloy fulfilled it the best metal fluidity.

(3) The higher applied infiltration pressure resulted in a decrease of defects size between the CF/CF and CSF/matrix, which meant more compact composites were obtained. Applying a higher-pressure lead to a decrease in the height of the composite, therefore, an increase in the CSFS volume fraction.

References

- [1] W. S. Lee, W. C. Sue and C. F. Lin: *Compos. Sci.* **60** (2000) 1975–1983.
- [2] Y. H. Zhang, G. H. Wu, G. Q. Chen, Z. Y. Xiu, Q. Zhang and C. Y. Wang: *Transactions of Nonferrous Metals Society of China*, **16** (2006) 1509–1512.
- [3] S. J. Chand: *Mater. Sci.* **35** (2000) 1303–1313.
- [4] J. K. Wessel: *Handbook of advanced materials: enabling new designs*, Oak Ridge, Tennessee, (2004) pp. 89–90.
- [5] M. Sanchez, J. Rams, and A. Urena: *Compos. Part A. Appl. Sci. Manuf.* **41** (2010) 1605–1611.
- [6] A. Daoud: *Mater. Sci. Eng. A*, **391** (2005) 114–120.
- [7] G. Sasaki, M. H. Lee, Y. B. Choi, K. Sugio and K. Matsugi: *ECCM15-15th European Conference on Composite Materials*, Venice, Italy, (2012).
- [8] J. M. Ting, and M. L. Lake: *J. Mater. Res.* **10** (1995) 247–250.
- [9] S. Zhou , X. Zhang, Z. Ding, C. Min, G. Xu, W. Zhu: *Composites A*, **38** (2007) 301-306.
- [10] A. M. K. Esawi, K. Morsi, A. Sayed, A. Abdel Gawad, P. Borah: *Mater. Sci. Eng. A*, **508** (2009) 167-173.
- [11] T. Shalu, E. Abhilash, M.A. Joseph: *J. Mater. Proc. Tech.* **209** (2009) 4809–4813.
- [12] H. Uozumi, K. Nakanishi, K. Inoue, T. Tsukada, N. Fuyama, T. Fujii and M. Yoshida: *J. Jpn. Inst. Light. Met.* **59** (2009) 562–568.
- [13] B. Moser, A. Rossoll, L. Weber, O. Beffort, A. Mortensen: *Composites A*, **32** (2001) 1067-1075.
- [14] Y. Q. Yao, Z. F. Xu, K. Sugio, Y. B. Choi, S. M Kang, R. D. Fu, and G. Sasaki: *Mater. Trans.* **56** (2015) 1693-1697.
- [15] F. Delannay, L. Froyen, and A. Deruyttere: *J. Mater. Sci.* **22** (1987) 1–16.
- [16] T. Rajan, R. Pillai, and B. Pai: *J. Mater. Sci.* **33** (1998) 3491–3503.
- [17] Y. M. Ryu, E. P. Yoon, and M. H. Rhee: *J. Mater. Sci. Lett.* **19** (2000) 1103–1105.
- [18] S. Ip, R. Sridhar, J. Toguri, T. Stephenson and A. Warner: *Mater. Sci. Eng. A*, **244** (1998) 31-38.
- [19] Mitsubishi Chemical, Inc., DIALEAD data sheet. (2009) Available at.

- http://www.mpi.co.jp/products/industrial_materials/pitch_based_carbon_fiber/pbcf001.html (accessed 11. 12. 09).
- [20] G. F. Cui, N. Li, D. Y. Li, J. Zheng and Q. L. Wu: *Surface and Coatings Technology*, **200** (2006) 6808–6814.
- [21] M. Yan, H. G. Ying and T. Y. Ma: *Surface Coating Technology*, **202** (2008) 5909–5913.
- [22] A. Ramalho and J. C. Miranda: *Wear*, **259** (2005) 828–834.
- [23] K. N. Srinivasan, R. Meenakshi, A. Santhi, P. R. Thangavelu and S. John: *Surface Engineering*, **26** (2010) 153–158.
- [24] Y. W. Riddle and T. O. Bailer: *JOM*, **57** (2005) 40–45.
- [25] S. M. Kang, Z. F. Xu, Y. B. Choi, K. Matsugi, H. Kuramoto and J. K. Yu: *Mater. Trans.* **57** (2016) 2139 – 2145.
- [26] H. Ashassi-Sorkhabi, S. H. Rafizadeh: *Surface Coating Technology*, **176** (2004) 318–326.
- [27] T. Nagai, K. Hodouchi and H. Matsbara: *Journal of The Surface Finishing Society of Japan*, **65** (2014) 396-398.
- [28] K. Krishnaveni, N. T. Sankara and S. K. Seshadri: *Surface Coating Technology*, **190** (2005) 115–121.
- [29] Y. B. Choi, Y. Kataoka, Z. F. Xu, K. Matsugi and G. Sasaki: *Mater. Trans.* **58** (2017) 1097–1099.
- [30] O. Kubaschewski, C. B. Alcock and P. J. Spencer. *Materials thermochemistry*. 6th ed. Pergamon Press, pp. 258–266.
- [31] M. H. Lee, Y. B. Choi, K. Sugio, K. Matsugi and G. Sasaki: *Compos. Sci. Technol.* **97** (2014) 1–5.

Chapter 4

Mechanical and thermal properties of CSF/Al matrix composites

4.1	Introduction	100
4.2	Evaluation methods and equipment.....	102
4.2.1	Hardness test.....	102
4.2.2	Relative density.....	102
4.2.3	Tensile test	102
4.2.4	Thermal conductivity.....	103
4.2.5	Observation of fracture surface.....	103
4.3	Results and discussion	104
4.3.1	Mechanical properties of CSF/Al matrix composites	104
4.3.1.1	Vickers hardness and relative density of CSF/Al matrix composites	104
4.3.1.2	Tensile properties and fracture surface of CSF/Al matrix composites	108
4.3.2	Thermal conductivity of CSF/Al matrix composites	121
4.4	Summary	129
	References	130

4.1 Introduction

In the fields of thermal management and engineering applications, composites materials with high thermal conductivity (TC), light weight, and high mechanical property are expected to utilize as an alternative to existing materials such as heat sink material [1-6] or internal engine parts [7-10]. Among the various reinforcements, carbon fibers (CFs) possess high thermal and electrical conductivity, extremely low CTE and excellent mechanical properties, which have attracted much attention and have been particularly considered as an ideal candidate for reinforcement in multifunctional composites and engineering applications [11-13]. Aluminum is a dominant matrix for fabricating composite, CF reinforced aluminum composite can combine the superior characteristics of CF and Al matrix, therefore, CF/Al matrix composites can be the promising materials for the heat sink components or structural material with high TC, light weight and good workability. Recently, much work has been devoted to mainly investigating the effect of CFs amount on the modified TC and the enhancement of the mechanical properties [14-17].

However, the analysis of the effect of matrix with various alloying elements on the properties of CF/Al matrix composites has been rarely studied. The alloying elements of matrix (such as silicon and nickel) make an important impact thermal and mechanical properties of composites. A suitable manufacturing process for AMCs is the point for achieving high performance composites with good combination of reinforcement and matrix. The low-pressure infiltration (LPI) method is the useful fabrication process for composites with cost saving and the possibility of large or complex structures [18-20].

In addition, the problems associated with the fabrication of CFs reinforced Al matrix composites are the poor wettability and chemical reactions between carbon and Al matrix. An effective way to solve problems is surface coating on CFs [21]. The coating materials used in this study were SiO₂ and nickel (Ni). SiO₂ played a role in not only improving the wettability and preventing chemical reactions between carbon and Al matrix, but also retaining the integrity and shape of CSF preform. As a new process without manufacturing preform was developed for CF/Al matrix composites, CFs were Ni plated for improving the wettability.

In this study, the TC and mechanical properties of CSFs reinforced Al and Al alloys composites by LPI process have been evaluated by fixing the volume fraction of CFs, in conjunction with the analysis of theoretical and experimental values. The effect of matrix with various alloying elements on the properties of composites has been investigated. The properties of composites fabricated by the process with SiO₂ binder and fabricated by the new process without preform manufacturing were evaluated and compared.

4.2 Evaluation methods and equipment

4.2.1 Hardness test

Hardness of the CSF/Al matrix composites were measured in a Vickers hardness tester. The values reported for Vickers hardness represented the average of five separate measurements taken at randomly selected points using a load of 3Kg for 10 s.

4.2.2 Relative density

Densities of CSF/Al matrix composites fabricated with SiO₂ binder were measured with the water immersion method by Archimedes' principle. The relative density was the ratio of the experimental density to the theoretical density. For Ni plated CSF/Al matrix composites, due to the formation of Al₃Ni intermetallic compounds, the relative density was calculated by image analysis of microstructures of composites.

4.2.3 Tensile test

Plate tensile specimens with a thickness of 2 mm and a gauge length of 18 mm (Fig. 5-2) were cut from the composites in accordance with ASTM test method E8M-11. Tensile tests were carried out using a precision universal testing machine (AG-50KNX STD, SHIMADZU Inc., Japan) with a strain rate of 0.5 mm/min, the sampling time of 1s at room temperature. The strain gauges (YEFLA-2, t=Tokyo Measuring Instruments Lab.) was used for strain analysis.

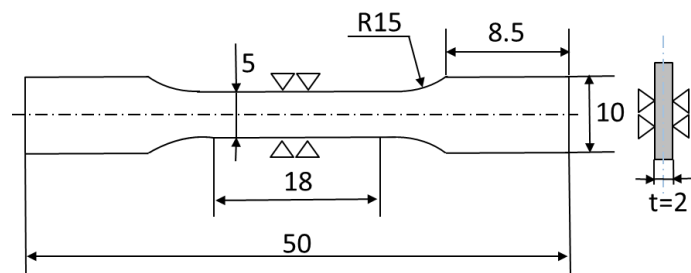


Fig. 4-1 Shape and dimension of tensile specimens (Unit: mm).

4.2.4 Thermal conductivity

Thermal conductivity of CSF/Al matrix composites fabricated with SiO₂ binder and Ni plated CSF/Al matrix composites without preform manufacturing was evaluated by laser flash method thermal constants measuring system (TC-9000H, ULVAC-RIKO Inc., Japan) at the room temperature in air. The schematic illustration was shown in Fig. 4-2. The specimen size of CF/Al composites was $\phi 10 \times h 1.5$. One side (front side) of the thin circular disc specimen was placed in the laser flash apparatus was irradiated with instantaneous heat source by laser beam and the temperature was detected by thermocouple at the other side (back side). The thermal conductivity is calculated as follows:

$$\lambda = \alpha \cdot \rho \cdot C_p \quad (4-1)$$

where λ , α , ρ and C_p are thermal conductivity ($\text{W} \cdot \text{m}^{-1} \cdot \text{K}^{-1}$), thermal diffusivity ($\text{m}^2 \cdot \text{s}^{-1}$), density ($\text{Kg} \cdot \text{m}^{-3}$) and specific heat ($\text{J} \cdot \text{g}^{-1} \cdot \text{K}^{-1}$) of the sample, respectively. The thermal diffusivity is also calculated as follows:

$$\alpha = 0.39 \cdot L^2 / t_{1/2} \quad (4-2)$$

where L is specimen thickness and $t_{1/2}$ (ms) is the half of the time which reaches to maximum temperature of specimen after irradiation by laser. The $t_{1/2}$ of the CSF/Al composites was measured by the laser flash apparatus.

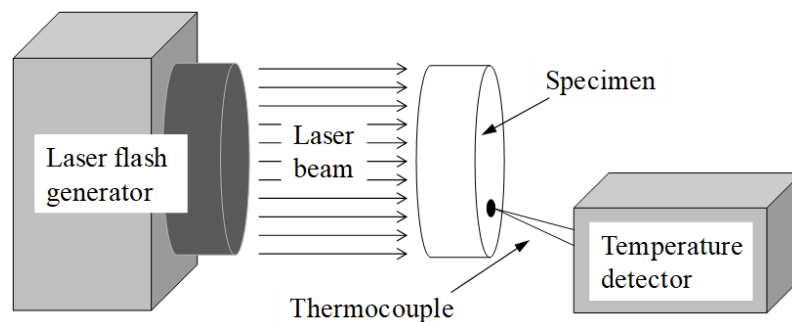


Fig. 4-2 Schematic diagram of laser flash method.

4.2.5 Observation of fracture surface

Microstructures of the fracture surface after tensile test of CSF/Al matrix composites were observed using an Electron Probe Micro-Analyzer (EPMA, JXA-8900RL).

4.3 Results and discussion

4.3.1 Mechanical properties of CSF/Al matrix composites

4.3.1.1 Vickers hardness and relative density of CSF/Al matrix composites

For developing the Al matrix composites with light weight and expected performance, CSF/Al matrix composites fabricated with SiO₂ binder and Ni plated CSF/Al matrix composites fabricated without preform manufacturing were fabricated by LPI process.

Figure. 4-3 shows the Vickers hardness and relative densities of CSF/Al matrix composites as well as CSF-CNF/Al matrix composite fabricated with SiO₂ binder preform (0.4 MPa). The relative density of CSF/A1070, A356 alloy and A336 alloy composite was 95.8%, 96.5% and 97.2%, respectively. The relative density of CSF-CNF/A336 alloy composite was 96.5%. Relative density is decided by the microstructure and matrix composition of composite. The lowest relative density of CSF/A1070 composite resulted from the defects with large size as shown in Fig. 2-9 (a), which caused by entrapped gases, poor wettability of the CSF by matrix and the poor fluidity of A1070 Al. The increased of the relative density of CSF/A356 alloy and A336 alloy composite was due to presence of alloying elements in Al alloys matrix, Si element could increase the infiltration rate by decreasing the viscosity of matrix and the existence of Mg in alloys enhanced the wettability of CSF with the Al matrix. Noticed that the A336 alloy possesses the highest content of Si and Mg elements, as a result, the highest relative density was obtained. The relative density of CSF-CNF/A336 alloy composite was relatively lower than CSF/A336 alloy composite. As shown in Fig. 2-9 (d), CNFs were presented as clusters dispersed at the corner of CSFs, the interspace was hard to be fully infiltrated resulted in more defects being retained in the composites.

The Vickers hardness of A1070, A356 alloy and A336 alloy is found to be 19.1 Hv, 47.8 Hv and 67.3 Hv, respectively. CSF/A1070, A356 and A336 alloy composites presented hardness of 33.5 Hv, 52.4 Hv and 74.3 Hv, respectively, as shown in Figs. 4-3 (a)-(c), which were all harder than their respective matrix. Indeed, the Vickers

hardness of the CSF/A1070, A356 alloy and A336 alloy composite was increased by about 76%, 9.6% and 11% relative to that of the respective matrix. This proves that the introduction and the dispersion of CSFs dramatically increase the hardness. Besides of the dispersion strengthening of CSFs, the difference of coefficient of thermal expansion between Al matrix and CSFs, CSFs could restrict the dislocation to increase dislocation density which also increased the hardness of composite. The Hardness of CSF-CNF/A336 alloy composite was 66.7 Hv as shown in Fig. 4-3 (d), almost the same with A336 alloy but decreased by 10.8% than that of CSF/A336 alloy composite. The lower relative density caused by the agglomeration of CNF lead to a weakening of dispersion strengthening to the composite which decreased the hardness.

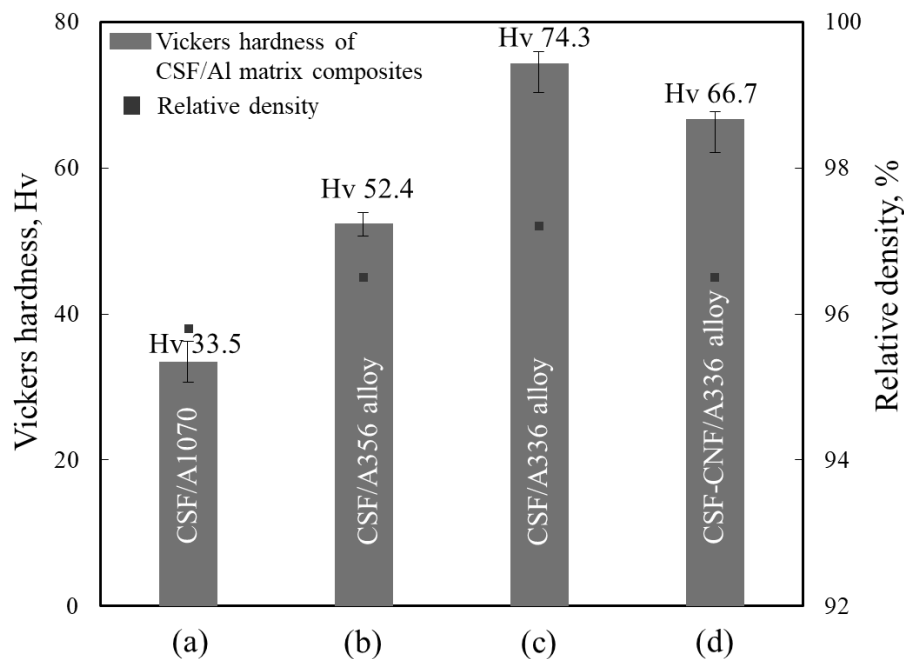


Fig. 4-3 Vickers hardness and relative density of CSF/Al matrix composites fabricated with SiO₂ binder preform (0.4MPa): (a) CSF/A1070 composite, (b) CSF/A356 alloy composite, (c) CSF/A336 alloy composite and (d) CSF-CNF/A336 alloy composite.

Figure. 4-4 shows the Vickers hardness and relative densities of Ni plated CSF/Al matrix composites fabricated without preform manufacturing (0.4 MPa). The relative density of the Ni plated CSF/A1070, A356 alloy and A336 alloy composites was 97.8%, 98.5% and 99.0%, respectively. The increase of relative density was related to the composition of matrix, and the Ni plated CSF/A336 alloy composite presented the highest relative density than the other composites which meant higher densification. Figs. 4-4 (a)-(c) show the Vickers hardness of Ni plated CSF/A1070, A356 alloy and A336 alloy composites was 41.3 Hv, 58.8 Hv and 88.4 Hv, respectively, which presented an improvement of 116.2%, 23.1% and 31.4% as compared to their respective matrix. The introduction of CSF, generation of Al_3Ni phase and the solid solution strengthening caused by Si phase precipitation in Al alloys composites contributed to the increase of hardness. A336 alloy possessed the highest content of Si (12 mass%) and Ni (1.5 mass%) elements, therefore, the highest content of IMCs and precipitate in Ni plated CSF/A336 alloy composite enables it to possess the highest hardness.

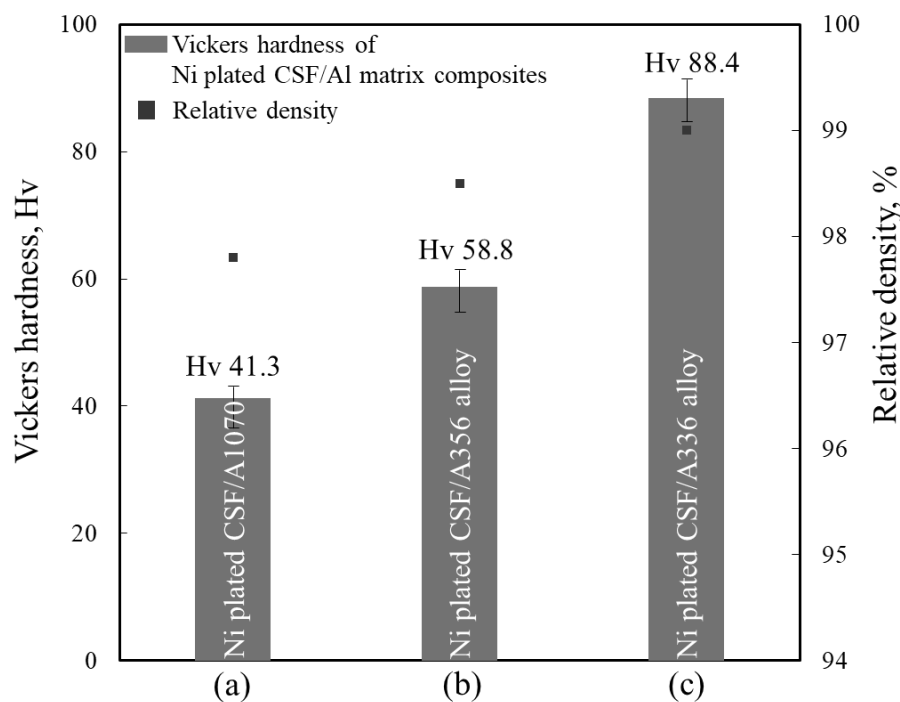


Fig. 4-4 Vickers hardness and relative density of Ni plated CSF/Al matrix composites fabricated without preform manufacturing (0.4MPa): (a) Ni plated CSF/A1070 composite, (b) Ni plated CSF/A356 alloy composite and (c) Ni plated CSF/A336 alloy composite.

For analyzing the properties of composites fabricated by the process with SiO₂ binder and without preform manufacturing, the comparison of Vickers hardness and relative density of CSF/Al matrix composites with SiO₂ binder and Ni plated CSF/Al matrix composites without preform manufacturing were summarized in Table 4-1. It is observed that the relative densities and Vickers hardness of Ni plated CSF/Al matrix composites were all higher than that of CSF/Al matrix composites with SiO₂ binder. It implied that the Ni plated CSF/Al composite without preform manufacturing exhibited a better CSF dispersion and wettability which achieved a higher relative density compared to that of CSF/Al matrix composite with the SiO₂ binder. Meanwhile, it is noteworthy that besides the introduction of CSFs played a role in strengthening the hardness, the generation of Al₃Ni IMCs also contributed to the increase of hardness of the composites. Consequently, for the composite with the same type matrix, CSFs plated with Ni reinforced composite formed a more pronounced enhancement to hardness than that with SiO₂ binder.

Table 4-1 Comparison of Vickers hardness and relative density of CSF/Al matrix composites fabricated with SiO₂ binder and Electroless Ni plating (0.4 MPa).

CSF/Al matrix composites	Vickers hardness (Hv)	Relative density (%)
CSF/A1070 composite with SiO ₂ binder	33.5	95.8
Ni plated CSF/A1070 composite	41.3	97.8
CSF/A356 alloy composite with SiO ₂ binder	52.4	96.5
Ni plated CSF/A356 alloy composite	58.8	98.5
CSF/A336 alloy composite with SiO ₂ binder	74.3	97.2
Ni plated CSF/A336 alloy composite	88.4	99.0

4.3.1.2 Tensile properties and fracture surface of CSF/Al matrix composites

The tensile stress–strain curves of the Ni plated CSF/Al matrix composites fabricated without preform manufacturing under 0.4 MPa were shown in Fig. 4-5. The tensile properties of composites and their respective matrix are summarized in Table 4-2. It can be observed that the ultimate tensile strength (UTS) and Young's modulus increased by changing the matrix from A1070 to A336 alloy in Figs. 4-5 (a)-(c), and the CSF/A336 alloy composite possessed the highest UTS than the other two kinds of composites due to the highest content of Si precipitate and Al_3Ni compounds. However, the Al_3Ni brittle intermetallic compounds decreased the plasticity of the CSF/A336 alloy composite lead to the lowest elongation.

For the A1070 matrix, the UTS and yield strength was 67.9 MPa and 19.1 MPa, respectively. With reinforcing by Ni plated CSF, the UTS and yield strength was obviously improved to 90.3 MPa and 37.1 MPa, respectively as shown in Table 4-2. The A1070 matrix possessed no alloying elements with a lower tensile property, the addition of CSFs and the generation of Al_3Ni compounds can produce high dislocation density significantly enhanced the mechanical property of A1070 matrix. However, the Young's modulus and elongation of Ni plated CSF/A1070 composite were reduced than A1070 matrix, the reduced ductility in this composite may be attributed to the limited ductility of the CSFs as well as the generation of Al_3Ni brittle compounds which increased the brittleness of A1070 matrix.

As for the comparison of Ni plated CSF/Al alloys composites and Al alloys matrix, the tensile properties of Ni plated CSF/A356 alloy composite shows almost the same with A356 alloy matrix, the tensile properties of Ni plated CSF/A356 alloy composite were decreased than A336 alloy matrix. A less effective reinforcing effect was achieved. The reduction of strength might be due to insufficient bonding strength between CSF and matrix and the orientation of fibers in the composites. The direct strengthening capacity of CSFs which contains predominantly strong interfacial bonding strength and fibers fracture during the tensile process. However, the Ni plated layer was dissolved into the molten Al which improved the wettability, CSFs were exposed to Al, because

the surfaces of the fibers were quite smooth there was very little mechanical bonding with matrix. In addition, the small defects at the interface of CSF and matrix which produced more sites for crack initiation and thus a lower load bearing capacity of the composites. On the other hand, short fibers were distributed in three-dimensional random orientation in composites, fewer fibers were paralleled to the tensile direction lead to an insufficient stress transmission of fibers. In the case of weak interface binding, some fibers were pulled out before they fractured, which didn't provide a good reinforcing effect.

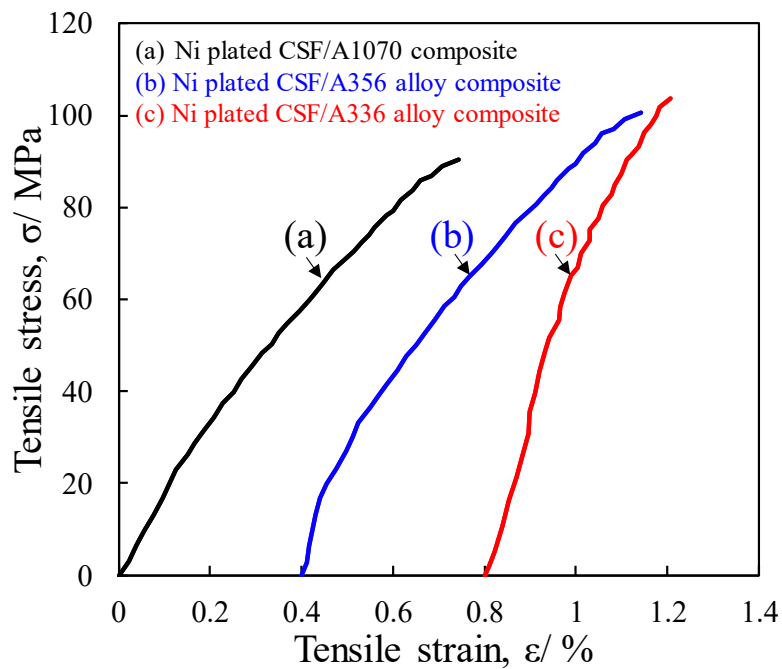


Fig. 4-5 Tensile stress–strain curves of Ni plated CSF/Al matrix composites fabricated without preform manufacturing (0.4 MPa): (a) Ni plated CSF/A1070 composite, (b) Ni plated CSF/A356 alloy composite and (c) Ni plated CSF/A336 alloy composite.

Table 4-2 Tensile properties of Al matrix and Ni plated CSF/Al matrix composites fabricated without preform manufacturing (0.4MPa).

Matrix	E (GPa)	σ_{UTS} (MPa)	0.2% σ_{YS} (MPa)	ϵ (%)
A1070	68.6	67.9	19.1	32.1
CSF/A1070	18.9	90.3	37.1	0.75
A356 alloy	15.7	96.7	32	2.1
CSF/A356 alloy	22.4	100.5	33.1	0.74
A336 alloy	44.9	204.8	79.7	1.0
CSF/A336 alloy	32.5	103.8	30.7	0.41

The fracture surfaces of the A1070 and Al alloys matrix are shown in Fig. 4-6. The fracture surface of A1070 shows the presence of many dimples (Fig. 4-6 (a) and (b)), and the image analysis revealed a strain concentration and large deformation which indicated that the fracture mechanism was a ductile fracture. For the A356 and A336 alloys in Fig. 4-6 (d) and (f), the main fracture mechanism was ductile fracture, while the brittle fracture occurred at the place of Si and IMC, a lot of cleavage stages were observed. The image analysis revealed nearly no strain concentration and deformation to the A356 and A336 alloys.

Figure 4-7 shows the fracture surfaces of Ni plated CSF reinforced composites fabricated under 0.4 MPa without preform manufacturing. The fracture mechanism of Ni plated CSF/A1070 composite was changed to brittle fracture, and lots of large size defects were also observed as shown in Fig. 4-7 (a) and (b). The A1070 matrix possesses no alloying elements with relatively limit tensile properties. The increased UTS of A1070 composite than A1070 matrix was attributed to the presence of CSFs and the formation of Al_3Ni in composites, which could increase the resistance to crack propagation, as a result of enhancement of the tensile property of composite. Fig. 4-7 (c) shows fibers pull out and debonding generated by the high number of defects between CSF/CSF and CSF/matrix which was described in detailed in microstructure

analysis in Chapter 3, therefore, the enhancement effect to tensile property was weakened accordingly. The fracture mechanism of Ni plated CSF/Al alloys composites were brittle fracture while cleavage stages were seldom observed by the addition of CSFs as shown in Fig. 4-7 (d) and (h). Defects with reduced size were observed compared to 1070 composites as shown in Fig. 4-7 (e) and (i). However, in Fig. 4-7 (f) and (j), lots of fibers debonding and fibers pull-out were observed at the fracture surfaces of CSF/Al alloys composites. Al alloys matrix possess a high content of alloying elements which fulfill them high tensile strength. The defects in composites increased the possibility of minute cracks generation, also the interface of CSFs and Al matrix shows poor bonding characteristic, cracks propagated along the interface with rarely propagated through the fibers which inevitably led to the failure of the material with low strength than Al alloys matrix.

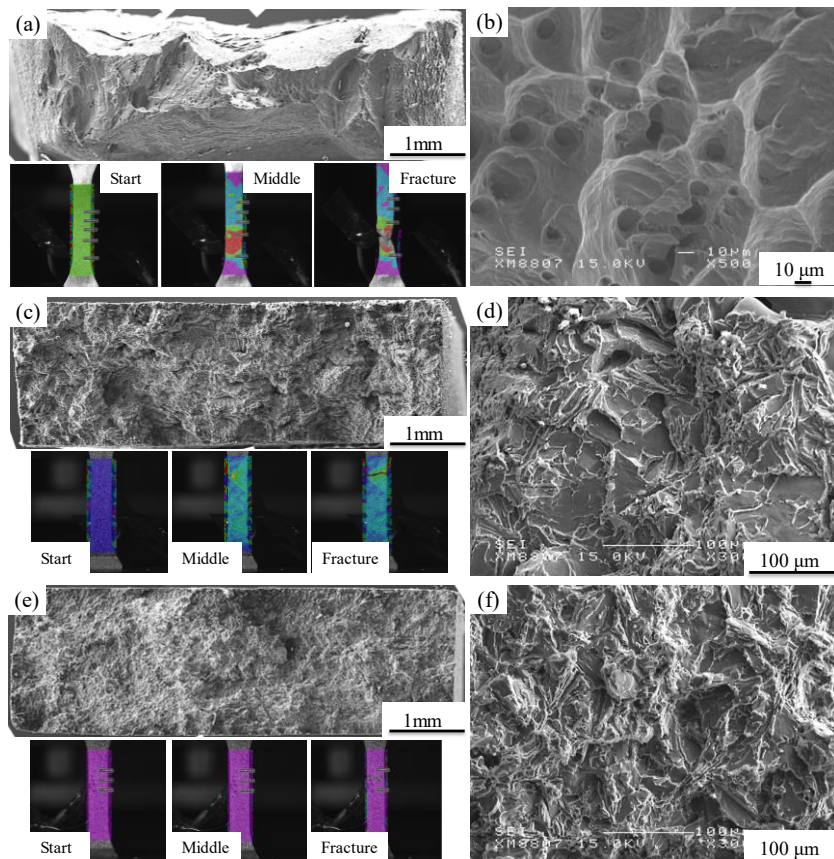


Fig. 4-6 Tensile fracture surfaces and image analysis of Al matrix:
 (a), (b) A1070, (c), (d) A356 alloy and (e), (f) A336 alloy.

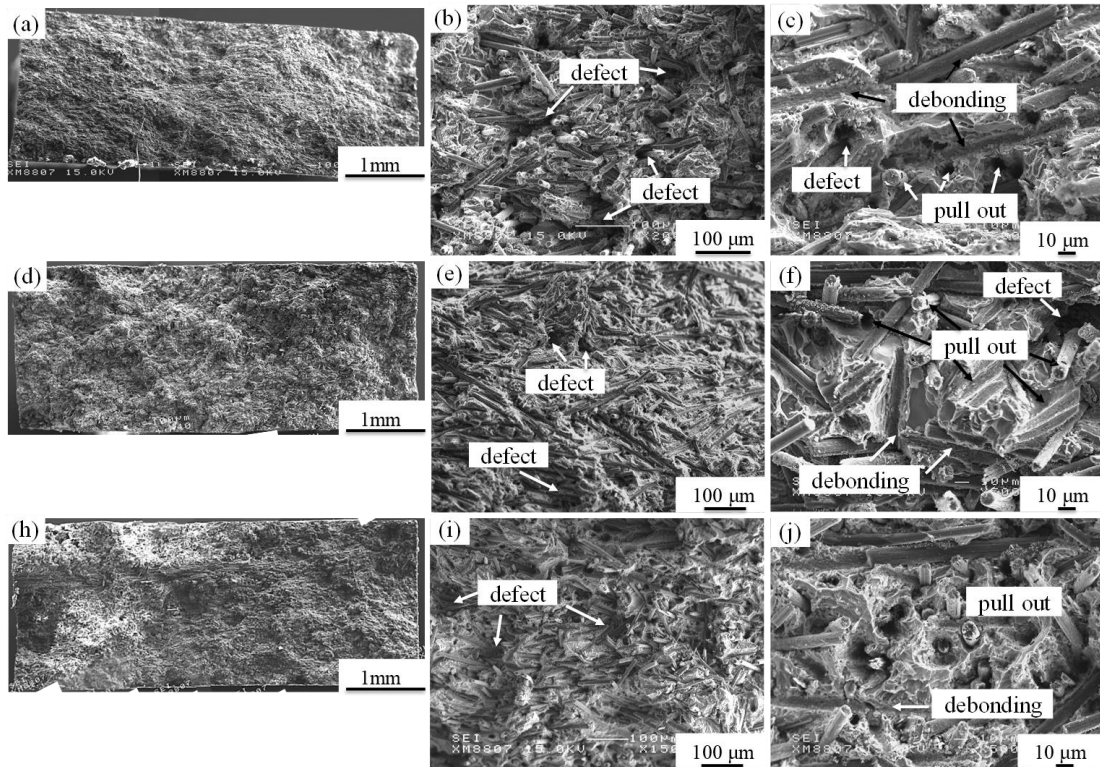


Fig. 4-7 Tensile fracture surfaces of Ni plated CSF/Al matrix composites fabricated without preform manufacturing (0.4 MPa): (a)-(c) Ni plated CSF/A1070 composite, (d)-(f) Ni plated CSF/A356 alloy composite and (h)-(j) Ni plated CSF/A336 alloy composite.

In order to further improve the tensile property of Ni plated CSF/Al matrix composites fabricated without preform manufacturing, Ni plated CSF/Al matrix composites were fabricated under 0.8 MPa, the tensile properties of composites fabricated under 0.4 and 0.8 MPa was compared and analyzed. Figure 4-8 shows the tensile stress–strain curves of the Ni plated CSF/Al matrix composites fabricated without preform manufacturing under 0.4 and 0.8 MPa. It was observed that the CSF/Al matrix composites fabricated without preform manufacturing under 0.8 MPa showed a slightly higher UTS than the composites fabricated under 0.4 MPa which was due to the higher relative density was accomplished by higher pressure. However, the strength enhancement was not significant.

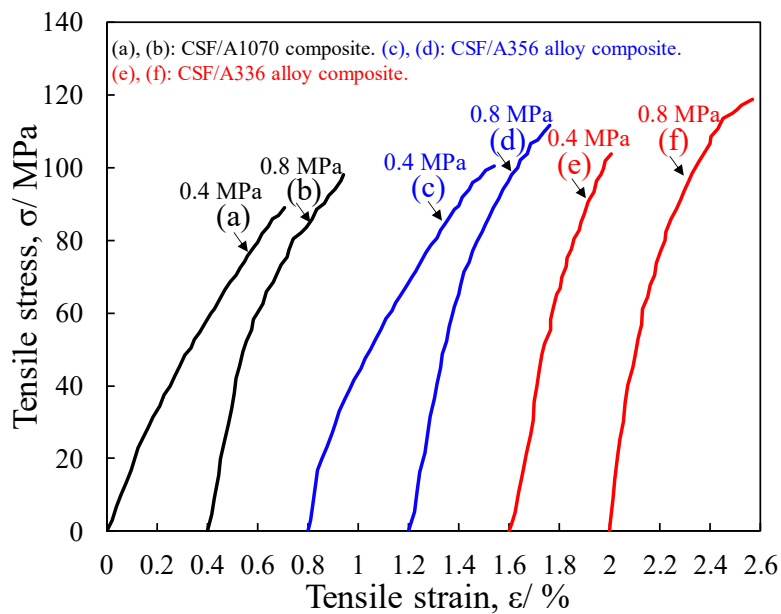


Fig. 4-8 Tensile stress–strain curves of CSF/Al matrix composites fabricated without preform manufacturing (0.4 and 0.8 MPa): (a), (b) Ni plated CSF/A1070 composites, (c), (d) Ni plated CSF/A356 alloy composites and (e), (f) Ni plated CSF/A336 alloy composites.

Figure 4-9 shows the tensile fracture surfaces of Ni plated CSF/Al matrix composites fabricated without preform manufacturing (0.4 MPa and 0.8 MPa). It was pointed out that many defects were generated in the composites (0.4 MPa) together with a large number of fibers pulled out and debonding due to the weak bonding strength between CSFs and matrix as shown in Fig. 4-9 (a), (c) and (e). As for the same matrix composites fabricated under the condition of 0.8 MPa as shown in Fig. 4-9 (b), (d) and (f), a decrease of defects amount by applying a higher infiltration pressure was observed, which lead to an enhance of tensile strength. Relative less but unavoidably fibers pulled out and debonding was also observed. The weak interface bonding strength between CSFs and matrix limited the further improve tensile properties.

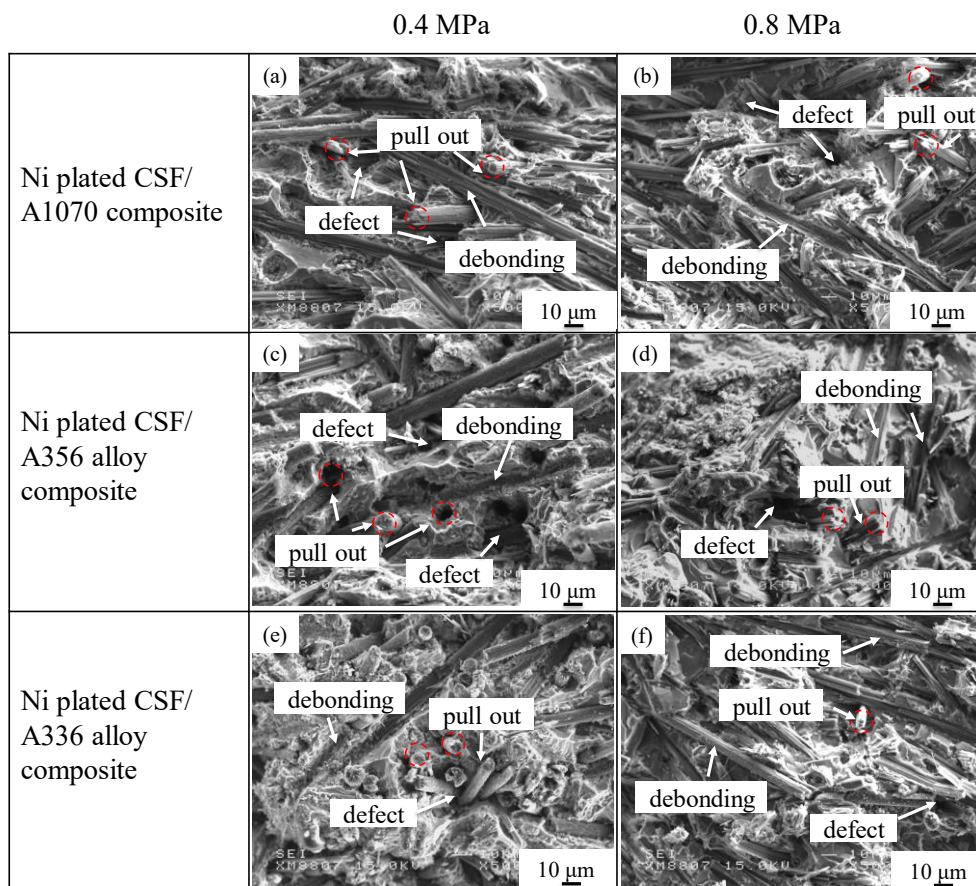


Fig. 4-9 Tensile fracture surfaces of Ni plated CSF/Al matrix composites (0.4 MPa and 0.8 MPa): (a), (c), (e) 0.4 MPa, and (c), (d), (f) 0.8 MPa.

Figure 4-10 shows the tensile stress–strain curves of the CSF/Al matrix composites fabricated under 0.8 MPa without preform manufacturing process and with SiO₂ binder preform, respectively. The tensile properties of composites fabricated with SiO₂ binder were used for comparison with the properties of composites fabricated without preform manufacturing. The tensile stress-strain curves of composites fabricated by two process show the same tendency, the fracture mechanism of all composites was supposed to be brittle fracture due to the small strain. It was observed that the CSF/Al matrix composites fabricated without preform manufacturing can achieve a higher UTS than the composites fabricated by the conventional process with SiO₂ binder. The UTS of Ni plated CSF/A336 alloy composites fabricated without preform manufacturing possessed the highest UTS than the other composites due to a higher relative density and content of alloying elements of A336 alloy matrix.

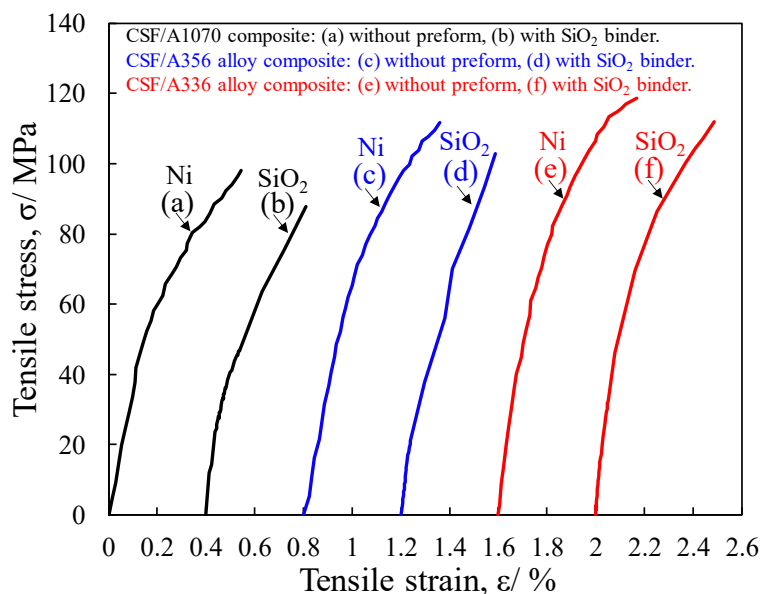


Fig. 4-10 Tensile stress–strain curves of CSF/Al matrix composites fabricated under 0.8 MPa without preform manufacturing and with SiO₂ binder: (a), (c) and (e) Ni plated CSF/Al matrix composites fabricated without preform manufacturing and (b), (d) and (f) CSF/Al matrix composites fabricated with SiO₂ binder preform.

The fracture surfaces of the Ni plated CSF/Al matrix composites fabricated under 0.8 MPa without preform manufacturing were shown in Fig. 4-11. The fracture surfaces of CSF reinforced composite exhibited essentially brittle fracture, as shown in Figs. 4-11 (a), (d) and (e). The fracture surfaces of Ni plated CSF/A1070 composites under 0.8 MPa revealed that the dimples of A1070 matrix were obviously decreased left some residual dimples filled with CSFs, some defects were also observed in Fig. 4-11 (b). In Fig. 4-11 (c), less fibers pulled out and debonding contributed to strength enhancement. The fracture surfaces of CSF/Al alloys composites as shown in Figs. 4-11 (f) and (j) had revealed much fewer defects were observed by applying a higher infiltration pressure, fibers pulled out and debonding was also observed due to the poor interface bonding strength between CSFs and matrix. Especially, the morphology of IMCs emerged at the fracture surfaces in all composites as shown in Figs. 4-11 (c), (f) and (j).

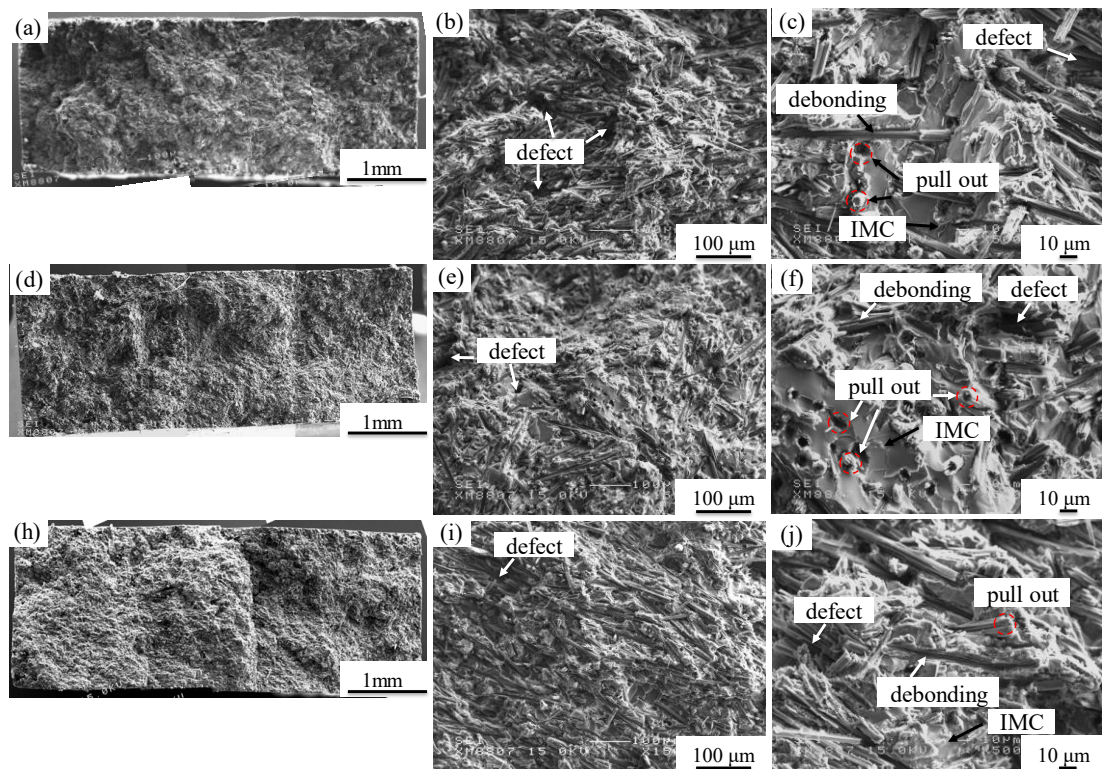


Fig. 4-11 Tensile fracture surfaces of Ni plated CSF/Al matrix composites fabricated without preform manufacturing (0.8 MPa): (a)-(c) Ni plated CSF/A1070 composite, (d)-(f) Ni plated CSF/A356 alloy composite and (h)-(j) Ni plated CSF/A336 alloy composite.

The fracture surfaces of the CSF/Al matrix composites fabricated under 0.8 MPa with SiO₂ binder preform were shown in Fig. 4-12. The fracture surfaces of composites all exhibited brittle fracture, as shown in Figs. 4-12 (a), (d) and (e). It is noticed that many defects were observed at the fracture surfaces as shown in Figs. 4-12 (b), (e) and (i), these defects manifested because of the agglomeration of CSFs by the SiO₂ binder in preform due to which molten Al could not infiltrate in between the CSFs cluster. The fracture surface of CSF/A1070 composite with SiO₂ binder as shown in Fig. 4-12 (c) revealed large size defects with lots fibers pulled out and debonding, as a result, a lower strength than the Ni plated CSF/A1070 composite without preform manufacturing (0.8 MPa). In Figs. 4-12 (f) and (j), fibers pulled out and debonding were widely existed at the fracture surface, defects were generated at the place of intertwined CSFs clusters, and the tensile fracture was prone to occur at the fiber agglomeration place, which caused a decrease of tensile strength than the CSF/Al alloys composites without preform manufacturing (0.8 MPa).

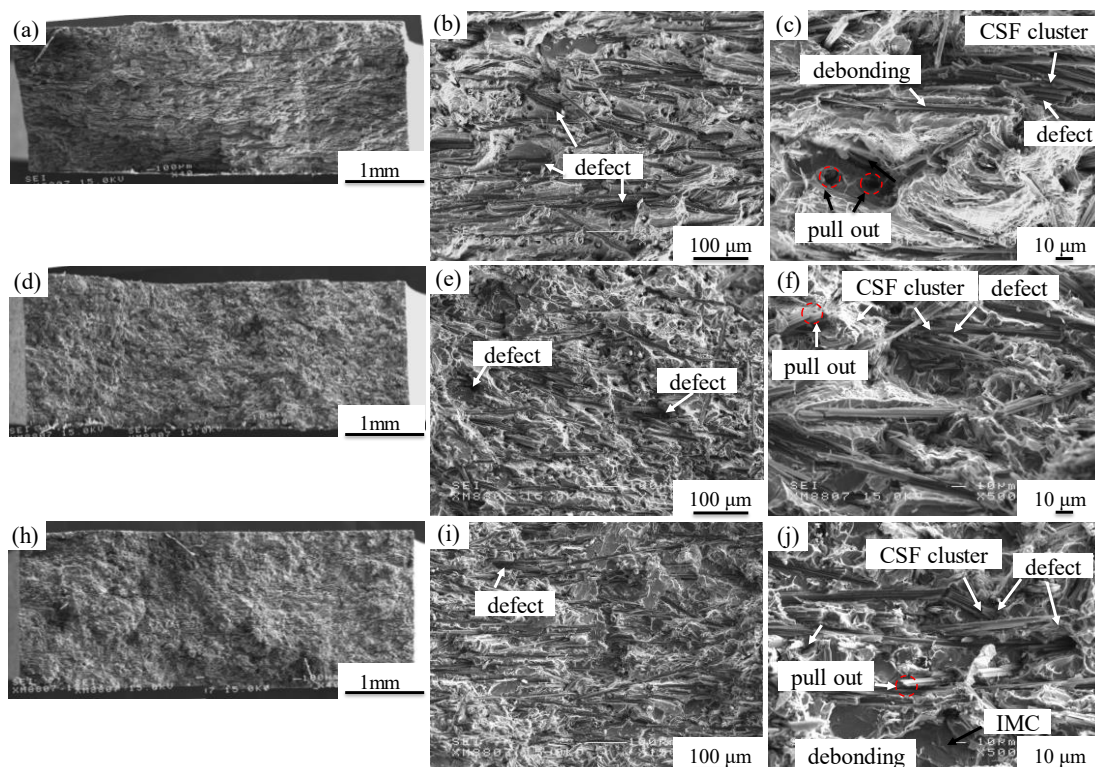


Fig. 4-12 Tensile fracture surfaces of CSF/Al matrix composites fabricated with SiO₂ binder preform (0.8 MPa): (a)-(c) CSF/A1070 composite, (d)-(f) CSF/A356 alloy composite and (h)-(j) CSF/A336 alloy composite.

In the case of randomly oriented short-fiber reinforced composites, the theoretical strength was calculated according to the Hirsch' model ^[22] as described in Chapter 1. The theoretical ultimate tensile strength value of Ni plated CSF with 10 vol.% reinforced A1070, A356 alloy and A336 alloy composites is 115.2 MPa, 255.9 MPa and 277.4 MPa, respectively. The experiment value of Ni plated CSF/A1070 composite (0.8 MPa) showed a more keeping to the theoretical value which proved that the addition of CSF could enhance the mechanical property of A1070 soft matrix effectively. However, the experiment value of Ni plated CSF/Al alloys composites is much lower than theoretical values. The theoretical tensile strength of the CSF reinforced Al matrix composites is determined by both the tensile strength of the base metal and the maximum value of CF. However, a lot of CSFs pulled-out and fibers debonding were observed at the fracture surface of the composite due to insufficient bonding strength between CSF and matrix, fibers fracture was rarely observed, fibers did not provide sufficient resistance to tensile stress.

Table 4-3 summarized the tensile properties of CSF/Al matrix composites fabricated without preform manufacturing under different pressure (0.4 MPa and 0.8 MPa) and with SiO₂ binder preform under 0.8 MPa. For the composites fabricated without preform manufacturing under 0.4 MPa and 0.8 MPa, by increasing the fabrication pressure, the UTS, yield strength and Young's modulus properties of composites (0.8 MPa) slightly increased than the properties of composites (0.4 MPa). The higher fabrication pressure achieved a higher relative density with smaller size defects which contributed to the increase of tensile properties. However, the unavoidable fiber pulled out and debonding due to the weak bonding strength between CSFs and Al limited the further improve tensile properties of composites. For the comparison of composites fabricated without preform manufacturing and with SiO₂ binder preform under 0.8 MPa. The UTS and yield strength of composites without preform manufacturing was higher than the composites with SiO₂ binder preform. The Ni plated CSFs showed a better wettability with Al matrix which can achieve a higher relative density contributed to higher tensile properties.

Table 4-3 Tensile properties of CSF/Al matrix composites fabricated without preform manufacturing (0.4 MPa and 0.8 MPa) and with SiO₂ binder preform (0.8MPa).

Composites	0.4 MPa				0.8 MPa				0.8 MPa			
	without preform				without preform				with SiO ₂ binder preform			
	E (Gpa)	σ_{UTS} (MPa)	$\sigma_{0.2}$ (MPa)	ϵ (%)	E (Gpa)	σ_{UTS} (MPa)	$\sigma_{0.2}$ (MPa)	ϵ (%)	E (Gpa)	σ_{UTS} (MPa)	$\sigma_{0.2}$ (MPa)	ϵ (%)
CSF/A1070	18.9	90.3	37.1	0.75	35.2	98.1	38.2	0.54	56.3	87.8	25.8	0.41
CSF/A356 alloy	22.4	100.5	33.1	0.74	37.0	111.7	35.3	0.56	37.0	102.8	21.1	0.39
CSF/A336 alloy	32.5	103.8	30.7	0.41	55.6	118.8	41.5	0.57	65.1	112.0	32.0	0.49

Among the composites fabricated under the same conditions, CSF/A336 alloy composites possessed the best mechanical properties. Therefore, a summary and comparison of the microstructure and fracture surfaces of CSF/A336 alloy composites fabricated without preform manufacturing (0.4 and 0.8 MPa) and fabricated with SiO₂ binder (0.8 MPa), respectively, were summarized and compared in Fig. 4-13.

In Fig. 4-13 (a) and (b), the Ni plated CSF/A336 alloy composite (0.4 MPa) presented a high relative density of 99.0% with small size (about 2 μm) defects. Lots of fibers pulled out and debonding were observed due to the weak interface bonding. In Fig. 4-13 (c) and (d), the Ni plated CSF/A336 alloy composite (0.8 MPa) presented the highest relative density of 99.4% with the smallest size (about 1 μm) defects. The highest relative density contributed to the highest tensile properties than other composites. Less but unavoidable fibers pulled out and debonding were also observed. As a comparative composite, CSF/A336 alloy fabricated with SiO₂ binder (0.8 MPa) as shown in Fig. 4-13 (e) and (f), possessed the lowest relative density of 97.8% with the largest size (about 30 μm) defect, the large size defects manifested due to the agglomeration of CSFs by the SiO₂ binder in the preform, molten Al could not infiltrate into the narrow space between the CSFs cluster. Fracture mainly occurred at the place of intertwined CSFs clusters, fibers pulled out and debonding were observed, which all caused a decrease of tensile strength.

Compared with the composites fabricated by the conventional process with SiO₂ binder. The composites fabricated without preform manufacturing possessed the following excellent characteristics. CSFs were more randomly dispersed in the matrix. The Ni plated layers dissolved and reacted with Al matrix which increased the wettability leads to a higher relative density, the formation of Al₃Ni compounds leads to a higher tensile property. Therefore, the new process without preform manufacturing proposed in this research is expected to replace the traditional fabrication process, aiming for further developing short fibers reinforced composites.

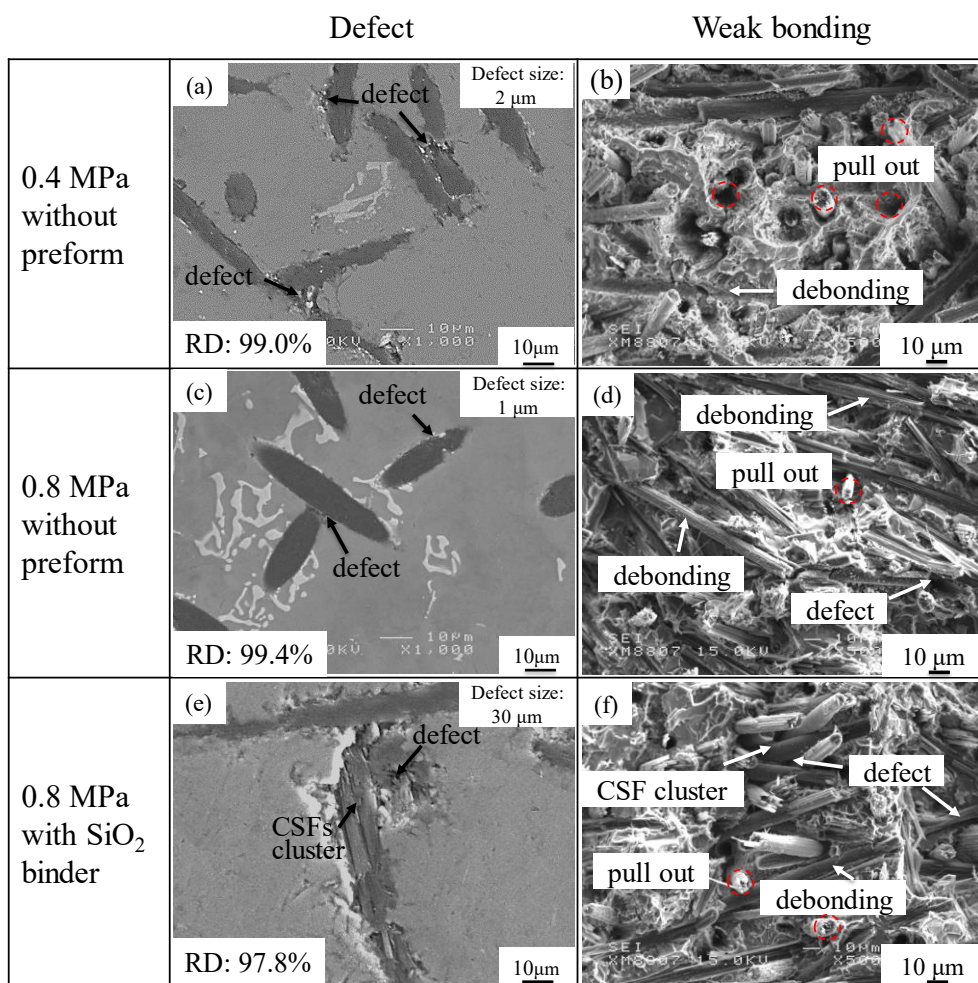


Fig. 4-13 Comparison of microstructures and fracture surfaces of CSF/A336 alloy composites: (a) Ni plated CSF/A336 alloy composites without preform manufacturing (0.4 MPa), (b) Ni plated CSF/A336 alloy composites without preform manufacturing (0.8 MPa) and (c) CSF/A336 alloy composites with SiO₂ binder (0.8 MPa).

4.3.2 Thermal conductivity of CSF/Al matrix composites

The TC properties of CSF/Al matrix composites fabricated with SiO₂ binder preform and without preform manufacturing, respectively, have been investigated, in conjunction with their theoretical values calculated by the model derived by Nan et al. [23] The theoretical model is suitable for a three-dimensionally randomly oriented occasion with considering the anisotropy in TC of CF, the aspect ratio and volume fraction of the fibers, as well as the interfacial thermal resistance at the fiber/matrix interface. The theoretical model equations and explanations are as follow:

$$K_{eff} = K_m \frac{3 + 2f [\beta_x (1 - L_x) + \beta_z (1 - L_z)]}{3 - f (2\beta_x L_x + \beta_z L_z)} \quad (4.3)$$

where f is volume fraction of the CF, 10vol.% in this study. K_m is the TC of the matrix, A1070, A356 alloy and A336 alloy were used as the matrix in this study with TC of 237 W·m⁻¹·K⁻¹, 159 W·m⁻¹·K⁻¹ and 125W·m⁻¹·K⁻¹. β_x , β_y and β_z are expressed in eqs. (4.4) and (4.5)

$$\beta_x = \beta_y = \frac{K_x - K_m}{K_m + L_x (K_c - K_m)} \quad (4.4)$$

$$\beta_z = \frac{K_z - K_m}{K_m + L_z (K_c - K_m)} \quad (4.5)$$

L_x and L_z are well-known geometrical factors dependent on the CF aspect ratio p , aspect ratio p is expressed as l/d , l and d are the diameter and length of the CF, respectively, which is 2.5mm and 11 μ m, therefore, the aspect ratio p is 230. For $p > 1$ fibers, L_x and L_z are are given by eqs. (4.6) and (4.7)

$$L_x = \frac{p^2}{2(p^2 - L_x)} - \frac{p}{2(p^2 - L_x)^{3/2}} \cosh^{-1} p \quad (4.6)$$

$$L_z = 1 - 2L_x \quad (4.7)$$

K_x^c and K_y^c are K_z^c are calculated by the following eqs. (4.8) and (4.9).

$$K_x^c = K_y^c = \frac{K_d^c}{1 + \frac{2a_k K_d^c}{dK_m}} \quad (4.8)$$

$$K_z^c = \frac{K_l^c}{1 + \frac{2a_k K_l^c}{lK_m}} \quad (4.9)$$

where K_d^c and K_l^c represent thermal conductivities of the CF in transverse and longitudinal directions. The CSFs with high TC of $800 \text{ W}\cdot\text{m}^{-1}\cdot\text{K}^{-1}$ through the longitudinal direction which was provided by the company. Although the transverse TC of K13D2U CSFs was unknown from the company, that was assumed extremely low TC based on the K-1100 CFs (BP Amoco Chemicals) which had similar fiber internal structure with K13D2U CFs and represented extremely low transverse TC of $10 \text{ W}\cdot\text{m}^{-1}\cdot\text{K}^{-1}$. a_k is called Kapitza radius and expressed in (4.10).

$$a_k = R_{Bd} K_m \quad (4.10)$$

where R_{Bd} is a coefficient of the interfacial thermal resistance, which controls the characteristics of interfacial heat transfer. Here $8.3 \times 10^{-8} \text{ W}^{-1}\cdot\text{m}^2\cdot\text{K}$ was used for the coefficient [24]. The theoretical value of CSF/A1070, A356 alloy, and A336 alloy composites was 242.4, 179.7, and $151.5 \text{ W}\cdot\text{m}^{-1}\cdot\text{K}^{-1}$, respectively.

Figure 4-14 shows the TC of CSF/Al matrix composites fabricated with SiO_2 binder preform under 0.4 MPa. The CSF/A1070 composite as shown in Fig.4-14 (a) showed a value of $175.5 \text{ W}\cdot\text{m}^{-1}\cdot\text{K}^{-1}$, which was the highest than other composites and corresponding to 73.1% of the theoretical value. It can be supposed that heat loss was mainly conducted to the large size and number of defects between CSF/CSF and fiber-matrix. Fig.4-14 (b) and (c) shows the TC of CSF/A356 and A336 alloy composites was $114.3 \text{ W}\cdot\text{m}^{-1}\cdot\text{K}^{-1}$ and $113.5 \text{ W}\cdot\text{m}^{-1}\cdot\text{K}^{-1}$, respectively, which was corresponded to 80.3% and 74.9% of the theoretical values. The generation of IMCs and precipitation of Si caused a decrease of TC of CSF/Al alloys composites than CSF/A1070 composite. The highest content of alloying elements in A336 alloy resulted in the highest content of IMCs and Si phase in its corresponding composite, which further reduced the TC of the composite. Furthermore, oxide interface layers were generated between CSF and Al matrix in all CSF reinforce composites with SiO_2 binder by the reaction of SiO_2 and Al matrix as described in Chapter two. The oxide interfaces give rise to the thermal interfacial resistance, which reduced the TC of composites. TC of the composites is

remarkably reduced than the theoretical TC of composites by the equation of Nan's prediction model. It was attributed to the thermal resistance at the CSF/Al interface and CSF/CSF interface. However, the magnitude of thermal resistance at the CSF/Al interface and CSF/CSF interface is unclear which needs further investigations.

The TC of CSF-CNF/A336 alloy composite was $98.4 \text{ W}\cdot\text{m}^{-1}\cdot\text{K}^{-1}$ as shown in Fig. 4-14 (d). Although CNF has a much higher TC of $1200 \text{ W}\cdot\text{m}^{-1}\cdot\text{K}^{-1}$ than CF of $800 \text{ W}\cdot\text{m}^{-1}\cdot\text{K}^{-1}$ along the longitudinal direction, the TC of CSF-CNF/A336 alloy composite was much lower than that of CSF/A336 alloy composite. In general, the TC of fiber reinforced composites depends on the porosity and dispersion of fibers in composites as well as the interface layer between fibers and matrix. In the case of CSF-CNF/A336 alloy composite, the poor dispersion of CNFs caused CNFs clusters entangled at the inner corner of cross CSFs lead to the formation of defects. The above phenomenon disturbed the thermal transport, resulting in lower TC of CSF-CNF/A336 alloy composites. For improving the property of CSF-CNF/A336 alloy composite as expect, the CNFs should be further dispersed such as using vibration milling to decrease the CNFs agglomeration and Cu or Ni layer coated on CNFs would improve the wettability between CNF and matrix to reduce porosity and defects in the composite.

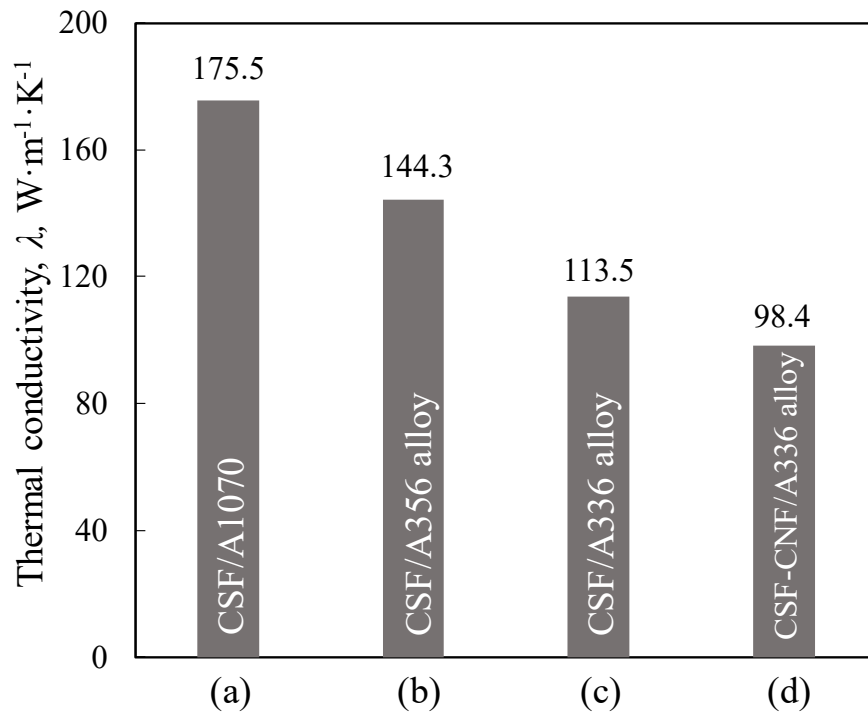


Fig. 4-14 TC of CSF/Al matrix composites fabricated with SiO_2 binder preform (0.4MPa): (a) CSF/A1070 composite, (b) CSF/A356 alloy composite, (c) CSF/A336 alloy composite and (d) CSF-CNF/A336 alloy composite.

Figure 4-15 shows the TC of Ni plated CSF/Al matrix composites without preform manufacturing under 0.4 MPa and 0.8 MPa, respectively. It is noticed that the TC of Ni plated CSF/A1070, A356 alloy, and A336 alloy composites fabricated under 0.4 MPa showed the values of 152.3, 135.8, and 106.7 $\text{W}\cdot\text{m}^{-1}\cdot\text{K}^{-1}$, respectively, as shown in Figs. 4-15 (a), (c), (e). The TC of composites fabricated under 0.8 MPa was 167.1, 147.6, and 121.6 $\text{W}\cdot\text{m}^{-1}\cdot\text{K}^{-1}$, respectively, as shown in Figs. 4-15 (b), (d), (f). The same decrease trend of TC was observed which can be attributed to the difference of matrix of A1070, A356 alloy, and A336 alloy. It is important to emphasize that A1070 contained almost no other alloying elements except aluminum which provided strong thermal and electron conductivity, however, the A356 alloy and A336 alloy possessed high amounts of alloying elements and precipitate in composites had a remarkable bad effect on TC of composites.

Figs. 4-15 (a) and (b) show the TC of Ni plated CSF/A1070 composite fabricated under 0.4 and 0.8 MPa. A higher TC of composite fabricated by 0.8 MPa was achieved than composite fabricated by 0.4 MPa. It is emphasized that an increase of TC can be obtained by applying a higher fabrication pressure. In addition, by applying higher pressure, according to the, a higher of volume fraction of CSFs (13.7 Vol. %, higher than 10 Vol. %) in per unit area of composite was achieved as described in Chapter 3 (microstructure analysis), and an increase of relative density was also achieved as analyzed above. These all contributed to an increase of TC of the Ni plated CSF/A1070 composite fabricated under 0.8 MPa. However, the TC of Ni plated CSF/A1070 composite (0.8 MPa) corresponded to 62.9% of the theoretical value. According to the microstructure analysis, 3.6 vol.% Al_3Ni compound was generated by the reaction of Ni plated layer with Al matrix. In addition, the existed defects in composite caused high interfacial thermal resistance. These phenomena caused a high divergence between the experimental and theoretical TC values of CSF/A1070 composite.

Figs. 4-15 (b) and (d), (e) and (f) show the TC of Ni plated CSF/A356 alloy and A336 alloy composites fabricated under different pressure. The values also revealed that a higher TC can be obtained by a higher fabrication pressure. It is noticed that the Ni plated CSF/A336 alloy composite presented the lowest TC compared with composites fabricated under the same pressure, and the TC of Ni plated CSF/A356 alloy (0.8 MPa)

corresponding to 80.0% of the theoretical value. Ni plated CSF/A336 alloy composite possessed the highest content of Al_3Ni compounds than other composites. The highest amount of Al_3Ni compounds was generated by not only the Ni plated layer but also the high content of Ni (1.5 mass%) in A336 alloy matrix. The Al_3Ni compound with low TC to be approximately $35 \text{ W}\cdot\text{m}^{-1}\cdot\text{K}^{-1}$ acted a role of the thermal resistance to the heat flow and leads to degradation of the thermal properties of composites [25]. In addition, the precipitate was also a factor that weakens the TC of composites. A336 alloy possessed the highest content of Si than A356 alloy, resulting in a higher degree of Si phase precipitation in Ni plated CSF/A336 alloy composite. The higher degree of supersaturation of Si phase resulting in severe distortion of the crystal lattice and provide additional interfacial resistance which would further obstruct to effective thermal conduction through the matrix. As a result, the Ni plated CSF/A336 alloy composite exhibited the lowest TC. For the generation of Al_3Ni compound and the precipitation of Si phase in Ni plated CSF/Al alloy composites which provided additional interfacial resistance caused a disparity between the experimental and theoretical values.

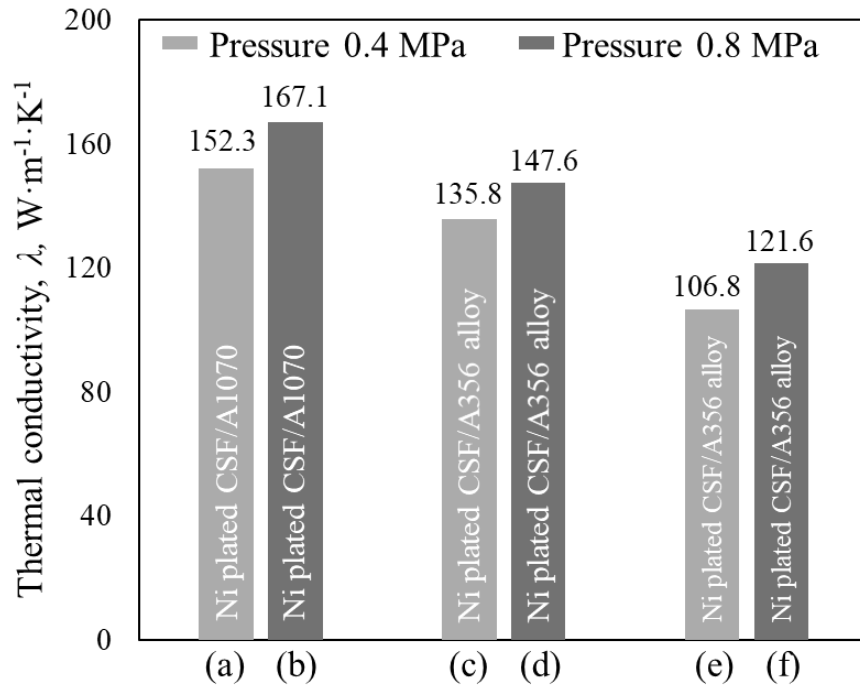


Fig. 4-15 TC of Ni plated CSF/Al matrix composites fabricated without preform manufacturing (0.4MPa and 0.8 MPa): (a) Ni plated CSF/A1070 composite, (b) Ni plated CSF/A356 alloy composite and (c) Ni plated CSF/A336 alloy composite.

The TC comparison of CSF/Al matrix composites with SiO₂ binder (0.4 MPa) and Ni plated CSF/Al matrix composites without preform manufacturing (0.4 and 0.8 MPa) were summarized in Table 4-4. It is concluded that the TC of Ni plated CSF/Al matrix composites were slightly lower than that of CSF/Al matrix composites with SiO₂ binder. The introduction of Ni plating leads to the formation of Al₃Ni compounds in composites which introduced a much newer interface, meanwhile, the Al₃Ni possessed a low TC of 35 W·m⁻¹·K⁻¹, the two reasons resulted in a relative lower TC. By increasing the fabrication pressure, a higher relative density of Ni plated CSF/Al matrix composites attributed to an increase of TC.

Table 4-4 Comparison of TC of CSF/Al matrix composites fabricated with SiO₂ binder (0.4 MPa) and without preform manufacturing (0.4 and 0.8 MPa).

Composites	0.4 MPa	0.4 MPa	0.8 MPa
TC (W·m ⁻¹ ·K ⁻¹)	with SiO ₂ binder	without preform	without preform
CSF/A1070 composite	175.5	152.3	167.1
CSF/A356 alloy composite	144.4	135.8	147.6
CSF/A336 alloy composite	113.5	106.8	121.6

4.4 Summary

(1) The relative density of CSF/Al matrix composites with SiO₂ binder (0.4 MPa) was ranged from 95.8% to 97.2%. The CSF/Al matrix composites without preform manufacturing (0.4 MPa) are capable of achieving higher densification (greater than 97.8% relative density, highest 99.0%).

(2) All CSF/Al matrix composites were harder than their respective matrix due to the introduction of CSFs. The hardness of Ni plated CSF reinforced composites was higher than that of composites with SiO₂ binder due to the generation of Al₃Ni compounds. The Ni plated CSF/A336 alloy composite (0.4 MPa) showed the highest hardness due to the highest content of Al₃Ni compounds and Si precipitate.

(3) For Ni plated CSF/Al matrix composites fabricated without preform manufacturing under 0.4 MPa and 0.8 MPa. With applying a higher fabrication pressure, an increase in Young's modulus, UTS and yield strength of the composite was achieved, while the elongation dropped. The Ni plated CSF/Al matrix composite without preform manufacturing exhibited higher tensile strength than the composites with SiO₂ binder due to the formation of Al₃Ni compounds. The CSF reinforced composites all revealed the brittle fracture mechanism as the addition of CSFs.

(4) For the same fabrication condition of containing binder and without binder, CSF/A1070 composites both presented the highest TC compared to other composites. A higher amount of Si phase precipitate and IMCs in CSF/A336 alloy composite due to a high content of 12mass% Si, 1.5mass% Ni and 1.3mass% Mg elements in A336 alloy, which resulted in the lowest TC. Comparison of TC of CSF/Al matrix composites fabricated with SiO₂ binder and without binder, the TC of Ni plated CSF reinforced composites was relative lower which caused by the additional generation of Al₃Ni compounds.

References

- [1] J. M. Molina, J. Narciso, L. Weber, A. Mortensen and E. Louis: *Mater. Sci. Eng. A*, **480** (2008) 483-488.
- [2] C. Zweben: *JOM*, **50** (1998) 47-51.
- [3] G. Korb, J. Koráb and G. Groboth: *Composites A*, **29** (1998) 1563-1567.
- [4] K. J. Euh and S. B. Kang: *Mater. Sci. Eng. A*, **395** (2005) 47-52.
- [5] C. Zweben: *Power El. Tech.*, **32** (2006) 40-47.
- [6] J.M. Molina, J. Narciso, L. Weber, A. Mortensen and E. Louis: *Mater. Sci. Eng. A*, **480** (2008) 483-488.
- [7] S. F. Moustafa: *Wear* **185** (1995) 189–195.
- [8] W. Ames and A.T. Alpas: *Metall. Mater. Trans. A*, **26** (1995) 85–98..
- [9] S. C. Tjong, K.C. Lau and S.Q. Wu: *Metall. Mater. Trans. A*, **30** (1999) 2551–2555.
- [10] A. Wilson and A.T. Alpas: *Wear*, **196** (1996) 270–278.
- [11] D. D. Edie: *Carbon*, **36** (1998) 345-362.
- [12] T. Suzuki and H. Umehara: *Carbon*, **37** (1999) 47–59.
- [13] L. Laffont and M. Monthieux, V. Serin: *Carbon*, **40** (2002) 767-780.
- [14] K. C. Chang, K. Matsugi, G. Sasaki and O. Yanagisawa: *JSME Int. J.* **48** (2005) 205 209.
- [15] T. P. D. Rajan, R. M. Pillai and B. C. Pal: *J. Mater. Sci.* **33** (1998) 3491-3503.
- [16] R. S. Bushby and V. D. Scott: *Compos. Sci. Technol.* **57** (1997) 119-128.
- [17] H. Yanling and R.J. Young: *J. Mater. Sci.* **29** (1994) 4027.
- [18] Y. B. Choi, G. Sasaki, K. Matsugi, O. Yanagisawa: *Mater. Trans.* **46** (2005) 2156-2158.
- [19] Y. B. Choi, G. Sasaki, K. Matsugi, N. Sorida, S. Kondoh, T. Fujii, O. Yanagisawa: *JSME A*, **49** (2006) 20-24.
- [20] Y. B. Choi, K. Matsugi, G. Sasaki, K. Arita and O. Yanagisawa: *Mater. Trans.* **47** (2006) 1227-1231.
- [21] S. R. Bakshi, A. K. Keshri, V. Singh, S. Seal and A. Agarwal, *J. Alloys Compd.* **481** (2009) 207-213.
- [22] T. J. Hirisch: *J. Am. Con. Inst.* **59** (1962) 427-452.

- [23] C.W. Nan, G. Liu, Y. H. Lin and M. Li: *Appl. Phys. Lett.* **85** (2004) 3549-3551.
- [24] C.W. Nan, Z. Shi and Y. Lin: *Chem. Phys. Lett.* **375** (2003) 666–669.
- [25] Y. Terada, K. Ohkubo, T. Mohri and T. Suzuki: *Mater. Trans.* **43** (2002) 3167-3176.

Conclusions

The purpose of present research is to develop the carbon short fiber reinforced Al matrix composites with satisfactory mechanical and thermal properties by the cost-effective fabrication process. The traditional manufacturing of short fiber reinforced composites by liquid processes requires preform manufacturing using inorganic binders (such as SiO₂, Al₂O₃, TiO₂ binder etc). However, conventional preform manufacturing techniques using inorganic binder are nontrivial procedures requiring high-energy inputs and preparation time for binder sintering process. Therefore, a novel alternative fabrication process without preform manufacturing was developed for carbon short fiber (CSF) reinforced Al matrix composite by low- pressure infiltration method. The low-pressure infiltration process enables complex/large shape and cost saving fabrication. In this study, CSF/Al matrix composites were fabricated with SiO₂ binder preform and CSF/Al matrix composites were fabricated without preform manufacturing, respectively. The effects of matrix on microstructure, mechanical and thermal properties were investigated. Meanwhile, the properties of composites that fabricated with SiO₂ binder preform and without preform manufacturing, respectively, were compared and evaluated. The conclusions of this thesis are summarized as follows:

1. The study on the fabrication of CSF/Al and CSF-CNF/Al matrix composites fabricated with SiO₂ binder preform by low-pressure infiltration process. (Chapter 2)

Prior to the fabrication of CSF-CNF/Al composite by the low-pressure infiltration process, the decision of the fabrication conditions for the CSF-CNF preform was studied. A different ratio of CSF: CNF (5:5, 7:3, 9:1 and 9.5:0.5) was carried out to investigate the best CNF dispersion. With decreasing the content of CNFs, CNFs agglomeration in preform was weakening accordingly. CNFs were presented the best distribution at the condition of CSF: CNF by 9.5:0.5. Microstructure analysis of CSF

preform revealed that the CSFs were cross linked and clustered together by SiO₂ binder, meanwhile, SiO₂ binder was coated on the surface of CSFs. As for CSF-CNF preform, CNFs were stuck together at the corner of CSFs bridges by SiO₂ binder.

Fabrication of CSF/Al and CSF-CNF/Al matrix composites SiO₂ binder preform was carried out by low-pressure infiltration process, infiltration pressure was 0.4 MPa. In all CSF/Al matrix composites, CSFs were random distributed in the matrix, while, defects were formed by the CSFs cluster with a size of 25 μm (CSF/A1070 composite), 20 μm (CSF/A356 alloy composite), and 10 μm (CSF/A1070 composite). In CSF-CNF/Al composite, CNFs were entangled at the intersection of CSFs lead to large size defects (approximately 60 μm). Oxide layer was discovered between CSF and Al matrix, which was generated by the interfacial reaction of SiO₂ binder and Al matrix.

2. The development of a new fabricating process without preform manufacturing. The study on the fabrication of Ni plated CSF/Al matrix composites by low-pressure infiltration. (Chapter 3)

Ni plated CSFs were prepared using an electroless plating process, with the Ni homogeneously deposited on the surface of CSFs. The Ni plated CSFs were put into graphite mold with a height of 10 mm to achieve a volume fraction of 10 vol.%. Al ingot was placed on the CSFs, the total mold was put into the furnace heated to 625K for 2h for Ni recrystallization, and then heated to 1073K for infiltrating Al into CSFs. In all Ni plated CSF/Al matrix composites, groups of Al₃Ni compounds were generated in the matrix and near the surface of CSFs, no Al₄C₃ was generated. The Ni plated CSF/A336 alloy composite possessed the highest content of Al₃Ni compounds due to the highest content of Ni element of A336 alloy promoted the generation of compounds. Meanwhile, the smallest defect size was presented in Ni plated CSF/A336 alloy composite due to the highest Si element of A336 alloy fulfilled it the best metal fluidity.

3. The study on the mechanical properties and thermal conductivities of the CSF/Al matrix composites fabricated with SiO₂ binder preform and without preform manufacturing, respectively. (Chapter 4)

The relative density of CSF/Al matrix composites with SiO₂ binder (0.4 MPa) was ranged from 95.8% to 97.2%. The CSF/Al matrix composites without preform manufacturing (0.4 MPa) are capable of achieving higher densification (greater than

97.8% relative density). By increasing the fabrication pressure, a higher relative density can be achieved. The Ni plated CSF/A336 alloy composite fabricated under 0.8 MPa presented the highest relative density of 99.4%. As for fabrication pressure of 0.4 MPa, the hardness of Ni plated CSF reinforced composites without preform manufacturing was higher than the composites fabricated with SiO₂ binder due to the strengthening of Al₃Ni compounds.

For the composites fabricated without preform manufacturing, a slight increase of tensile properties was achieved by applying higher pressure. The weak bonding strength between CSF and matrix in the composites fabricated by the new process limited the enhancement of tensile strength. A comparison of tensile properties of the composites fabricated under 0.8 MPa, with SiO₂ binder and Ni plated CSF reinforced composites without preform manufacturing was conducted. It revealed that the tensile properties of Ni plated CSF reinforced composites were slightly higher than the composites fabricated with SiO₂ binder.

As concerned to the composites fabricated under the same condition by the process with SiO₂ binder and without preform manufacturing, respectively. CSF/A1070 composites all presented the highest thermal conductivity (TC) compared to Al alloys composites due to the A1070 matrix possesses no alloying elements. The higher amount of Si phase precipitate and IMCs in CSF/A336 alloy composite due to the high content of 12mass% Si, 1.5mass% Ni and 1.3mass% Mg elements in A336 alloy, which resulted in the lowest TC. In addition, the composites fabricated without preform manufacturing (0.4 MPa) could reach a TC similar to the composites fabricated with SiO₂ binder although the generation of compounds.

After a systematic analysis of the CSF/Al matrix composites fabricated with SiO₂ binder and without preform manufacturing. The new fabrication process developed in this research can achieve a higher relative density, hardness, tensile properties, and approximately equal TC compared to the composites fabricated by the traditional process using SiO₂ binder preform. Furthermore, the new process without preform manufacturing is provided with the characteristics of simple operation process, energy saving and high production efficiency which is expected for further developing the CSF/Al matrix composites.

Acknowledgements

I would like to express my sincere gratitude to Assistant Professor Yongbum Choi for his great guidance and insight throughout this study. He gave me full support not only on my research, but also on my life and career, which has played an important role in both of my professional and personal development. I am also greatly indebted Professor Kazuhiro Matsugi and Assistant Professor Zhefeng Xu. They gave me so much positive help on the research, the accumulation of the knowledge and my life, and I have learnt so much from them. In addition, I would like to express my heartfelt thanks to Professor Gen Sasaki, Associate Professor Kenjiro Sugio, Professor Wenchang Liu, Professor Jinku Yu and Professor Xingang Liu for their technical advice and experimental assistance.

I would like to thank Mr. Shaoming Kang, Mrs. Meiqi Yu, Mr. Fei Gao, Mr Yujiao Ke, Mr. Xilong Ma, Mr. Zeze Xiao and Mrs Siran Chen for considerable assistance and help in my experiments and my life. Moreover, I would also like to thank all the past and present members of Property Control of Materials Laboratory, in Department of Mechanical Physical Engineering, Hiroshima University, for their enthusiastic help to both of my life and study.

Finally, my thanks would go to my beloved family for their loving considerations and great confidence in me all through these years. Grateful to my wife for unconditional support and care over the years. I also owe my sincere gratitude to my friends who gave me their help and time in helping me work out my problems during the difficult course of the thesis.

Published papers in regard to this thesis

1. **X. Meng**, Y. B. Choi*, K. Matsugi, Z. F. Xu, W. C. Liu. Microstructures of carbon fiber and hybrid carbon fiber carbon nano fiber reinforced aluminum matrix composites by low-pressure infiltration process and their properties. *Materials transactions*. 2018(59)12: 1935-1942. (Chapter 2 & 4)

2. **X. Meng**, Y. B. Choi*, K. Matsugi, W. T. Hu, W. C. Liu. Development of short carbon fiber reinforced aluminum matrix composites by low pressure infiltration process. *Materials Science and Engineering*. 2019(547)012024: 1-6. (Chapter 2 & 4)

3. **X. Meng**, Y. B. Choi*, K. Matsugi, W. C. Liu. Development of carbon short fiber reinforced Al based composite without preform manufacturing. *Materials transactions*. 2020(61)3: in press. (Chapter 3 & 4)

Presentations

1. **Xuan Meng**, Yong Bum Choi, Kazuhiro Matsugi, Zhefeng Xu and Wenchang Liu. Microstructure and Texture of Ti/Al/Mg Five-ply Laminated Composites Prepared by Hot-roll Bonding. 日本軽金属学会中国四国支部第9回講演大会 July 29, 2017, Aihime, Japan ; Aihime University. 優秀講演賞.

2. **Xuan Meng**, Yong Bum Choi, Kazuhiro Matsugi, Zhefeng Xu and Wenchang Liu. Development of hybrid carbon fiber and carbon nano fiber reinforced Al composites. 日本金属学会2018年春期講演大会. March 19-21, 2018, Tokyo, Japan; Chiba Institute of Technology University.

3. **Xuan Meng**, Yong Bum Choi, Kazuhiro Matsugi, W. T. Hu and Wenchang Liu. Development of carbon short fiber reinforced aluminum matrix composites by low pressure infiltration process. The 1st International Conference on Design and Application of Engineering Materials; Sept. 6-7, 2018, Bandung, Indonesia.

4. **X. Meng**, Y. B. Choi, K. Matsugi. 高機能性を有する炭素短繊維強化金属基複合材料の開発. 広島大学若手研究者による研究シーズ発表会, 2019年3月11日.

5. **X. Meng**, Y. B. Choi, K. Matsugi, Hiroki Shibata. Microstructure and Properties of Carbon Short Fiber Reinforced Aluminum and Aluminum Alloy Matrix Composite by Low-pressure Infiltration Method. 日本金属学会2019年秋期講演大会. Sept. 11-13, 2019, Okayama, Japan; Okayama University.

6. **X. Meng**, Y. B. Choi, K. Matsugi. Effect of matrix on characteristics for multipurpose of carbon short fiber reinforced composite. The 12th Korea-Japan Joint Symposium on Composite Materials. Dec.5-7, 2019, Changwon, Korea.